UNIVERSIDAD AUTÓNOMA DE SAN LUIS POTOSÍ

FACULTAD DE CIENCIAS QUÍMICAS

POSGRADO EN CIENCIAS FARMACOBIOLÓGICAS

TÍTULO DEL TRABAJO

Polímeros de impresión molecular para la liberación de antibióticos en úlceras de biomodelos con diabetes inducida

TESIS PARA OBTENER EL GRADO DE

DOCTORADO EN CIENCIAS FARMACOBIOLÓGICAS

PRESENTA:

VANESSA SARAHÍ GALVÁN ROMERO

DIRECTORA DE TESIS: Dra. Denisse Atenea de Loera Carrera

CO-DIRECTOR DE TESIS: Dr. Rogelio Flores Ramírez

San Luis Potosí, S. L. P. Julio 2026

Este proyecto se realizó en el Laboratorio de Salud Total de la Coordinación para la Innovación y Aplicación de la Ciencia y Tecnología y en el Laboratorio de Antimicrobianos, Biopelículas y Microbiota del Centro de Investigación en Ciencias de la Salud y Biomedicina de la Universidad Autónoma de San Luis Potosí, en el periodo comprendido entre agosto de 2022 y julio de 2026, bajo la codirección de la Dra. Denisse Atenea de Loera Carrera y el Dr. Rogelio Flores Ramírez.

El programa de Doctorado en Ciencias Farmacobiológicas de la Universidad Autónoma de San Luis Potosí pertenece al Sistema Nacional de Posgrados de Calidad (SNP) del SECIHTI, registro 003383. Número de la beca otorgada por SECIHTI: **1078903** Número de CVU.

Los datos del trabajo titulado polímeros de impresión molecular para la liberación de antibióticos en úlceras de biomodelos con diabetes inducida se encuentran bajo el resguardo del Facultad de Ciencias Químicas y pertenecen a la Universidad Autónoma de San Luis Potosí.

UNIVERSIDAD AUTÓNOMA DE SAN LUIS POTOSÍ
Facultad de Ciencias Químicas
Centro de Investigación y Estudios de Posgrado
Posgrado en Ciencias Farmacobiológicas
Programa de Doctorado

Formato D13

Aprobación de Tema de Tesis

San Luis Potosí SLP a 07/ 23 /2026

Comité Académico

La presente es para que quede asentado que el tema de Tesis de Doctorado:
Polímeros de impresión molecular para la liberación de antibióticos en úlceras de biomodelos con diabetes inducida

del estudiante: _Vanessa Sarahí Galván Romero_, que se llevará a cabo en el laboratorio de Laboratorio de Salud Total de la Coordinación para la Innovación y Aplicación de la Ciencia y Tecnología y en el Laboratorio de Antimicrobianos, Biopelículas y Microbiota del Centro de Investigación en Ciencias de la Salud y Biomedicina de la Universidad Autónoma de San Luis Potosí, es APROBADO.

Sin más por el momento, quedo de Uds.

A T E N T A M E N T E

Dra. Claudia Escudero Lourdes

Coordinador del Posgrado

UNIVERSIDAD AUTÓNOMA DE SAN LUIS POTOSÍ

FACULTAD DE CIENCIAS QUÍMICAS

POSGRADO EN CIENCIAS FARMACOBIOLÓGICAS

TÍTULO DEL TRABAJO

Polímeros de impresión molecular para la liberación de antibióticos en úlceras de biomodelos con diabetes inducida

TESIS PARA OBTENER EL GRADO DE

DOCTORADO EN CIENCIAS FARMACOBIOLÓGICAS

PRESENTA:

VANESSA SARAHÍ GALVÁN ROMERO

SINODALES:

PRESIDENTE:

Dr. Sergio Zarazúa Guzman _____

SECRETARIO:

Dra. Denisse Atenea de Loera Carrera _____

VOCAL:

Dr. Rogelio Flores Ramírez _____

VOCAL:

Dra. Luz Eugenia Alcántara Quintana _____

VOCAL:

Dr. Mario Aurelio Martínez Jiménez _____

San Luis Potosí, S. L. P JULIO 2026

INTEGRANTES DEL COMITÉ TUTORIAL ACADÉMICO

Directora de Tesis:

Dra. Denisse Atenea de Loera Carrera

Facultad de Ciencias Químicas

Universidad Autónoma de San Luis Potosí, San Luis Potosí, S.L.P.

Codirector de Tesis:

Dr. Rogelio Flores Ramírez

Coordinación para la Innovación y Aplicación de la Ciencia y la Tecnología

Universidad Autónoma de San Luis Potosí, San Luis Potosí, S.L.P.

Asesores de tesis:

Dr. Sergio Zarazúa Guzman

Facultad de Ciencias Químicas

Universidad Autónoma de San Luis Potosí, San Luis Potosí, S.L.P.

Dra. Luz Eugenia Alcántara Quintana

Coordinación para la Innovación y Aplicación de la Ciencia y la Tecnología

Universidad Autónoma de San Luis Potosí, San Luis Potosí, S.L.P.

Dr. Mario Aurelio Martínez Jiménez

Unidad de quemados y cuidado de heridas, Hospital Central Ignacio Morones Prieto.

UNIVERSIDAD AUTÓNOMA DE SAN LUIS POTOSÍ
Facultad de Ciencias Químicas
Centro de Investigación y Estudios de Posgrado
Posgrado en Ciencias Farmacobiológicas
Programa de Doctorado

Formato D5

Carta Cesión de Derechos

San Luis Potosí SLP a 07/ 23 /2026

En la ciudad de *San Luis Potosí* el día *22* del mes de *Julio* del año *2026.* El que suscribe *Vanessa Sarahí Galván Romero* Alumno(a) del programa de posgrado *Ciencias Farmacobiológicas* adscrito a *Facultad de Ciencias Químicas* manifiesta que es autor(a) intelectual del presente trabajo terminal, realizado bajo la dirección de: *Dra. Denisse Atenea de Loera Carrera y Dr. Rogelio Flores Ramírez* y cede los derechos del trabajo titulado *Polímeros De Impresión Molecular Para La Liberación De Antibióticos En Úlceras De Biomodelos Con Diabetes Inducida* a la **Universidad Autónoma de San Luis Potosí**, para su difusión con fines académicos y de investigación.

Los usuarios de la información no deben reproducir de forma total o parcial texto, gráficas, imágenes o cualquier contenido del trabajo si el permiso expreso del o los autores. Éste, puede ser obtenido directamente con el autor o autores escribiendo a la siguiente dirección *rogelio.flores@uaslp.mx y vannegalvan@hotmail.com.* Si el permiso se otorga, el usuario deberá dar el agradecimiento correspondiente y citar la fuente del mismo.

_____

Vanessa Sarahí Galván Romero

UNIVERSIDAD AUTÓNOMA DE SAN LUIS POTOSÍ
Facultad de Ciencias Químicas
Centro de Investigación y Estudios de Posgrado
Posgrado en Ciencias Farmacobiológicas
Programa de Doctorado

Formato D28

Carta de Análisis de Similitud

San Luis Potosí SLP a 07/ 23 /2026

L.B. Reyna Nayeli Ortíz Quintero
Biblioteca de Posgrado FCQ

Asunto: Reporte de porcentaje de similitud de tesis de grado

Por este medio me permito informarle el porcentaje de similitud obtenido mediante Ithenticate para la tesis titulada Polímeros De Impresión Molecular Para La Liberación De Antibióticos En Úlceras De Biomodelos Con Diabetes Inducida presentada por el autor Vanessa Sarahí Galván Romero. La tesis es requisito para obtener el grado de Doctorado en el Posgrado en Ciencias Farmacobiológicas. El análisis reveló un porcentaje de similitud de 9% excluyendo referencias y metodología.

Agradezco sinceramente su valioso tiempo y dedicación para llevar a cabo una exhaustiva revisión de la tesis. Quedo a su disposición para cualquier consulta o inquietud que pueda surgir en el proceso.

Sin más por el momento, le envío un cordial saludo.

A T E N T A M E N T E

_____

Coordinador Académico del Posgrado

en Ciencias Farmacobiológicas

DEDICATORIA

A mis padres, por su apoyo incondicional, por confiar en mí y por acompañarme en cada etapa de este camino. Gracias, mamá y papá, por ser una parte fundamental de este logro.

A mis hermanos, por su cariño, comprensión y por estar presentes aun en los momentos de mayor distancia y trabajo.

Y a mí misma, por la constancia, la disciplina y la fortaleza para continuar incluso cuando el camino se volvió difícil.

Este logro también es de ustedes.

AGRADECIMIENTOS

La conclusión de esta tesis representa el cierre de una etapa de un gran aprendizaje académico, profesional y personal. Este camino no habría sido posible sin el el apoyo de las personas que estuvieron presentes durante estos cuatro años.

Agradezco especialmente al Dr. Rogelio Flores, por brindarme la oportunidad de desarrollar este proyecto bajo su dirección, por la confianza y por motivarme a buscar nuevas oportunidades de crecimiento profesional.

A la Dra. Denisse Atenea, la Dra. Luz Alcántara, el Dr. Sergio Zarazúa, el Dr. Mario Martínez y el Dr. Fidel Martínez Gutiérrez, por acompañarme durante este proceso académico y por compartir conmigo su tiempo, experiencia y conocimientos. Agradezco profundamente su apoyo, sus consejos y cada una de sus observaciones, que no solo contribuyeron a enriquecer y mejorar este proyecto, sino también a fortalecer mi desarrollo profesional.

A mis amigos de laboratorio, Bere, Ruth, Sam, Fer y María, por compartir conmigo las dificultades y los logros incluso los días de platicas largas. Gracias por su ayuda, su compañía y por hacer mis días más divertidos.

A mis amigos del posgrado (Rodri y Omar) que hemos pasado juntos desde el día uno de carrera y ahora del doctorado.

A las personas que conocí durante mis estancias de investigación en Japón y España, gracias por recibirme, orientarme y compartir conmigo sus conocimientos y experiencias. Su compañía y amistad hicieron de esta etapa algo inolvidables.

Finalmente, agradezco profundamente a mis papás, a mis hermanos, a toda mi familia y a los que hoy ya no están. Gracias por su amor, paciencia y apoyo incondicional; por confiar en mí y acompañarme incluso en la distancia. Su presencia y respaldo fueron esenciales para alcanzar esta meta.

Resumen

En este trabajo se realizaron materiales poliméricos basados en la técnica de impresión molecular denominados MIPs (polímeros de impresión molecular) como sistemas para la liberación localizada y controlada de amoxicilina, piperacilina y tazobactam, incorporados de manera individual o combinada. Los MIPs se sintetizaron mediante un método no covalente llamado coprecipitación, utilizando ácido láctico como monómero funcional. Los materiales se caracterizaron mediante espectroscopía ATR-FTIR, microscopía electrónica de barrido de emisión de campo, punto de carga cero, estudios de adsorción y ensayos de liberación *in vitro* a pH 5.4 y 7.4. La eficacia y seguridad de los materiales se evaluó frente a cepas de referencia ATCC y aislamientos clínicos de *Escherichia coli*, *Staphylococcus aureus* y *Pseudomonas aeruginosa*, y en fibroblastos dérmicos humanos normales. Los MIPs presentaron eficiencias de adsorción superiores al 90 %, con un mejor ajuste al modelo de Langmuir y SIPs. Los perfiles de liberación fueron dependientes del pH y los tratamientos basados en MIPs alcanzaron concentraciones mínimas inhibitorias de 0.09 ± 0.08 μg mL^{-1} frente a *E. coli* y de 0.83–1.56 μg mL^{-1} frente a *S. aureus*. Además, el sistema MIP-PT produjo una reducción bacteriana completa en 180 min para *S. aureus* y en 90–120 min para *P. aeruginosa*. Los materiales mostraron una viabilidad celular superior al 70 %. Respaldando el potencial de los MIPs como vehiculos para la administración local y controlada de antibióticos.

Palabras clave: polímeros de impresión molecular; liberación controlada; antibióticos; actividad antibacteriana; citocompatibilidad.

Abstract

In this study, polymeric materials based on the molecular imprinting technique, known as molecularly imprinted polymers (MIPs), were developed as systems for the localized and controlled delivery of amoxicillin, piperacillin, and tazobactam, incorporated either individually or in combination. The MIPs were synthesized using a noncovalent coprecipitation method, with lactic acid as the functional monomer. The materials were characterized by ATR-FTIR spectroscopy, field-emission scanning electron microscopy, point of zero charge determination, adsorption studies, and *in vitro* release assays at pH 5.4 and 7.4. Their efficacy and safety were evaluated against ATCC reference strains and clinical isolates of *Escherichia coli*, *Staphylococcus aureus*, and *Pseudomonas aeruginosa*, as well as in normal human dermal fibroblasts. The MIPs exhibited adsorption efficiencies above 90%, with the Langmuir and Sips models providing the best fit. Drug release profiles were pH-dependent, and MIP-based treatments achieved minimum inhibitory concentrations of 0.09 ± 0.08 μg mL^{-1} against *E. coli* and 0.83–1.56 μg mL^{-1} against *S. aureus*. In addition, the MIP-PT system produced complete bacterial reduction within 180 min for *S. aureus* and within 90–120 min for *P. aeruginosa*. The materials obtained cell viability above 70%, supporting the potential of MIPs as carriers for the localized and controlled delivery of antibiotics.

Keywords: molecularly imprinted polymers; controlled release; antibiotics; antibacterial activity; cytocompatibility**.**

ÍNDICE

ÍNDICE DE TABLAS Y FIGURAS

1. Introducción

1.1 Resistencia antimicrobiana: un problema global de salud pública

Las enfermedades infecciosas continúan siendo una causa importante de morbilidad y mortalidad a nivel mundial, pero su tratamiento se ha vuelto más complejo debido a la aparición y propagación de microorganismos resistentes a los antimicrobianos (World Health Organization, 2023). La resistencia antimicrobiana (RAM) se define como la capacidad heredada o adquirida de los microorganismos para sobrevivir o proliferar frente a concentraciones de un antimicrobiano que normalmente los inhibiría o eliminaría (UNEP, 2022). En el caso de las bacterias, este fenómeno representa un desafío clínico relevante, ya que reduce la eficacia de los antibióticos y limita las opciones terapéuticas disponibles. La resistencia puede ser intrínseca, cuando forma parte de las características naturales del microorganismo, o adquirida, cuando surge por mutaciones, incorporación de ADN externo o transferencia horizontal de genes mediante elementos genéticos móviles (UNEP, 2022; World Health Organization, 2023).

Las consecuencias de la RAM no se limitan al fracaso terapéutico individual, sino que también incrementan el riesgo de complicaciones, favorecen la diseminación de microorganismos resistentes y elevan los costos asociados al diagnóstico, tratamiento y control de infecciones. Se ha estimado que la RAM bacteriana estuvo asociada con 4.95 millones de muertes en 2019, de las cuales 1.27 millones fueron atribuibles directamente a este fenómeno (Murray et al., 2022). Aunque el desarrollo de nuevos antibióticos sigue siendo necesario, la innovación antibacteriana continúa siendo limitada frente a la rápida emergencia de mecanismos de resistencia y a barreras científicas, regulatorias, económicas y de acceso (Sullivan et al., 2024; World Health Organization, 2023). Por ello, se requieren estrategias complementarias que preserven la utilidad clínica de los antibióticos existentes, optimicen su uso y reduzcan exposiciones innecesarias (Davies, 2010; UNEP, 2022; World Health Organization, 2023). En este contexto, los sistemas de liberación controlada, como los polímeros de impresión molecular, pueden contribuir a modular

la liberación del antibiótico, prolongar su exposición local y mejorar su desempeño terapéutico en el sitio infeccioso (Wassif et al., 2021).

1.2 Patógenos prioritarios y desafíos terapéuticos en infecciones bacterianas

La identificación de patógenos bacterianos prioritarios permite orientar la investigación, el desarrollo de nuevos antibacterianos y las estrategias de prevención frente a la resistencia antimicrobiana. En 2024, la OMS actualizó su lista de patógenos prioritarios con base en criterios como mortalidad, carga de enfermedad, incidencia, tendencias de resistencia, transmisibilidad, tratabilidad, capacidad de prevención y estado del desarrollo de nuevos tratamientos (WHO, 2024). Entre los microorganismos de mayor relevancia se encuentran bacterias Gram negativas resistentes a antibióticos críticos, como *Escherichia coli*, *Klebsiella pneumoniae*, *Pseudomonas aeruginosa* y *Acinetobacter baumannii*, así como *Staphylococcus aureus* resistente a meticilina, debido a su impacto clínico en infecciones hospitalarias, bacteriemias, infecciones asociadas a dispositivos médicos y lesiones de piel y tejidos blandos (Blair et al., 2014; Ciofu et al., 2022; WHO, 2024).

En heridas infectadas, *S. aureus* y *P. aeruginosa* son especialmente relevantes por su capacidad para colonizar tejido lesionado, formar biopelículas y persistir en microambientes inflamatorios o crónicos (Goswami et al., 2023; Versey et al., 2021). En estos casos, la eficacia terapéutica no depende únicamente de la susceptibilidad in vitro del microorganismo, sino también de factores locales como pH, exudado, oxigenación, matriz extracelular, perfusión tisular, material necrótico e interacciones microbianas dentro del biofilm (Ciofu et al., 2022; Goswami et al., 2023; Versey et al., 2021).

Aunque la administración sistémica de antibióticos por vía oral, intravenosa o intramuscular sigue siendo esencial en infecciones diseminadas o profundas, puede ser limitada en infecciones localizadas, ya que solo una fracción del fármaco alcanza el sitio infeccioso en forma activa y durante el tiempo necesario (Aparicio-Blanco et al., 2024; Choi et al., 2023; Gao et al., 2018). Además, aumentar la dosis

sistémica no siempre mejora proporcionalmente la concentración local y puede incrementar efectos adversos, alterar la microbiota y favorecer presión selectiva sobre bacterias no objetivo (Davies, 2010; Gullberg et al., 2011; Tamma et al., 2017). Por ello, las estrategias de administración local y liberación controlada representan alternativas complementarias para mejorar la disponibilidad del antibiótico en el sitio de infección y reducir la exposición sistémica innecesaria (Aparicio-Blanco et al., 2024; Choi et al., 2023; Gao et al., 2018).

1.3 Limitaciones de la terapia antimicrobiana convencional

Los antibióticos son esenciales para el tratamiento de infecciones bacterianas; sin embargo, su uso puede asociarse con efectos adversos cuya aparición depende de la familia farmacológica, la dosis, la duración del tratamiento, la vía de administración, la función renal o hepática, las comorbilidades y el uso concomitante de otros medicamentos (Tamma et al., 2017). Entre las manifestaciones descritas se incluyen alteraciones gastrointestinales, dermatológicas, renales, hepáticas, hematológicas y neurológicas, así como reacciones de hipersensibilidad, prolongación del intervalo QT e infecciones oportunistas, incluidas las causadas por *Clostridioides difficile* (Tamma et al., 2017). En pacientes hospitalizados tratados con antibióticos sistémicos durante al menos 24 h, Tamma et al. (2017) reportaron que el 20 % presentó al menos un evento adverso, y que cada 10 días adicionales de terapia se asociaron con un incremento del 3 % en el riesgo de dichos eventos.

Este problema adquiere mayor relevancia cuando se requieren dosis elevadas o tratamientos prolongados para infecciones difíciles de erradicar, ya que el aumento de la exposición sistémica puede incrementar la toxicidad y favorecer presión selectiva sobre comunidades bacterianas no objetivo (Davies, 2010; Gullberg et al., 2011; Tamma et al., 2017). Además, en infecciones localizadas, las concentraciones plasmáticas no siempre reflejan la cantidad de antibiótico libre y activo en el tejido infectado, especialmente en presencia de barreras tisulares, biopelículas, exudado, variaciones de pH, hipoxia o comunidades polimicrobianas (Choi et al., 2023; Ciofu et al., 2022; Goswami et al., 2023; Versey et al., 2021; Wassif et al., 2021). Por ello, los sistemas de liberación local y controlada buscan aumentar y sostener la

concentración del antimicrobiano en el sitio de infección, modular su exposición temporal y reducir la exposición sistémica innecesaria (Aparicio-Blanco et al., 2024; Choi et al., 2023; Gao et al., 2018).

1.4 Úlceras del pie diabético infectadas: microambiente, patógenos y desafíos terapéuticos

Las úlceras del pie diabético constituyen una complicación crónica y multifactorial, cuyo desarrollo se relaciona principalmente con la interacción entre neuropatía periférica, enfermedad vascular, alteraciones biomecánicas, traumatismos repetitivos y control metabólico deficiente ((Bulton et al., 2020; Márquez-Godínez et al., 2014; Pavón Núñez et al., 2016). La enfermedad vascular periférica reduce la perfusión del miembro inferior y compromete el aporte de oxígeno y nutrientes al tejido lesionado, mientras que la neuropatía diabética modifica la sensibilidad, la función motora y el control autonómico del pie (Boulton & Rayman, 2020; Tesfaye et al., 2010). En una población de pacientes con pie diabético, Pavón-Núñez et al. (2016) identificaron enfermedad vascular periférica en 72.1 % y neuropatía en 59.8 % de los casos, lo que evidencia la frecuente coexistencia de ambos componentes.

La neuropatía sensitiva produce pérdida de la sensibilidad protectora y disminuye la percepción del dolor, por lo que pequeñas lesiones, presiones repetitivas o traumatismos pueden pasar inadvertidos. La neuropatía motora favorece debilidad muscular, deformidades y redistribución anormal de las presiones plantares, mientras que la afectación autonómica puede alterar la sudoración y contribuir a la sequedad y fisuración de la piel (Boulton & Rayman, 2020; Tesfaye et al., 2010). Además, la duración prolongada de la diabetes y el control glucémico insuficiente se han asociado con un mayor riesgo de desarrollar pie diabético; Márquez-Godínez et al. (2014) reportaron que una evolución de la enfermedad mayor de diez años y una HbA1c ≥7 % se relacionaron significativamente con dicho riesgo. Como se representa en la **Figura 1**, la interacción entre angiopatía, neuropatía, alteraciones inmunológicas y traumatismos facilita la formación de una lesión que puede progresar cuando se acompaña de isquemia, edema e infección.

Una vez que se pierde la integridad de la piel, la perfusión deficiente, la hipoxia, la inflamación persistente, el exudado y el tejido desvitalizado pueden retrasar la reparación tisular y favorecer la proliferación microbiana (Boulton & Rayman, 2020; Tesfaye et al., 2010; Versey et al., 2021). Entre los microorganismos asociados con las úlceras infectadas se encuentran *S. aureus*, *P. aeruginosa* y distintas especies de Enterobacterales, incluida *E. coli*. Estos microorganismos pueden coexistir en comunidades polimicrobianas y formar biopelículas que disminuyen su susceptibilidad a los antimicrobianos y dificultan su eliminación por la respuesta inmunitaria del hospedero (Ciofu et al., 2022; Versey et al., 2021).

En etapas avanzadas, la infección puede extenderse hacia tejidos blandos profundos, articulaciones y hueso, dando lugar a osteomielitis y aumentando el riesgo de procedimientos quirúrgicos y amputación (Boulton & Rayman, 2020; Pavón Núñez et al., 2016). En el estudio de Pavón-Núñez et al. (2016), 32 % de los pacientes presentaba lesiones Wagner grado III y 38.5 % requirió tratamiento quirúrgico. El manejo de estas lesiones debe ser multidisciplinario e integrar control metabólico, desbridamiento, descarga de presión, valoración vascular y tratamiento antimicrobiano cuando exista infección clínica (Boulton & Rayman, 2020).

La administración sistémica de antibióticos puede verse limitada por la perfusión deficiente del tejido y por las características del microambiente infeccioso. Por ello, los sistemas de liberación local y controlada se investigan como estrategias complementarias para mantener concentraciones terapéuticas en la lesión y reducir la exposición sistémica innecesaria(Aparicio-Blanco et al., 2024; Choi et al., 2023; Gao et al., 2018).

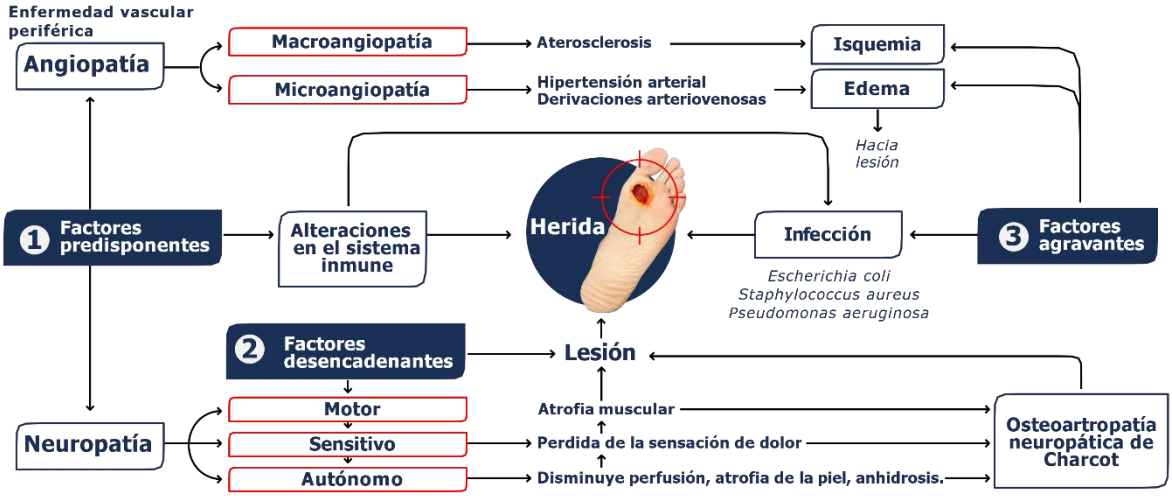

***Figure 1**. Factores predisponentes, desencadenantes y agravantes relacionados con el desarrollo y progresión de las úlceras del pie diabético infectadas.*

1.5 Sistemas de liberación controlada de fármacos

1.5.1 Conceptos generales y clasificación

Los sistemas de liberación controlada de fármacos son plataformas farmacéuticas diseñadas para modular la forma en que un principio activo se libera y alcanza el organismo o un sitio terapéutico específico (Langer & Peppas, 2003). A diferencia de las formulaciones de liberación inmediata, estos sistemas buscan regular la velocidad, duración, localización o condición de liberación del fármaco, con el propósito de mantener concentraciones terapéuticas más estables, reducir fluctuaciones entre niveles subterapéuticos y potencialmente tóxicos, y mejorar la relación entre eficacia y seguridad (Adepu & Ramakrishna, 2021; Liechty et al., 2010; Uhrich et al., 1999). Aunque los términos liberación sostenida, prolongada y controlada suelen emplearse de manera cercana, la liberación controlada implica un mayor grado de diseño sobre la cinética, el sitio o el estímulo que regula la salida del fármaco desde una matriz o vehículo (Adepu & Ramakrishna, 2021; Kamaly et al., 2016).

Estos sistemas pueden clasificarse según su perfil temporal, arquitectura, material, escala o vía de administración. De acuerdo con el perfil de liberación, pueden ser

sostenidos, prolongados, retardados, pulsátiles o activados por estímulos como pH, temperatura, actividad enzimática, potencial redox o biomoléculas específicas adep(Adepu & Ramakrishna, 2021; Kamaly et al., 2016; Li & Mooney, 2016). Según su arquitectura, incluyen sistemas tipo matriz, reservorio y sistemas particulados como microesferas, nanopartículas, nanocápsulas, micelas, liposomas y dendrímeros, cuya composición y estructura influyen en la estabilidad, distribución y cinética de liberación (Kamaly et al., 2016; Liechty et al., 2010). Desde el punto de vista del material, pueden ser poliméricos, lipídicos, inorgánicos, híbridos o basados en biomateriales; entre ellos, los sistemas poliméricos destacan por la posibilidad de ajustar su composición, degradabilidad, porosidad, entrecruzamiento, funcionalización y respuesta a estímulos (Kamaly et al., 2016; Uhrich et al., 1999).

En aplicaciones antimicrobianas, las plataformas locales como partículas, hidrogeles, apósitos, membranas o matrices poliméricas son de interés porque pueden incrementar la concentración del antibiótico en el sitio de infección, prolongar su exposición y reducir la exposición sistémica innecesaria (Aparicio-Blanco et al., 2024; Choi et al., 2023; Gao et al., 2018; Wassif et al., 2021). No obstante, su desempeño depende de la interacción entre el material, el fármaco, la arquitectura del sistema y las condiciones del microambiente infectado, como pH, exudado, actividad enzimática, biopelículas y estado del tejido (Choi et al., 2023; Ciofu et al., 2022; Kamaly et al., 2016).

1.5.2 Ventajas terapéuticas de los sistemas de liberación controlada de antimicrobianos

Los sistemas de liberación controlada de antimicrobianos ofrecen diversas ventajas terapéuticas frente a las formas de administración convencionales, principalmente al permitir una liberación más sostenida y dirigida del principio activo. Estas plataformas pueden contribuir a mantener concentraciones terapéuticas adecuadas durante periodos prolongados, aumentar la disponibilidad del fármaco en el sitio de infección y disminuir la exposición sistémica. Asimismo, pueden reducir la frecuencia de administración, proteger al antimicrobiano frente a procesos de

degradación e incorporar propiedades funcionales adicionales. En la **Tabla 1** se resumen las principales ventajas terapéuticas asociadas con estos sistemas.

Table 1*. Principales ventajas terapéuticas de los sistemas de liberación controlada de antimicrobianos*

	Ventaja terapéutica
Control de la concentración terapéutica	Mantienen niveles más estables del fármaco y reducen fluctuaciones entre concentraciones subterapéuticas o potencialmente tóxicas.
Menor frecuencia de administración	Pueden reducir el número de dosis necesarias y favorecer la adherencia al tratamiento.
Mayor disponibilidad local	Incrementan la concentración del fármaco en el sitio de acción, especialmente en infecciones localizadas.
Menor exposición sistémica	Disminuyen la distribución hacia tejidos no blanco y pueden reducir efectos adversos.
Contacto antimicrobiano prolongado	Mantienen el antibiótico por más tiempo en el sitio infeccioso, favoreciendo su interacción con las bacterias.
Protección del fármaco	Pueden proteger moléculas sensibles frente a degradación química o biológica.
Propiedades funcionales adicionales	Permiten incorporar características como biodegradabilidad, bioadhesión, respuesta a estímulos o modificación superficial.

(Adepu & Ramakrishna, 2021; Aparicio-Blanco et al., 2024; Choi et al., 2023; Gao et al., 2018; Kamaly et al., 2016; Li & Mooney, 2016; Liechty et al., 2010; Tamma et al., 2017; Versey et al., 2021)

1.6 Aplicaciones biomédicas de los sistemas poliméricos de liberación de fármacos

Los sistemas de liberación controlada han sido explorados en diversas áreas biomédicas, incluyendo oncología, enfermedades cardiovasculares, vacunación, terapia hormonal, enfermedades inflamatorias, regeneración tisular, analgesia, terapia génica y tratamiento de infecciones (Adepu & Ramakrishna, 2021). Su utilidad depende de la necesidad terapéutica específica, como prolongar la exposición al fármaco, dirigirlo hacia un sitio determinado, disminuir la toxicidad sistémica o responder a condiciones del microambiente biológico (Kamaly et al., 2016; Li & Mooney, 2016).

En enfermedades infecciosas, estas plataformas se han estudiado para mejorar la administración de antibióticos, antifúngicos y otros agentes antimicrobianos, particularmente en infecciones persistentes, localizadas o asociadas con biopelículas (Aparicio-Blanco et al., 2024; Choi et al., 2023). Sistemas como nanopartículas, liposomas, micropartículas, hidrogeles, películas, apósitos y matrices poliméricas pueden incrementar la concentración local del agente terapéutico, modular su liberación y prolongar su permanencia en el sitio afectado (Choi et al., 2023; Wassif et al., 2021). Esto resulta relevante en heridas crónicas, infecciones cutáneas, osteomielitis e infecciones asociadas a implantes, donde el microambiente puede presentar exudado, variaciones de pH, hipoxia, inflamación persistente, tejido necrótico y biopelículas (Ciofu et al., 2022; Goswami et al., 2023; Versey et al., 2021).

Dentro de estas plataformas, los polímeros tienen un papel central por su versatilidad química, estructural y funcional (Langer & Peppas, 2003; Liechty et al., 2010; Uhrich et al., 1999). Pueden diseñarse como matrices, membranas, hidrogeles, micropartículas, nanopartículas, fibras, películas o implantes, ajustando propiedades como composición, masa molecular, porosidad, degradabilidad, funcionalización superficial y grado de entrecruzamiento (Kamaly et al., 2016; Li & Mooney, 2016). La liberación del fármaco puede depender de difusión, hinchamiento, erosión, degradación o interacciones fisicoquímicas entre el fármaco y el material. Por ello, su diseño debe considerar simultáneamente la estabilidad, solubilidad y actividad del agente terapéutico, así como la biocompatibilidad del

polímero y su desempeño en el sitio de aplicación (Adepu & Ramakrishna, 2021; Aparicio-Blanco et al., 2024; Choi et al., 2023).

1.7 Polímeros de impresión molecular

1.7.1 Fundamentos de la impresión molecular

Los polímeros de impresión molecular (MIPs) son materiales sintéticos diseñados para reconocer selectivamente una molécula plantilla o compuestos estructuralmente relacionados (Belbruno, 2018; L. Chen et al., 2016). Su síntesis se basa en la polimerización de monómeros funcionales y agentes entrecruzantes en presencia de la plantilla; al retirarla, quedan cavidades con complementariedad química, espacial y funcional hacia la molécula objetivo (Belbruno, 2018; Cormack & Elorza, 2004). Debido a esta “memoria química”, los MIPs pueden actuar como receptores artificiales estables y adaptarse a distintos formatos, como partículas, películas, membranas o hidrogeles (Belbruno, 2018; L. Chen et al., 2016). En el ámbito farmacéutico, sus sitios impresos pueden favorecer la carga, retención y liberación controlada de fármacos, diferenciándolos de matrices poliméricas convencionales (Bărăian et al., 2022; Lawai et al., 2024; Liu & Poma, 2021a; Mathieu et al., 2024).

1.7.2 Componentes empleados en la síntesis de MIPs

La síntesis de polímeros impresos molecularmente requiere la selección adecuada de distintos componentes, cuya naturaleza y proporción determinan la formación de los sitios de reconocimiento y las propiedades finales del material. La molécula plantilla establece la estructura de las cavidades impresas, mientras que los monómeros funcionales participan en las interacciones responsables del reconocimiento molecular. A su vez, el agente entrecruzante aporta estabilidad a la matriz, el porógeno regula características como la porosidad y la accesibilidad de los sitios de unión, y el iniciador permite comenzar el proceso de polimerización. En la **Tabla 2** se describen las funciones principales de cada componente empleado en la síntesis de MIPs, así como algunos ejemplos generales de su aplicación.

Table 2. *Función de los componentes empleados en la síntesis de polímeros impresos molecularmente.*

Componente del proceso de síntesis	Descripción	Ejemplos
Molécula plantilla	Es el componente central de la impresión molecular, ya que define características los sitios de reconocimiento.	Analitos ambientales, fármacos, antibióticos, metabolitos o análogos estructurales de la molécula objetivo.
Monómeros funcionales	Interactúan con la plantilla durante la etapa de prepolimerización mediante interacciones covalentes, no covalentes o mixtas. Su selección depende de los grupos funcionales de la plantilla y de las interacciones deseadas.	Monómeros con grupos ácidos, básicos, neutros, hidrofílicos, hidrofóbicos, aromáticos o capaces de formar puentes de hidrógeno.
Agente entrecruzante	Proporciona rigidez y estabilidad a la matriz polimérica, conservando la estructura tridimensional de las cavidades impresas. Su proporción influye en la accesibilidad, difusión y estabilidad de los sitios de reconocimiento.	Entrecruzantes que forman redes poliméricas rígidas o semirrígidas, empleados según la aplicación del MIP.
Porógeno o solvente de polimerización	Disuelve los componentes de la mezcla de prepolimerización y contribuye a definir la porosidad, morfología, área superficial y	Solventes polares, próticos o menos competitivos, seleccionados según la

Componente del proceso de síntesis	Descripción	Ejemplos
	accesibilidad de los sitios de unión. También puede afectar las interacciones plantilla-monómero.	solubilidad de los componentes, estabilidad de la plantilla y método de síntesis.
Iniciador	Genera especies reactivas que inician la polimerización, principalmente en métodos radicalarios. Su tipo y concentración, junto con la temperatura, tiempo de reacción y presencia de oxígeno, influyen en la formación de la red, morfología y tamaño de partícula.	Iniciadores térmicos o fotoquímicos empleados en polimerización radicalaria.

(Bărăian et al., 2022; Belbruno, 2018; L. Chen et al., 2016; Cormack & Elorza, 2004; Hasanah et al., 2021a; Lawai et al., 2024; Liu & Poma, 2021a; Lusina & Cegłowski, 2022a; Naghavi et al., 2024)

1.7.3 Métodos de síntesis y propiedades fisicoquímicas de los MIPs

Los MIPs pueden sintetizarse mediante distintos métodos, como polimerización en bloque, precipitación, emulsión, suspensión, superficie, sol-gel o electropolimerización, cuya elección depende de la aplicación, morfología, tamaño de partícula y accesibilidad de los sitios impresos (Belbruno, 2018; Cormack & Elorza, 2004; Hasanah et al., 2021a). La polimerización en bloque es simple, pero genera partículas irregulares; la precipitación produce partículas más uniformes, aunque requiere mayor cantidad de solvente; y la emulsión permite controlar tamaño y morfología, pero puede implicar residuos o interferencias (Naghavi et al., 2024; Yang & Shen, 2022). Su desempeño depende de propiedades como porosidad,

carga superficial, composición química, estabilidad y grado de entrecruzamiento, que influyen en la carga, reconocimiento y liberación del fármaco (Lawai et al., 2024; Liu & Poma, 2021a).

1.8 Polímeros de impresión molecular como sistemas de liberación controlada de fármacos

1.8.1 Mecanismos de carga, retención y liberación de fármacos en MIPs

Los polímeros de impresión molecular (MIPs) han evolucionado desde materiales empleados principalmente en aplicaciones analíticas, como extracción en fase sólida, cromatografía, sensores y reconocimiento molecular, hacia plataformas con potencial en sistemas de liberación controlada de fármacos (Belbruno, 2018; Cormack & Elorza, 2004). Esta transición se sustenta en su capacidad para formar cavidades complementarias a una molécula plantilla, lo que permite no solo reconocer analitos, sino también cargar, retener y liberar moléculas terapéuticas de forma modulada (Liu & Poma, 2021a; Lusina & Cegłowski, 2022a). Estudios tempranos, como el de MIPs impresos con teofilina, mostraron mayor afinidad y liberación más sostenida frente a polímeros no impresos, apoyando el uso de cavidades impresas como sitios de retención selectiva (Andersson & Nicholls, 1997; Liu & Poma, 2021a).

En estos sistemas, la carga del fármaco puede realizarse durante la síntesis, cuando el fármaco actúa como plantilla, o posteriormente mediante adsorción en cavidades impresas y regiones no específicas de la matriz (Bărăian et al., 2022; Liu & Poma, 2021a). Las interacciones responsables pueden incluir puentes de hidrógeno, fuerzas electrostáticas, hidrofóbicas, dipolo-dipolo, Van der Waals, interacciones π-π o coordinación, dependiendo de la estructura del fármaco, los grupos funcionales del polímero y el medio empleado (L. Chen et al., 2016; Hasanah et al., 2021a; Karim et al., 2005). Sin embargo, no toda la carga corresponde necesariamente a sitios impresos, por lo que la comparación con polímeros no impresos es esencial para demostrar el efecto real de la impresión molecular (Belbruno, 2018; Ndunda, 2020).

La liberación del fármaco depende del equilibrio entre afinidad fármaco-polímero, accesibilidad de los sitios impresos, difusión, hinchamiento, erosión, degradación y condiciones del medio (Kamaly et al., 2016; Lawai et al., 2024; Li & Mooney, 2016). Factores como composición química, densidad de entrecruzamiento, porosidad, área superficial, tamaño de partícula, carga superficial, hidrofilicidad y propiedades del fármaco influyen directamente en la cinética de liberación (Lawai et al., 2024; Liu & Poma, 2021a). Además, variables experimentales como pH, fuerza iónica, temperatura, agitación y condiciones sink pueden modificar el perfil obtenido, por lo que los modelos cinéticos deben interpretarse junto con la caracterización fisicoquímica, adsorción, selectividad y actividad biológica del fármaco liberado, especialmente en aplicaciones antimicrobianas (Aparicio-Blanco et al., 2024; Choi et al., 2023; Gao et al., 2018).

1.9 Ventajas y limitaciones de los MIPs como sistemas de liberación de fármacos

Los MIPs presentan ventajas como sistemas de liberación de fármacos debido a su capacidad de reconocimiento molecular, lo que puede favorecer mayor carga, afinidad, retención selectiva y liberación modulada frente a matrices no impresas (Alvarez-Lorenzo & Concheiro, 2004; Bărăian et al., 2022; Liu & Poma, 2021a). Además, destacan por su estabilidad química y estructural, así como por la posibilidad de ajustar su composición, porosidad, hidrofilicidad y respuesta a estímulos (Belbruno, 2018; Hasanah et al., 2021a; Lawai et al., 2024). No obstante, su aplicación farmacéutica enfrenta limitaciones asociadas con heterogeneidad de sitios, remoción incompleta de plantilla, residuos de síntesis, biocompatibilidad, reproducibilidad y validación de actividad biológica del fármaco liberado (Bărăian et al., 2022; Lawai et al., 2024; Ndunda, 2020).

2. Antecedentes

2.1 Evolución de los MIPs hacia aplicaciones biomédicas

Los MIPs son materiales poliméricos diseñados para reconocer de manera preferencial una molécula determinada. Su preparación se basa en la polimerización de uno o varios monómeros funcionales en presencia de una molécula plantilla. Antes y durante la formación de la red polimérica, la plantilla establece interacciones específicas con los monómeros, mientras que un agente entrecruzante estabiliza a la matriz polimérica. Posteriormente, la plantilla se elimina y deja cavidades tridimensionales complementarias en tamaño, geometría y distribución de grupos funcionales. Estas cavidades pueden volver a unir la molécula original o compuestos estructuralmente relacionados mediante un mecanismo que suele compararse con el reconocimiento entre una llave y su cerradura (Belbruno, 2018; Haupt & Mosbach, 2000; Lusina & Cegłowski, 2022a)

La idea de generar materiales con memoria molecular se remonta a los experimentos de Polyakov de 1931 con sílice preparada en presencia de diferentes solventes. El campo fue reactivado durante las décadas de 1970 y 1980 mediante los trabajos de Wulff, Sarhan, Arshady y Mosbach. Durante varias décadas, los MIPs se utilizaron principalmente como fases estacionarias cromatográficas, sorbentes para extracción en fase sólida, elementos de reconocimiento en sensores y sustitutos sintéticos de anticuerpos (Liu & Poma, 2021a). En 1998 se demostró que un polímero impreso con teofilina podía unirla de manera selectiva al compararla con cafeína y liberarla más lentamente que un polímero no impreso, lo que constituyó uno de los primeros antecedentes directos de su uso como vehículo farmacéutico (Norell et al., 1999).

La transición de los MIPs desde aplicaciones predominantemente analíticas hacia sistemas de liberación de fármacos se ha favorecido por el desarrollo de hidrogeles impresos, nanoMIPs, materiales compatibles con medios acuosos, matrices con mayor biocompatibilidad o biodegradabilidad y sistemas sensibles a estímulos. En este contexto, los MIPs han sido investigados como alternativas que pueden mejorar la eficacia y la seguridad de los tratamientos actuales para padecimientos como

infecciones, cáncer, úlceras corneales, asma, hipertensión, enfermedad de Alzheimer, depresión, artritis reumatoide, glaucoma y hepatitis crónica (H. Chen et al., 2018; Cirillo et al., 2010; Moghadam Omranipour et al., 2015; Ruela et al., 2016; Shadabfar et al., 2020; Wu et al., 2015). Sin embargo, su traslación clínica continúa siendo limitada, debido a que una parte considerable de la evidencia disponible corresponde a estudios *in vitro* y solo un número reducido de materiales ha sido evaluado *in vivo*. Si bien la elevada estabilidad química y estructural de los MIPs constituye una ventaja para preservar los sitios de reconocimiento y controlar la liberación del fármaco, esto puede convertirse en una limitación cuando el material debe degradarse o eliminarse después de su administración (Bărăian et al., 2022; Liu & Poma, 2021a).

2.2 Aplicaciones de los MIPs en la liberación de fármacos

El uso de MIPs como sistemas de liberación de agentes antimicrobianos surge como una estrategia para mejorar la administración local y sostenida de antibióticos en infecciones donde la terapia convencional puede presentar baja disponibilidad en el sitio de acción, toxicidad sistémica o limitaciones farmacocinéticas (Aparicio-Blanco et al., 2024; Choi et al., 2023; Gao et al., 2018). En estos sistemas, el antibiótico puede emplearse como molécula plantilla durante la síntesis, generando cavidades con complementariedad parcial hacia su estructura química. Posteriormente, dichas cavidades pueden participar en procesos de recarga, retención y liberación modulada, siempre que sean accesibles y que la afinidad fármaco-polímero permita una liberación efectiva (Alvarez-Lorenzo & Concheiro, 2004; Lawai et al., 2024; Liu & Poma, 2021a). A diferencia de matrices poliméricas convencionales, cuya liberación depende principalmente de difusión, porosidad, hinchamiento, erosión o degradación, los MIPs pueden incorporar interacciones específicas como puentes de hidrógeno, interacciones electrostáticas, hidrofóbicas, dipolo-dipolo, Van der Waals o π-π (L. Chen et al., 2016; Hasanah et al., 2021a; Kamaly et al., 2016; Karim et al., 2005; Li & Mooney, 2016).

Los antibióticos son moléculas de interés para la impresión molecular debido a la diversidad de grupos funcionales presentes en fluoroquinolonas, β-lactámicos,

tetraciclinas, aminoglucósidos y glicopéptidos, lo que permite diseñar interacciones con monómeros funcionales adecuados (Hasanah et al., 2021a; Karim et al., 2005; Zhao et al., 2023). Además, los sistemas multimolde o MT-MIPs, sintetizados con dos o más plantillas, representan una estrategia potencial para la carga y liberación simultánea de fármacos, particularmente en terapias combinadas como β-lactámicos con inhibidores de β-lactamasas; sin embargo, su aplicación farmacéutica es más compleja que en análisis químico, debido a posibles diferencias de solubilidad, ionización, afinidad, estabilidad y cinética de liberación entre los componentes (Blair et al., 2014; Lawai et al., 2024; Triadenda et al., 2022; WHO, 2024).

A pesar de su potencial, los MIPs antimicrobianos enfrentan retos importantes, como biocompatibilidad, biodegradabilidad, reproducibilidad, remoción completa de la plantilla, residuos de síntesis y validación de la actividad biológica del fármaco liberado (Bărăian et al., 2022; Liu & Poma, 2021a; Lusina & Cegłowski, 2022a; Ndunda, 2020). Por ello, su desarrollo debe incluir comparación con polímeros no impresos, caracterización fisicoquímica, cuantificación individual de los fármacos, estudios microbiológicos y evaluación de seguridad, antes de considerarlos plataformas terapéuticas aplicables frente a infecciones resistentes o localizadas (Aparicio-Blanco et al., 2024; Choi et al., 2023; Lawai et al., 2024).

En un estudio que involucró un MIP con clindamicina, la interacción de la clindamicina con el MIP se evaluó mediante FTIR. Se observó que la forma y la posición de los picos de los polímeros no impresos (NIPs) eran muy similares a las de los MIPs con clindamicina. El MIP presentó cavidades de unión heterogéneas y el proceso de adsorción siguió una cinética de pseudo-primer orden. Además, la liberación de clindamicina fue significativamente más controlada en comparación con una solución control de clindamicina ($p < 0.05$), alcanzando una liberación de hasta el 77 % después de 30 horas (Parisi et al., 2024).

En otro estudio, Kempe et al. desarrollaron y evaluaron polímeros de impresión molecular para la liberación sostenida de eritromicina mediante polimerización por precipitación de radicales libres. Las isotermas de unión mostraron que los MIPs de

eritromicina presentaron una mayor capacidad de unión para este antibiótico que los correspondientes polímeros no impresos. La eficiencia de carga de eritromicina fue del 87 %. Los estudios de liberación en un tampón fisiológico indicaron una liberación inicial rápida de aproximadamente el 25 % de la eritromicina incorporada durante el primer día, seguida de una liberación del 82 % después de una semana. El perfil de liberación fue descrito de mejor manera por el modelo de Korsmeyer-Peppas (Kempe et al., 2015).

3. Justificación

Las heridas crónicas, particularmente las úlceras asociadas con diabetes mellitus, representan un problema clínico complejo debido a las alteraciones vasculares, neuropáticas, inmunológicas y metabólicas que dificultan la reparación tisular. La disminución de la perfusión sanguínea, la pérdida de sensibilidad, la inflamación persistente y el deterioro de la respuesta celular favorecen la permanencia de la lesión, incrementan la susceptibilidad a la infección y retrasan el cierre de la herida. En casos avanzados, la infección puede extenderse hacia tejidos profundos y ocasionar celulitis, abscesos, osteomielitis, sepsis y amputaciones, con consecuencias importantes sobre la movilidad, la autonomía y la calidad de vida de los pacientes.

Aunque la administración sistémica de antibióticos constituye una estrategia terapéutica fundamental, su eficacia puede verse limitada por la reducción del flujo sanguíneo periférico asociado a la diabetes mellitus. Esta condición puede impedir que el fármaco alcance concentraciones terapéuticas suficientes en el sitio infectado, lo que favorece el uso de dosis elevadas o tratamientos prolongados, aumenta la exposición sistémica y eleva el riesgo de efectos adversos. Asimismo, las concentraciones insuficientes o fluctuantes pueden contribuir a la formación de bacterias resistentes.

La administración local de antimicrobianos es una alternativa que permite incrementar la concentración del fármaco en la herida y disminuir su distribución hacia tejidos no afectados. Sin embargo, las formulaciones convencionales pueden presentar rápida difusión, eliminación o pérdida del antibiótico, reduciendo el tiempo de contacto con las bacterias y la necesidad de administración frecuente. Por ello, se requieren sistemas capaces de retener y liberar los antibióticos de manera localizada y sostenida.

Los polímeros de impresión molecular constituyen una alternativa prometedora, ya que poseen cavidades de reconocimiento específicas capaces de retener moléculas farmacológicas y modular su liberación. Su desempeño puede ajustarse mediante la selección del monómero funcional, el entrecruzante, el porógeno y el método de

síntesis. Además, presentan estabilidad química, térmica y mecánica, y pueden diseñarse con adecuada citocompatibilidad.

La incorporación individual o combinada de moléculas con actividad antimicrobiana como amoxicilina, piperacilina y tazobactam resulta de interés por su actividad frente a microorganismos asociados con heridas infectadas. En este contexto, el presente trabajo propone desarrollar y caracterizar MIPs para la liberación localizada y controlada de estos antibióticos, evaluar su adsorción, liberación, actividad antimicrobiana y citocompatibilidad, y establecer su potencial como plataformas terapéuticas para el control de infecciones en úlceras diabéticas.

4. Hipótesis

Los polímeros de impresión molecular cargados con antibióticos permiten una liberación local y controlada del fármaco, conservando su eficacia antibacteriana frente a bacterias asociadas con heridas infectadas y manteniendo un perfil de biocompatibilidad adecuado en líneas celulares humanas.

5. Objetivos

5.1 Objetivo General

Sintetizar y caracterizar polímeros de impresión molecular cargados con amoxicilina y piperacilina-tazobactam, evaluando su capacidad como sistemas de liberación local y controlada, así como su eficacia antibacteriana frente a bacterias asociadas con heridas infectadas y su biocompatibilidad en líneas celulares humanas.

5.2 Objetivos Específicos

Etapa 1

- Diseñar y sintetizar polímeros de impresión molecular y polímeros no impresos dirigidos a amoxicilina y piperacilina-tazobactam mediante el método de coprecipitación.
- Desarrollar y validar un método analítico por cromatografía líquida de alta resolución acoplada a detector de arreglo de diodos para la cuantificación de amoxicilina, piperacilina y tazobactam.
- Caracterizar las propiedades morfológicas, fisicoquímicas y de carga superficial de los polímeros sintetizados, tanto impresos como no impresos.

Etapa 2

- Determinar la cinética de liberación del sistema AMO PIP-TAZ utilizando el método de difusión en celdas de Franz, evaluando

además la influencia del pH y la presencia de múltiples moléculas cargadas en la matriz polimérica sobre el perfil de liberación.

- Evaluar la actividad antimicrobiana de los MIPs mediante la técnica de microdilución en placa y la técnica de Miles & Misra, utilizando cepas bacterianas de referencia (ATCC) y cepas clínicas.
- Determinar el efecto citotóxico de los MIPs sobre fibroblastos dérmicos humanos mediante el ensayo colorimétrico MTT, con el fin de establecer su seguridad celular.

Manuscrito 1. *Development and evaluation of ciprofloxacin local controlled release materials based on molecularly imprinted polymers*

El presente capítulo corresponde al manuscrito en su versión previa a la publicación del artículo titulado *"Development and evaluation of ciprofloxacin local controlled release materials based on molecularly imprinted polymers"*. Publicado en la revista *European Journal of Pharmaceutics and Biopharmaceutics*.

Galván-Romero, V., Gonzalez-Salazar, F., Vargas-Berrones, K., Alcantara-Quintana, L. E., Martinez-Gutierrez, F., Zarazua-Guzman, S., & Flores-Ramírez, R. (2024). Development and evaluation of ciprofloxacin local controlled release materials based on molecularly imprinted polymers. *European Journal of Pharmaceutics and Biopharmaceutics*, *195*, 114178. doi.org/10.1016/j.ejpb.2024.114178

Development and evaluation of ciprofloxacin local controlled release materials based on molecularly imprinted polymers.

Abstract

The aim of this study was the molecular imprinting polymers (MIPs) assessment as a controlled release system of ciprofloxacin. The MIPs synthesis was performed by three different methods: emulsion, bulk, and co-precipitation. Lactic acid (LA) and methacrylic acid (MA) were used as functional monomers and ethylene glycol dimethacrylate as crosslinker. Also, nonimprinted polymers (NIPs) were synthesized. MIPs and NIPs were characterized by scanning electron microscopy, Fourier Transform Infrared Reflection, specific surface area, pore size, and release kinetics. Their efficiency against *Staphylococcus aureus* and *Escherichia coli*, and their cytotoxicity in dermal fibroblast cells were proven. Results show that MIPs are mesoporous materials with a pore size between 10-20 nm. A higher adsorption with the co-precipitation MIP with MA as a monomer was found. The release kinetics proved that a non-Fickian process occurred and that the co-precipitation MIP with LA presented the highest release rate (90.51 mg L^{-1}) in 8 hours. The minimum inhibitory concentration was found between 0.031-0.016 mg L^{-1} for *Staphylococcus aureus* and between 0.004-0.031 mg L^{-1} for the *Escherichia coli*. No cytotoxicity in cellular cultures was found; also, cellular growth was favored. This study demonstrated that MIPs present promising properties for drug administration and their application in clinical practice.

Keywords: Molecularly imprinted polymers; controlled delivery; minimum inhibitory concentration; ciprofloxacin

1. Introduction

The skin is the largest organ in the human body, acting as a protective barrier against noxious agents [1]. Damage caused by trauma alters its integrity and makes it susceptible to the growth of microorganisms that may aggravate the situation of immunosuppressed patients with diseases such as diabetes mellitus, arterial disease, and vasculitis; it also, prolongs the patient's healing process due to subjacent factors such as cellular senescence, inflammation, and ischemia, which interfere with healing [2].

The treatment of wounds with healing problems is performed by mechanical methods such as debridement, and topical or oral application of antimicrobial agents. However, debridement presents complications such as bleeding and pain and favors the development of infections [3]. In addition, the use of systemic antibiotics increases the risk of antimicrobial resistance, dysbiosis in the intestinal microbiota, and biofilm formation due to poor distribution at the wound site because of the pathophysiological conditions of the patient that prevent the arrival of a therapeutic agent to the wound [4, 5].

The most commonly used antibacterial agents for skin infections include fluoroquinolones such as ciprofloxacin (CPX)[6]. This compounds show an extensive antibacterial activity against *Escherichia coli* and *Staphylococcus aureus*, which are the most common bacteria responsible for wound infections[7]. Moreover, was approved in 1987 by the Food and Drug Administration and it is approved for the treatment of skin infections [8]. Therefore, CPX could be used for its local treatment increasing its safety and efficacy.

Topical cutaneous delivery of antibiotics has several advantages over oral delivery: they are non-invasive, easily accessible, self-administered, long-term release, low cost, and improve patients' health [9]. The current and successful delivery methods have a molecular mass of hundreds of Daltons, a high octanol-water partition coefficient, and require milligram doses [10]. The delivery strategy of a drug is vital to achieve efficiency; drug delivery systems (DDS) have been extensively studied and have experienced rapid growth in recent decades. These materials must have

a controlled release rate over an extended time, present biocompatibility, and not release toxic compounds.

Molecularly Imprinted Polymers (MIPs) are a current approach to drug delivery and are synthetic receptors with specific recognition sites for template molecules used for drug delivery in wounds due to their mechanical resistance and biocompatibility [11-13]. In recent studies, MIPs have been used for development in the design of DDS. Selective recognition of MIPs is determined during the polymer preparation using the appropriate monomers for the specific molecule [12]. Furthermore, in the non-covalent molecular imprinting approach, the functional monomer is chosen to provide non-covalent interactions with the template. The molecular imprinting technique involves template, functional monomer and crosslinker dissolved in a suitable solvent resulting in a highly crosslinked polymer due to the formation of the bonds between the template and the monomer during the synthesis process [13, 14]. Monomers such as methacrylic acid and lactic acid have been widely used in the development of DDS due to their biocompatibility [15]. MIPs offer some advantages that make them suitable devices, such as biocompatibility, low toxicity, biodegradability, low cost, and easy preparation [16]. Thus, the objective of this study was to synthesize, characterize and evaluate MIPs as ciprofloxacin delivery device. Also, to evaluate their efficiency and safety through minimum inhibitory concentration assays of common bacteria in wounds and with cytotoxicity in dermal fibroblast cells.

2. Materials and Methods

2.1. Materials

The following reagents were used for the MIPs and NIPs synthesis: lactic acid (LA), methacrylic acid (MA), ethylene glycol dimethacrylate (EDGMA), azobisisobutyronitrile (AIBN), polyvinyl alcohol (PVA), lauryl sulfate (SDS) and ciprofloxacin (CPX). All reagents were purchased from Sigma-Aldrich (Darmstadt, Germany). The organic solvents used were methanol and acetonitrile, purchased from Tedia Company Inc. (Fairfield Ohio, EE. UU). Chlorohydric acid (HCl) and orthophosphoric acid were purchased from Merck (Edo. De México).

2.2. Synthesis of molecularly imprinted polymers

The polymer synthesis was carried out with slight modifications based on previous work performed by our research group [17] using three non-covalent polymerization methods.

(i) Emulsion polymerization. First, 1.55 g of PVA and 0.1079 g of SDS were dissolved in 75 mL of hot water in a 100 mL flask with stirring at 200 rpm under nitrogen atmosphere (99.9% purity) with a hermetic seal. The polymerization mixture was prepared using the template molecule (CPX); the functional monomer (LA and MA) was dissolved in a 1:4 ratio using methanol as porogen, EDGMA as crosslinker, and AIBN as initiator. The polymerization mixture was added through a septum to the flask with the PVA and SDS. This mixture was kept at constant temperature (70°C) in a glycerin bath with steady stirring (100 rpm) for 24 h. Finally, polymers were washed with hot water (95 °C) to remove PVA and SDS residues.

(ii) Bulk polymerization. The template (CPX) was mixed with the functional monomer (LA and MA) in a 1:4 molar ratio (template: monomer), 5 mL of methanol as porogen, EDGMA as crosslinker, and AIBN as initiator. The reaction was carried out under a nitrogen atmosphere without stirring and in a glycerin bath at 70°C for 24 h. The obtained polymers were crushed in a mortar.

(iii) Co-precipitation polymerization. The same procedure and reaction conditions of the bulk polymerization were followed, but with an excess of porogen (25 mL) and magnetic stirring (100 rpm) in a glycerin bath at 70°C for 24 h.

NIPs for each synthesized polymer were also obtained and prepared under the same conditions as their corresponding MIPs. The analyte was removed before their characterization in the scanning electron microscopy and infrared spectroscopy, as well as the determination of the imprinting factor, the adsorption isotherms, the surface charge distribution, and the zero-charge point. The removal was performed by washing the MIPs ten times with 10 mL of methanol in an HCl solution of 0.1% (0.1 N), followed by sonication for 10 min and centrifuged for 10 min at 2000 rpm.

2.3. CPX determination by HPLC-FLD

The determination of CPX in the samples was performed using high-performance liquid chromatography coupled to a fluorescence detector (HPLC-FLD) (Agilent ®

1260 Infinity Series) with a Zorbax SB C18 (4.6 x 150 mm, 5 µm) column. The mobile phase consisted of 65% orthophosphoric acid (pH 3.4) and 35% of methanol at an isocratic flow rate of 0.6 mL min-1 with a processing time of 7 min. The sample volume was 10 µL, and the FLD wavelength was 278 nm and 455 nm of excitation and emission, respectively.

Method validation was performed following the guidelines for the validation of analytical methods for the determination of organic compounds at trace level, evaluating the detection (LOD) and quantification (LOQ) limit, linearity (R^2), sensitivity and precision. The linearity expressed by the correlation coefficient (R^2) and the sensitivity determined by the slope were determined by calculating the average of seven curves recorded for three days (3 for repeatability and 4 for reproducibility). The LOD was calculated using the equation: $LOD = X + 3SD_{blank}$(1) Where X is the concentration and SD is the standard deviation of the blank, and the LOQ was determined as follows: $LOQ = X + 10SD_{blank}$. (2)

2.4. Morphological characterization of MIPs/NIPs

The MIPs and NIPs micrographs were obtained using scanning electron microscopy with an FE-SEM system model Inspect F50, to evaluate their surface and morphology. The previous deposition of a gold thin film on each sample was performed with a Bal-TecÒ equipment model MED 020 using the sputtering technique. Each sample remained for 10 s in the equipment to ensure the formation of a 10 nm thick layer.

The analysis of the samples was carried out using an Everhart-Thornley (ETD) detector in secondary electron mode (SE), a voltage of 30kV, 0.17 nA, and 85 pA. The parameters considered were the magnification (x), the horizontal field width (DFW), and the working distance (WD).

2.5. Infrared Spectroscopy

The functional groups of the materials were evaluated using Attenuated Total Reflection Fourier-transform Infrared Spectroscopy (ATR-FTIR) (Thermo

Scientific®, model Nicolet iS10). The infrared spectra were obtained in a spatial range from 500 to 4000 cm^{-1}.

2.6. Specific area and pore diameter

The texture of the materials was determined by measuring the nitrogen adsorption-desorption at 77 K using an automatic adsorption instrument (Autosorb-IQ, Quantachrome Instrument Corp., Boynton Beach, FL, USA). The specific surface area (S_{BET}) was calculated with the Brunauer Emmett Teller (BET) method. On the other hand, the method Barrett, Joyner, and Halenda (BJH) was used to determine the pore size distribution.

2.7. Surface charge distribution and zero charge point

The MIPs and NIPs surface charge was determined by the acid-base titration proposed by Kuzin y Loskutov [18]. Fifty mL of a neutralizing solution (pH 2-12) was prepared. Twenty-five mL of this mixture was added to 0.1 mg of MIP or NIP in a centrifuge tube. In addition, 25 mL of each solution was used as blanks. It was shaken every 30 min for two hours. Finally, the pH was evaluated, and the potentiometric curves of the blank and the adsorbent were plotted.

The Zero Charge Point (ZCP) is the intersection between de potentiometric curves with the MIP or NIP solution and the blank. The surface charge distribution was calculated by plotting the potentiometric curves for the adsorbent and the blank. By graphical representation, the HCl volume was considered negative, and the NaOH volume was positive. The blank and adsorbent volumes were plotted at different pH values. The surface charge was determined with the following equation:

$$C_s = [C_N(V_B - V_A)/m] F \quad (3)$$

Where C_s is the adsorbent Surface charge at a specific pH value (C g^{-1}), C_N is the concentration of the neutralizing solution (mol L^{-1}), V_A is the volume of the NaOH or HCl (0.1 N) used to reach the specific pH using the adsorbent (L), V_B of the NaOH or HCl (0.1 N) used to reach the specific pH without the adsorbent (L), m is the MIP or NIP mass (g), and F is the Faraday constant (96485 C mol^{-1}).

2.8. Adsorption isotherms

The adsorption isotherms were performed to characterize the adsorption of CPX on the polymer surface using concentrations between 1-90 mg L^{-1} of CPX at 24°C. The equilibrium adsorption capacity q, (mg g^{-1}) was calculated using the following equation:

$$q_e = [(C_0 - C_e)V]/W \quad (4)$$

Where Co (mg L^{-1}) and Ce (mg L^{-1}) are the initial and equilibrium concentrations of the adsorbent, respectively. V (L) is the stock solution volume, and W (g) is the weight of the polymer used.

The equilibrium data obtained were fitted to the Langmuir, Freundlich and SIPS adsorption isotherm models to describe the interaction between adsorbent and adsorbate [19]. The Langmuir isotherm model is shown in the following equation:

$$q = (Kq_mC)/(1 + KC) \quad (5)$$

Where C (mg L^{-1}) is the concentration of the adsorbate at equilibrium, qm (mg L^{-1}) is the maximum adsorption capacity, and K (L mg^{-1}) is the affinity constant related to the adsorption energy.

The Freundlich isotherm model is presented in the following equation:

$$q = kC^{\frac{1}{n}} \quad (6)$$

Where k ($mg^{1-1/n}$ $L^{1/n}$ g^{-1}) is the adsorption capacity of the adsorbent and the constant n indicates the adsorption intensity, a value of n > 1.0 represents a favorable adsorption condition.

Finally, the SIPS isotherm model is described in the following equation:

$$q = (N_taC^m)/(1 + aC^m) \quad (7)$$

This model includes the characteristics of the Langmuir and Freundlich models, where a is the isotherm constant.

The software Statistica® (version 7.0) was used to fit the experimental data to the math models, and the model with the best correlation coefficient (R^2) was chosen for the following analysis.

2.9. Imprinting factor

To verify the selectivity of the MIPs against the template for the different functional monomer, a concentration of 5 mg L^{-1} of CPX was prepared in pH 6 milli-Q water. One mL was then passed through each of the MIPs following the isothermal assay methodology. Similarly, the NIPs were analyzed to be compared with their corresponding MIP.

The specificity of the MIPs and NIPs was estimated by the partition coefficient of CPX between the polymer and the solution. The partition coefficient was calculated by the following equations:

$$K = q_e/C_0 = q_e/\{C\,[1 - (\%R/100)]\} \quad (8)$$

$$\%R = \,[(C_0 - C)/C_0]100\% \quad (9)$$

where C_0 (mg L^{-1}) is the amount of analyte bound to the MIP or NIP, C (mg L^{-1}) is the concentration of each analyte remaining in the loading eluent, q_e is the amount of adsorbate bound to the adsorbent at equilibrium and $\%R$ in retention percentages. Also, the imprinting factor (IF) was used to evaluate the selectivity of each MIP against the template for which it was synthesized in the presence of the other NIPs similar in structure. The IF was calculated with the following equation:

$$IF = K_{MIP}/K_{NIP} \quad (10)$$

where K_{MIP} and K_{NIP} represent the partition coefficients of the compounds under study for the MIP and NIP, respectively.

2.10. Release kinetics

In vitro diffusion assays were performed to establish the release kinetics of the CPX linked to the MIPs during the synthesis. Every experiment was carried out at 37°C ± 0.5 °C in a diffusion Franz cell using polyvinyl difluoride (PVDF) filter paper with 700 mg of MIP corresponding to 20 mg of CPX The filter paper, previously soaked with the receptor medium, was placed between the donor and receptor cell compartments. Then, both chambers were fixed, and the receptor compartment was filled with 20 mL of phosphate buffer (pH 5.4) to simulate physiological skin conditions [20-22]. Finally, the samples were collected from the receptor compartment at different times (0, 0.25, 0.5, 1, 2, 3, 4, 5, 6, 7, and 8 h), and a new

phosphate buffer was added for further analysis (HPLC-FLD). Experiments were performed five times for each synthesized MIP.

The release profiles were fitted according to the Higuchi and Korsmeyer-Peppas equation:

$M_t = kt^{1/2}$ (11)

Where M_t is the quantity of drug release at a specific time *t*, and *k* is a constant.

$M_t/M_\infty = Kt^n M_t$ (12)

Where Mt is the fraction of the released drug at a time t, k is the diffusion constant $M\infty$, and n is the release exponent. The exponent n describes the release mechanism. In the quasi-Fickian diffusion, the value n < 0.5, and in the Fickian diffusion, *n* = 0.5. The drug fraction is proportional to the square root of time, and the drug diffusion is controlled by the diffusion itself. When n = 1, the equation corresponds to the zero-order model. Values for n between 0.5 and 1 express an anomalous process with input from different phenomena such as an ion exchange, and polymer chain relaxation, among others [23, 24].

2.11. Antimicrobial activity

The antimicrobial activity was evaluated using microdilution method to determine the minimum inhibitory concentration (MIC). This method was previously validated using reference strains from the American Type Culture Collection (ATCC) collection (*Staphylococcus aureus* ATCC 25923 and *Escherichia coli* ATCC 25922). Cut-off points were confirmed according to the Clinical and Laboratory Standards Institute (CLSI). The evaluations were carried out in five repetitions on three different days.

The antimicrobial activity of the polymers on two representative microorganisms was carried out. Gram-positive *S. aureus* ATCC 25923 and Gram-negative *E. coli* ATCC 25922 were evaluated. The strains of the microorganisms were kept in Mueller Hinton solid medium (211443, BBLTM). Both strains were incubated in a 96-well microplate in a humidified atmosphere with 5% CO_2 for 24 h. The microorganisms were exposed to different concentrations of MIPs and NIPs. The absence of turbidity in the well evidenced the final point. Experiments were performed in quintupled for

each MIP. The antimicrobial activities of the polymers were compared to analytical grade ciprofloxacin and to the range reported by the CLSI.

2.12. Cytotoxicity

The cytotoxicity of the polymers in dermal fibroblasts (HDFn) (PCS- 201-010) was assessed. The cells were kept in Dulbecco's modified Eagle's medium (DMEM, 30-2002 ATCC), supplemented with fetal bovine serum at 10% (v/v) (1600.036, Gibco) and penicillin-streptomycin at 1% (v/v) (13377820, ROCHE). The preparation was maintained at 37°C in a humified atmosphere of 5% CO_2 for 24 h. The cells ($1x10^4$ cells/well) were cultured in 96-well microplates.

Cell viability assays were carried out by metabolic reduction of resazurin to highly fluorescent resorufin (alamarBlue, Invitrogen) estimating the viable cells present.

The cells were treated with polymeric extract obtained in PBS for 24, 48, and 72 h. After incubation, 100 µL of alamarBlue was added to each well. After 4 h, absorbance was measured at 570 nm using a microplate reader (Multiskan FC, Thermo Scientific). Cells with DMEM medium were used as negative control and cells with hydrogen peroxide as positive control. Experiments were carried out in quintuplicate, and the viability percentage was calculated using the positive control as 100%. ANSI/AAMI/ISO 10993-5:2009 (R2014) Biological Evaluation of Medical Devices – Part 5: Tests For In Vitro Cytotoxicity.

2.13. Statistical analysis

Data normality tests were performed using Shapiro-Wilk, and parametric tests of inferential statistics were applied using analysis of variance (ANOVA) and Dunn´s *post hoc* test.

3. Results and discussion

Six MIPs and 6 NIPs were synthesized (**Table 1**), obtaining approximately 3 g of polymer. The analytic method for CPX quantification was validated. A linear range of 0.8-3.50 mg L^{-1} was achieved, with a linearity of 0.99 and a sensitivity of 254.1 (IC

95 %: 237.6 – 270.7), the LOD and LOQ were calculated by the slope method obtaining 0.39 and 0.82 mg L^{-1}, respectively.

Table 1. Code of the MIPs and NIPs synthesized for CPX.

Code	Polymer	Monomer	Polimerization method
M-LA-E	MIP	Lactic acid	Emulsion
N-LA-E	NIP	Lactic acid	Emulsion
M-MA-E	MIP	Methacrylic acid	Emulsion
N-MA-E	NIP	Methacrylic acid	Emulsion
M-LA-B	MIP	Lactic acid	Bulk
N-LA-B	NIP	Lactic acid	Bulk
M-MA-B	MIP	Methacrylic acid	Bulk
N-MA-B	NIP	Methacrylic acid	Bulk
M-LA-C	MIP	Lactic acid	Co-precipitation
N-LA-C	NIP	Lactic acid	Co-precipitation
M-MA-C	MIP	Methacrylic acid	Co-precipitation
N-MA-C	NIP	Methacrylic acid	Co-precipitation

MIP Molecular imprinting polymer, NIP non-molecular imprinting polymer

Figure 1 shows the bond formed between the monomers (LA and MA) with the CPX at acidic pH. The carboxylic group in both molecules (-COOH) can effectively interact with acceptors and donors through hydrogen (H) or electrostatics bonds in the CPX structure. The carboxylic group acquires a negative charge and the ability to establish ionic bonds due to the loss of an H atom. In addition, the oxygen atom can accept a hydrogen atom and form bonds with H donors. The non-ionized hydroxyl group present in the MA (-OH) is an H donor; therefore, it can interact with an H acceptor. Due to the presence of three amino groups, a carbonyl, and a carboxylic acid in the CPX structure, it can easily act as a hydrogen bond donor and acceptor. Also, the monomers can form ionic bonds during the printing process [23].

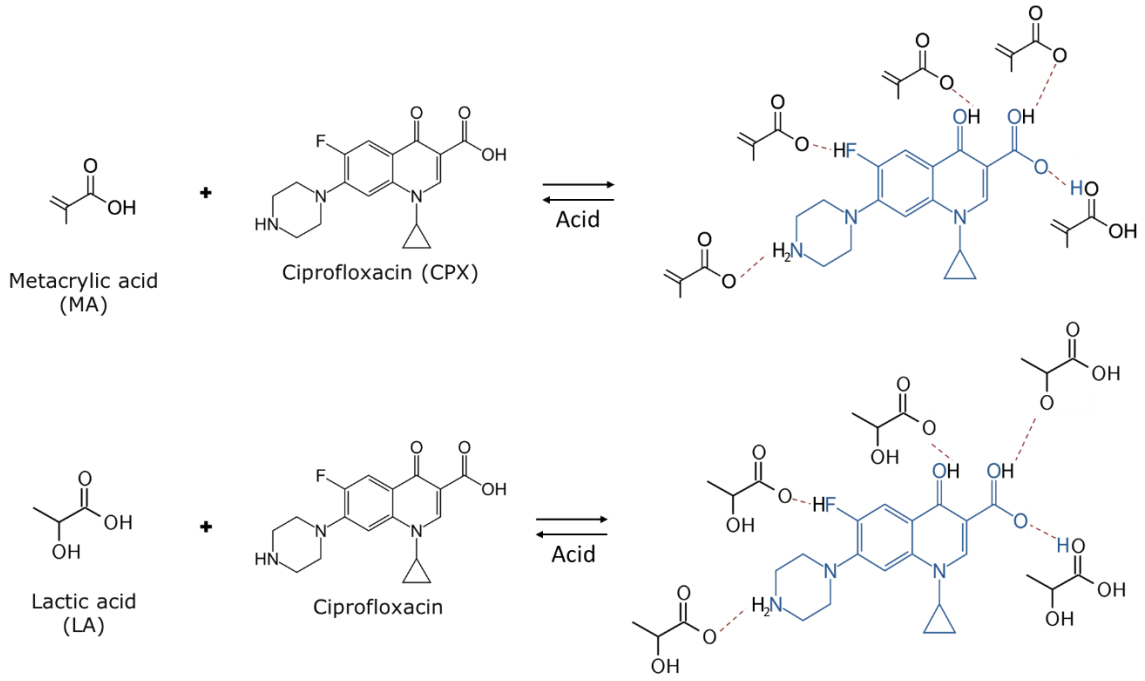

Figure 1. Proposed reaction scheme for the generation of interactions between the functional monomer (LA or MA) and the template molecule (CPX), acidic pH.

The polymer morphology was examined with a SEM showing different morphologies for each polymer. The surface of the spherical particles is formed by a polymeric network of the functional monomer and the cross-linker. The MIP emulsion with MA (**Figure 2**) presents an irregular morphology; when compared with its homologue without the drug, spherical particles with different sizes (approximately 5 µm) are observed. On the other hand, the MIP with LA as monomer showed spherical particles with a wide range of sizes (the largest being approximately 1 µm in diameter), and its corresponding NIP with particle sizes of 10 µm. The emulsion synthesis method is performed using two solutions: the polymerization mixture and the surfactant solution. The surfactant, under constant agitation, forms fine drops of polymerization mixture in the interphase, achieving spherical polymers. The drop size can be modified with the stirring rate, the surfactant concentration, and its nature [25].

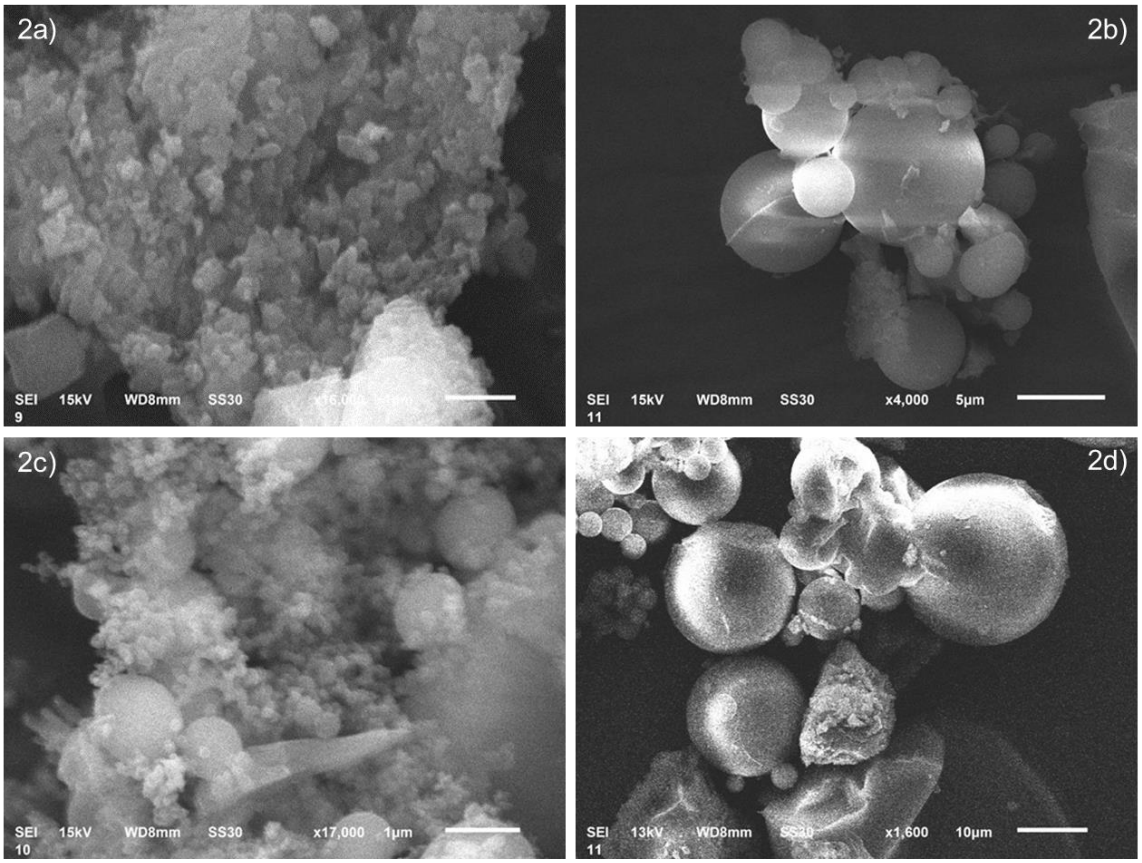

Fig. 2. Scanning electron microscope images for polymers made by the emulsion method 2a) M-MA-E, 2b) N-MA-E, 2c) M-LA-E and 2d) N-LA-E.
M, Molecular imprinting polymer; N, non-imprinting polymer; MA, methacrylic acid; LA, lactic acid and E, emulsion.

The polymers synthesized by the co-precipitation method, with MA as monomer (**Figure 3**), showed agglomerated particles with irregular morphology. On the other hand, MIPs with LA as monomer showed spherical morphology, even when agglomerates were present. Their homologues without CPX presented agglomerated and irregular particles. This synthesis method uses large quantities of solvent; therefore, the analyte concentration is low, and the polymer grows independently, Consequently, the bond between the functional monomer and the template presents better separation, allowing its former release. The precipitate obtained is loose and uniform, so it does not require grinding, resulting in a greater homogenization in its morphology [25].

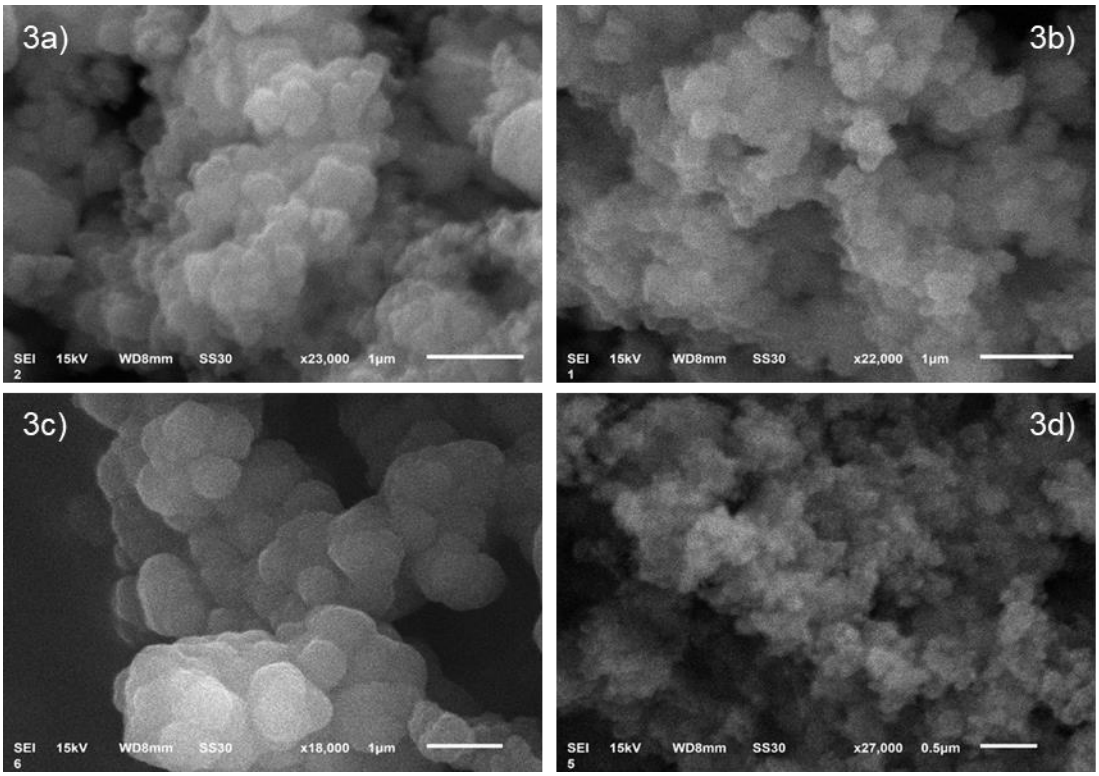

Fig. 3. Scanning Electron Microscope images for polymers made by the co-precipitation method 3a) M-MA-C, 3b) N-MA-C, 3c) M-LA-C and 3d) N-LA-C.
M, Molecular imprinting polymer; N, non-imprinting polymer; MA, methacrylic acid; LA, lactic acid; C, co-precipitation.

MIPs synthesized by the bulk method with MA as monomer (**Figure 4**) presented agglomerated spherical particles with a size of approximately 1 µm. Their respective NIPs were concentrated into smaller particles. MIPs with LA as monomer showed agglomerated spherical particles (<1 µm). The particles of the NIPs were agglomerated without a defined morphology. This behavior is due to the lack of agitation. The polymer obtained requires grinding, which may result in the alteration of the MIP structure, forming MIPs with irregular morphology and sizes [25].
The presence of CPX in the polymeric matrix during the synthesis, may interfere with the polymer morphology due to particle size deviation while being synthesized by the same method. This process has been previously described, and this

phenomenon occurs due to chemical interactions between the template and the monomer [26].

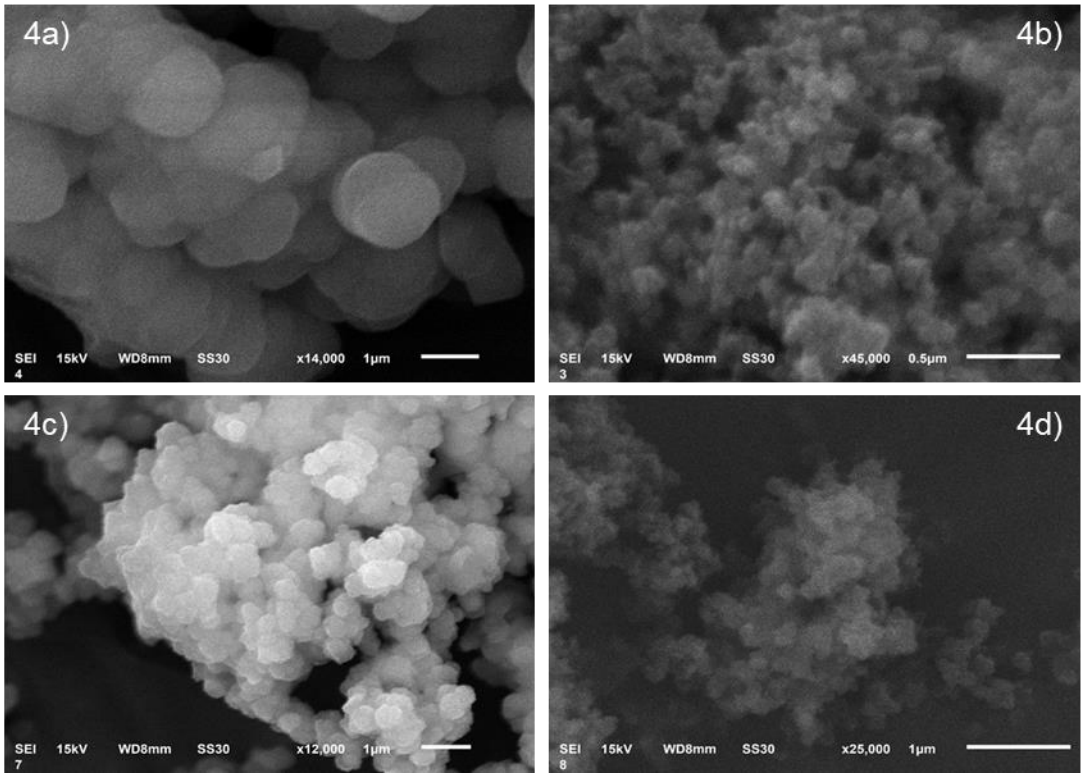

Fig. 4. Scanning Electron Microscope images for polymers made by the bulk method 4a) M-MA-B, 4b) N-MA-B, 4c) M-LA-B and 4d) N-LA-B.
M, Molecular imprinting polymer; N, non-imprinting polymer; MA, methacrylic acid; LA, lactic acid; B, bulk.

The specific area and the average pore diameter of the MIPs and NIPs were calculated using the BET and BJH methods. **Table 2** shows the results of the specific area in the range of 127 a 318 m^2 g^{-1}, which means that MIPs and NIPs are high porosity materials. Also, the pore diameters evidenced that all materials are mesoporous [27]. The specific area of the MIPs is smaller than that of NIPs because of the effectiveness of the template imprinting [28]. In addition, MA as the functional monomer improves pore formation because the diameter values are higher than those obtained with LA.

Table 2. *Textural properties of MIPs and NIPs.*

Parameters	SBET (m^2/g)	VP (cm^3/g)	Dp (nm)
M-MA-C	127	0.145	10.118
M-MA-B	410	0.922	12.714
M-MA-E	112	0.491	14.183
M-LA-C	155	0.049	4.354
M-LA-B	244	0.586	11.507
M-LA-E	209	0.352	9.567
N-MA-C	318	0.601	11.141
N-MA-E	403	1.452	19.858

SBET, Surface area; VP, pore volumen; Dp, pore diameter; M, Molecular imprinting polymer; N, non-imprinting polymer; MA, methacrylic acid; LA, lactic acid; C, co-precipitation.

The ATR-FTIR spectra for each polymer are shown in **Figure 5**. The CPX ATR-FTIR was characterized by a broad absorption band in the range of 3600-3000 cm^{-1} caused by the narrow vibration of n (-OH) groups. The narrow vibration of the n(C=O) bands appears near 1720 cm^{-1}, while the stretching vibration of C=C in the quinolone ring (under this range, the optical density of the deformation vibrations of the -NH bonds is light) appears near 1600 cm^{-1}. In the range of 1500-1400 cm^{-1}, the narrowing vibration of C-O groups appears, as well as the -COOC (ionized carboxyl group) vibrations. The stretching vibrations of the C-F bonds appear between 1050-1000 cm^{-1}. Therefore, the bands associated with the CPX molecule confirm that the template is imprinted.

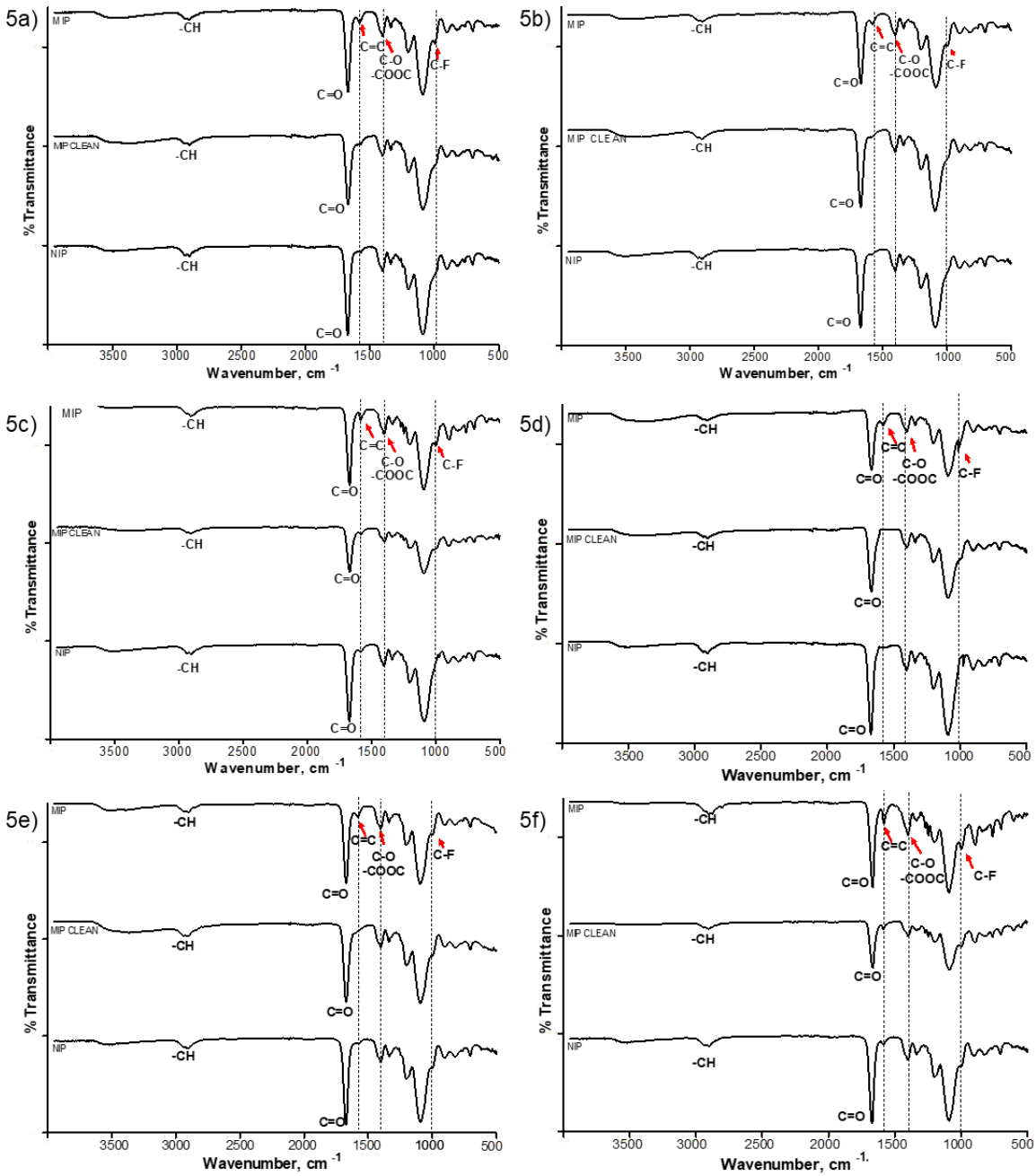

Fig. 5. Spectral ATR-FTIR 5a) M-LA-B, 5b) M-LA-C, 5c) M-LA-E, 5d) M-MA-B, 5e) M-MA-C and 5f) M-MA-E.

M, Molecular imprinting polymer; N, non-imprinting polymer; MA, methacrylic acid; LA, lactic acid; B, bulk; C, co-precipitation; E, emulsion.

Figure 6 shows the percentages of cumulative concentration obtained during the release process (8 h). During the first hour, an initial burst release was observed for the M-LA-C, M-LA-B, M-MA-E, and M-MA-B. The release increased gradually for the following 7 hours, except for the M-LA-C, where the increment was observed in the last 2 hours assessed. Differently, less than 10% of the release was reported for the polymers M-LA-E and M-MA-C during the 8 hours evaluated. The polymer made with the co-precipitation method and LA as monomer (M-LA-C) released 90.51 mg L^{-1} (45%) in 8 hours. The lowest release presented during the 8 hours of evaluation was the M-LA-E polymer with 9.1 mg L^{-1} (5%).

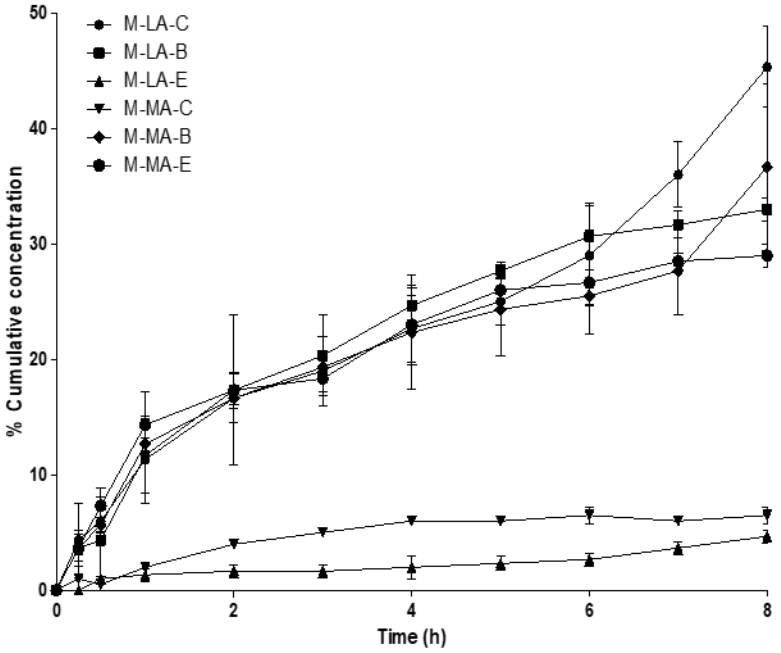

Fig. 6. Percentage of cumulative concentration release of the ciprofloxacin present in each of the MIPs. Each point represents the arithmetic mean ± SD of 5 independent experiments.

M, Molecular imprinting polymer; N, non-imprinting polymer; MA, methacrylic acid; LA, lactic acid; B, bulk; C, co-precipitation; E, emulsion.

CPX is a concentration-dependent bactericidal fluoroquinolone [29]. Therefore, it is suggested that the CPX concentration should be adequate for the elimination of microorganisms and that, in the following hours, release should be maintained, avoiding bacterial proliferation, resistance formation, and biofilm production [30]. In the release profile of CPX we can observe that this requirement is fulfilled since all MIPs have the capacity to release concentrations above the MIC reported in the CLSI, whose ranges are in μg mL^{-1}, from the first hour.

Higuchi and Korsmeyer-Peppas models were used to determine the kinetics and mechanism of CPX release. The logarithmic equation was calculated for all profiles. The value of *n*, provided information on the drug release kinetics for each MIP, giving results between 0.5 and 1 (**Table 3**). These data demonstrate that CPX release is due to the non-Fickian diffusion mechanism, which corresponds to the Korsmeyer-Peppas model.

Table 3. Kinetic data for the MIPs.

	Lactic acid			**Methacrylic acid**		
	M-LA-C	**M-LA-B**	**M-LA-E**	**M-MA-C**	**M-MA-B**	**M-MA-E**
n	0.64	0.62	0.85	0.60	0.61	0.55
K	3.00	3.00	0.38	1.47	2.96	3.04
R^2	0.9825	0.9827	0.8073	0.9597	0.9641	0.9442

M, Molecular imprinting polymer; N, non-imprinting polymer; MA, methacrylic acid; LA, lactic acid; B, bulk; C, co-precipitation; E, emulsion.

Four conventional categories of DDS are suggested: diffusion-controlled, swelling, erosion, and controlled drug release systems[31]. The release of the polymer developed in this study depends on the swelling mechanism. This behavior can be induced by pH stimulation and has been reported in monomers such as acrylic acid, MA, maleic anhydride, and N,N-dimethylaminoethylmethacrylate [32].

In this study, our results indicate that the molecule is released through a swelling-controlled mechanism depending on time and dissolution. The swelling mechanism refers to the water absorption capacity of the polymeric matrices, this property allows the drug molecule to desorb more easily by increasing the size of the binding cavities. In other words, a high degree of swelling will allow drug release at a much faster rate due to the crosslinking density of the polymeric matrix[33]. Therefore, the release profiles obtained allow us to predict that the polymer M-LA-C has a higher degree of swelling with a higher release compared to M-LA-E, indicating that, in the polymers made with LA, the emulsion method has a higher degree of crosslinking and therefore a greater control in the release compared to the co-precipitation method. In the case of MIPs synthesized with MA, the polymer made with the co-precipitation method presents lower release, demonstrating that not only the synthesis method interferes in this process but also its components.
An important point presented by the materials based on MIPs for the release, are the interactions between the molecule and the electrostatic charges that confer the functional monomers to the material, thus, we calculated the zero charge point (ZPC), this parameter indicates the pH at which the active sites are in their ionized form, in our study we obtained the ZPC of both monomers, 4.8 and 3.9 of MA and LA, respectively. This results in a pH value above these values (pH 5.4 of our solution), which will cause the active sites of the polymeric matrix to be in their ionized form releasing the CPX to the medium.
A gel-like material using a dendronized polymer loaded with CPX was developed by Garcia et al [34]. The results showed that the drug release was through a Fickian diffusion, the release was performed in different receptor media, in ultrapure water up to 8% and in NaCl 0.9% solution it was up to 50% in 24 h. The diffusion of the ionized species was prevented by the electrostatic gradient produced by the polyanion. Therefore, in NaCl solution as non-ionized species diffuse out of the complex environment, the equilibrium responds rapidly to provide fresh and free CPX [34]. Proving that the saline composition of the biological fluids would promote the release of CPX from the polymeric material.

The pH of the working solution favors the neutral molecule release in the developed materials. This behavior was verified with the surface charge and the zero-point charge. These characteristics are critical in the adsorption surface science and represent a fundamental role in adsorption processes. The adsorbent surface charge with acidic and basic groups depends significantly on the pH in solution and on the interaction between the adsorbent surface sites; the electrolyte species determines the ZPC [35]. The surface-active sites of an adsorbent can undergo protonation or deprotonation, depending on the pH in solution, developing a charged surface. In this regard, the polymers with MA and LA were 4.8 and 3.9 respectively, which means that, at the working pH, they are protonated, allowing neutral CPX to be released.

Previous studies reported the development of a MIP with nanofiber grafting using gentamicin sulfate and MA (1:5) as monomer. A 68% release in the imprinted polymer during the first 6 hours was determined, while a non-imprinted polymer released 98% in the first 8 hours. This investigation concluded that the specific interactions with a high affinity in the template-MIP allow better control of the drug release. The release was fitted to the Korsmeyes-Peppas model, and the gentamicin release was fitted to a non-Fickian model, demonstrating the diffusion of the drug molecule through the swollen gel[36].

Zhang et al., performed multiwalled carbon nanotubes coated crystalline liquid MIPs with levofloxacin (0.4 mg) (LVF), MA as commoner with a 1:4 ratio, 4-Methyl phenyl dicyclohexyl ethylene as a liquid crystalline monomer, EDGMA as a crosslinker were dissolved by chloroform. Acetonitrile was used as a medium in the release assay, which lasted 72 hours, 90% LVF release was demonstrated during the first 21 hours, and its release mechanism was by Fickian diffusion [37]. However, under physiological conditions, the release could present different behavior. In another investigation by Salguero et al., biopolymer films loaded with CPX were developed. These materials were designed for topical delivery using a double layer of hydroxide (LDH) and hyaluronan (HS). The release assay of the CPX film (LDH-CPX)/SH with 0.37 mg of CPX was performed for 8 hours. PBS was evaluated in a pH range of 5.8 to 7.4 to simulate physiological skin conditions and plasma exudates from damaged skin. The CPX release into the film CPX/HS at pH 5.8 and 7.4 was 68±6% and

73±4% respectively; and for the (LDH-CPX)/HS of 53±3 % and 46±4, respectively [29]. The developed polymers showed different behaviors after changing pH in the medium, and for the CPX/HS, a better release was observed. Therefore, the pH alteration in the system must be assessed to understand the release behavior of the MIP-CPX.

In comparison with the previously mentioned works, the MIPs developed in this work, achieved a greater control in the release of 9.1 mg L^{-1} (approximately 5%) up to 90.51 mg L^{-1} of CPX (approximately 45%) during the 8 h of study. Moreover, the release of the antibiotic not only depends on its dissolution, but also on the interaction of the polymeric matrix with the medium, demonstrating that the use of different monomers and synthesis methods interferes with the desorption capacity of CPX through the MIPs, using the same conditions.

Adsorption assays were performed to evaluate and establish the adsorption model of CPX on M-LA-C and M-MA-C polymers. The equilibrium data were fitted to the Freundlich, Langmuir, and SIPS models. The isothermal adsorption constants are shown in **Table 4**. The M-LA-C polymer was best fitted to the Freundlich model (R^2=0.9466), meaning that the adsorption occurs in a multilayer. This model describes that most surfaces are heterogenous and that multiple sites are available for the adsorption. The polymer M-MA-C showed a better fit with the Langmuir model (R^2=0.9169), representing that the adsorption is monolayer and homogenous with several specific unions.

Table 4 shows that the M-LA-C polymer presents a higher adsorption rate compared to the M-MA-C polymer. This behavior is explained by the best fit model for each MIP. These results explain the release capacity of both polymers, as M-LA-C releases higher amount of CPX compared to M-MA-C as shown in **Figure 6**.

Polímero	LANGMUIR	FREUNDLICH	SIPS

	qm (mg L^{-1})	K (L mg^{-1})	R^2	K (mg $^{1-1/n}$ $L^{1/n}g^{-1}$)	n	R^2	Nt	a	m	R^2
M-LA-C	4.4258	0.1025	0.4010	0.5478	1.7066	**0.9466**	4.62	0.1027	1	0.426
M-MA-C	3.6396	0.0599	**0.9169**	0.1911	1.3565	0.2347	3.0679	0.0348	1.3093	0.577

Table 4. Constants of the adsorption isotherms for the MIPs (10 mg of MIP, 15 minutes of contact, 1 mL of solution, temperature of the medium: 24°c, pH of the medium: 6).

Qm is the maximum amount of adsorbate (mg g^{-1}) on adsorbent at equilibrium. K is Langmuir's constant, k is Freundlich's constant, n is the exponent of the Freundlich isotherm, a and m are the SIPS isotherm constants, and R^2 is the correlation coefficient.

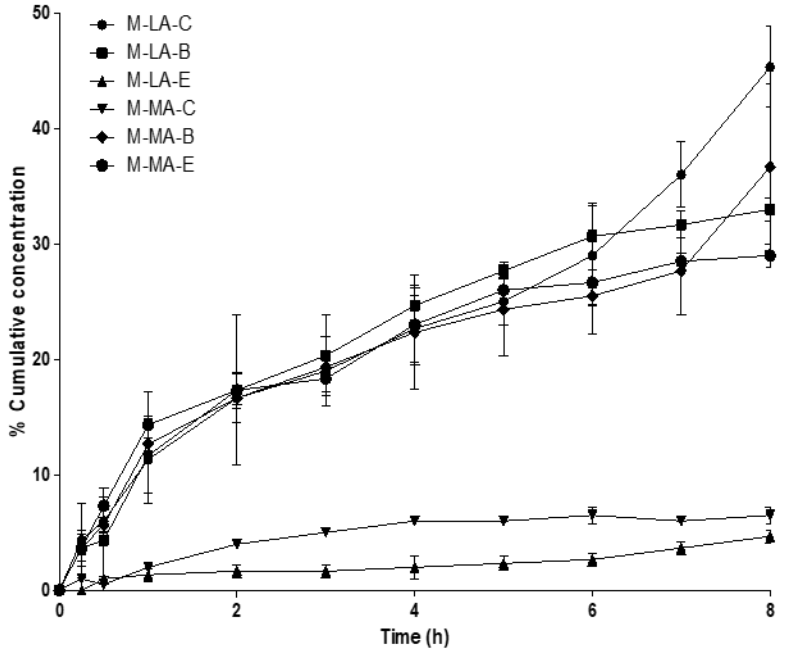

Fig. 6. Percentage of cumulative concentration release of the ciprofloxacin present in each of the MIPs. Each point represents the arithmetic mean ± SD of 5 independent experiments.

M, Molecular imprinting polymer; N, non-imprinting polymer; MA, methacrylic acid; LA, lactic acid; B, bulk; C, co-precipitation; E, emulsion.

The imprinting factor (IF) for the co-precipitation MIPs was calculated to evaluate the selectivity of the imprinted polymers against the molecule for each polymer; these values are presented in **Table 5.** It was observed in M-MA-C and M-LA-C polymers showed a high adsorption capacity (q_e) to adsorb CPX; besides, the K_{MIP} partition coefficient values are higher for CPX in M-LA-C than in M-MA-C. indicating higher specificity in the MIP performed with lactic acid. Additionally, the partition coefficient values determined for MIPs (K_{MIP}) and NIPs (K_{NIP}) and shown in **Table 5** ranged for 68.99 to 72.18 and from 35.82 to 47.21 mL g^{-1}, respectively. Higher partition coefficient values are considered adequate, indicating that MIPs are highly affine to CPX. The partition coefficient is a direct measure of the affinity of the adsorbent for the adsorbate under the conditions it is tested[27].

Table 5. Partition coefficients and imprinting factor of CPX on the corresponding MIP and NIP.

	C_0 (mg L^{-1})	C (mg L^{-1})	q_e (mg g^{-1})	%R	K (mL g^{-1})	IF
M-MA-C	5	1.5501	0.1725	68.9975	111.2775	2.4883
N-MA-C	5	2.6393	0.1180	47.2132	44.7207	
M-LA-C	5	1.3909	0.1805	72.1825	129.7430	4.6482
N-LA-C	5	3.2087	0.0896	35.8253	27.9123	

q_e amounts of adsorbate bound, %R percentage retention, K_{MIP} partition coefficients of MIP, K_{NIP} partition coefficients of MIP, IF imprinting factor

To evaluate the antimicrobial activity, analytical grade CPX was used to validate the method and MIC of 0.12-0.5 and 0.004-0.016 mg L^{-1} was obtained on *S. aureus* and *E. coli*, respectively. **Figure 6** shows that better release is achieved with the M-LA-C polymer.

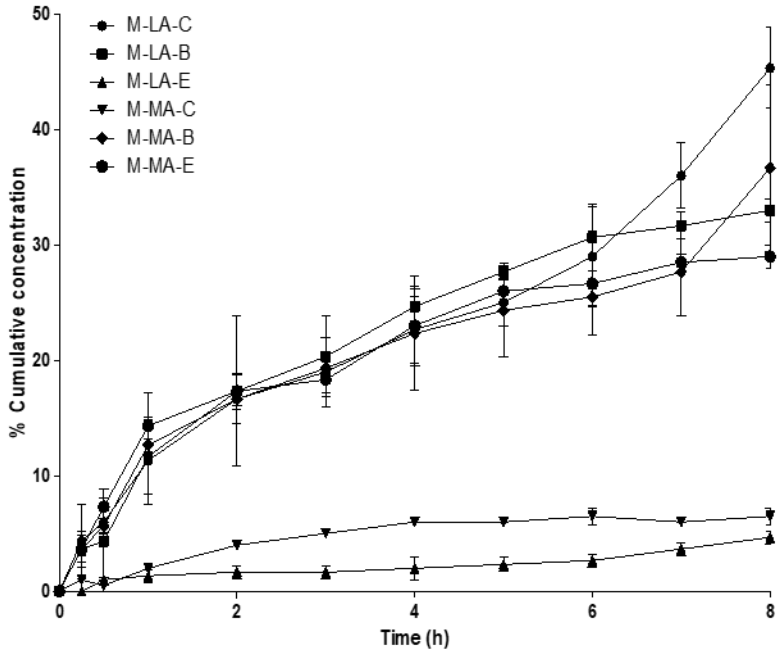

Fig. 6. Percentage of cumulative concentration release of the ciprofloxacin present in each of the MIPs. Each point represents the arithmetic mean ± SD of 5 independent experiments.

M, Molecular imprinting polymer; N, non-imprinting polymer; MA, methacrylic acid; LA, lactic acid; B, bulk; C, co-precipitation; E, emulsion.

The MIC values and ranges established by the CLSI are observed in **Table 6**. The antimicrobial activity of each polymer against *S. aureus* demonstrated an average MIC (±SD) of 0.031(± 0.0) mg L^{-1} for M-LA-B, M-MA-B of 0.016 mg L^{-1}(± 0.0), M-LA-C of 0.125 mg L^{-1}(± 0.0), M-LA-E of 0.062(± 0.0) mg L^{-1}, M-MA-C and 0.057(± 0.013) mg L^{-1} for M-MA-E (**Table 7**) . Experiments were performed in quintuplicate for each MIP. The best antimicrobial activity of each MIP evaluated was against Gram-negative *E. coli*. This result is interesting since the MIC shown by the analytical grade CPX was similar in four of the MIPs evaluated: 0.004 (± 0.0) mg L^{-1} for MIPs, 0.028 (± 0.006) mg L^{-1} with M-LA-E, and 0.014 mg L^{-1} (± 0.0) for M-MA-E. Experiments were performed in quintuplicate for each MIP. The similarities between the MICs obtained for the MIPs (M-LA-B and M-MA-B) against *E. coli* may be due to the synthesis method, which may interfere with the ability of the material to desorb

CPX regardless of the functional monomer used. This effect is also observed in the MIC obtained from M-LA-B, M-LA-C, M-MA-B and M-MA-C against *S. aureus*. On the contrary, M-MA-C and M-MA-E polymers show a greater influence of the presence of the functional monomer in obtaining the MIC.

Table 6. Antimicrobial activity of Ciprofloxacin analytical grade (average ± SD of 3 experiments) shown against the planktonic form of E. coli (ATCC 25922) and S. aureus (ATCC 25923), and parameters of CLSI.

	Ciprofloxacin	
	Analytical Grade	**CLSI**
MIC (mg L^{-1}) ±SD *E. coli*	0.004 ± 0	0.004-0.016
MIC (mg L^{-1}) ±SD *S. aureus*	0.031 ± 0	0.12-0.5

MIC, minimum inhibitory concentration; CLSI, Clinical and Laboratory Standards Institute.

Table 7. Antimicrobial activity (average ± SD of 3 experiments) of MIPs and NIPs shown against the planktonic form of *E. coli* (ATCC 25922) and *S. aureus* (ATCC 25923).

	Lactic acid				Methacrylic acid			
Polymer	**M-LA-C**	**M-LA-B**	**M-LA-E**	**N-LA-C**	**M-MA-C**	**M-MA-B**	**M-MA-E**	**N-AM-C**
MIC (mg L^{-1}) ± SD *E. coli*	0.004± 0	0.004±0	0.028±0.006	---	0.004±0	0.004±0	0.014±0.003	---
MIC (mg L^{-1}) ± SD *S. aureus*	0.016 ±0	0.031±0	0.125±0	---	0.062±0	0.031±0	0.057±0.013	---

MIC, minimum inhibitory concentration; M, Molecular imprinting polymer; N, non-imprinting polymer; MA, methacrylic acid; LA, lactic acid; C, co-precipitation; SD, standard deviation.

The NIPs did not exhibit microbial inhibition, which indicates that the components of MIP synthesis could not inhibit the bacteria; therefore, the activity corresponds exclusively to the CPX released through the MIPs.

Bacteria commonly isolated from infected wounds are *S. aureus* (Gram-positive) and *E. coli* (Gram-negative)[39]; therefore, broad-spectrum antibiotics are needed for their treatment [40]. Ciprofloxacin is ideal for the treatment of these infections due to its efficiency against Gram-positive and Gram-negative bacteria[41].

Previous studies have demonstrated that the use of MIPs is efficient for the elimination of different microorganisms found in infections, these studies evaluated MIPs with several methods: the disk diffusion assay, biological broth method and broth microdilution method. Research performed by Kioomars et al., shows how a CPX hydrogel is used for antibiotic delivery in ocular systems, using MA as monomer and EDGMA as crosslinker and 2-hydroxyethyl methacrylate (HEMA) as the solvent and backbone monomer. The antimicrobial tested was determined by the biological broth method and broth microdilution method. Results show that the antimicrobial activity of the MIPs compared to the NIPs loaded with CPX was more efficient against *P. aeruginosa* y *S. Aureus,* proving the selectivity of CPX in the MIPs [23]. Similarly, Hui et al., produced silicone hydrogel contact lenses loaded with CPX using HEMA, polivinilpirrolidona, methacryloxy propyl tris (trimethylsiloxy) silane and acrylic acid using a molecular imprinting technique. The MIC of the tested organism was determined by the broth microdilution method. *Pseudomonas aeruginosa* was previously isolated from a human case of MK, and the results showed a bacterial growth inhibition from 0.4 μg mL^{-1}.In addition, the bacterial inhibition was evaluated for three days, achieving a significative bacteria decrease ($p>0.05$); however, the difference between each lense was not significative [42]. On the other hand, Salguero and collaborators produced biopolymer films loaded with CPX (0.35 mg) for topical delivery using a double layer of hydroxide (LDH) and hyaluronan (HS). Antimicrobial activity was investigated by disk diffusion assay to evaluate the ability to inhibit the growth of *S. aureus*. A 6 mm CPX/HS film exhibited an inhibition halo of 38 ± 1 mm, slightly higher than the (LHD-CPX)/HS of 33 ± 1 mm and 12 ± 1 mm for HS [29]. However, most studies compared antibacterial activity between the developed materials without proving their efficiency in regulating organisms. Differently, our study demonstrates how the MIPs achieved the CPX release within the MIC range established by the CLSI, proving their efficiency against *S. aureus* and *E. coli*.

In addition, a MIP grafted onto nanofibers was developed using MA as monomer and gentamicin sulfate as template using different ratios (MIP1 1:5, MIP2 1:10 and MIP3 1:20, gentamicin: MA). The antimicrobial activity was evaluated with the disk

diffusion assay for *E. coli* and *S. aureus*. All nanofibers composed with MIP presented significant differences in the bacterial inhibition halo against the control group (8 mm for *E. coli* and 13.5 mm for *S. aureus* in the control group). The *S. aureus* halos for MIP1, MIP2, and MIP3 were 11 mm, 9.5 mm, and 7.5 mm, respectively [36]. These studies verify that the use of MIPs allows adequate release to act effectively against bacteria.

Cell viability was determined by evaluating dermal fibroblasts (HDFn) with the alamarBlue assay. This assay consists of the reducing ability of living cells to convert resazurin to fluorescent resorufin [43].

Cell viability was assessed by exposing MIPs extracts to PBS at 24, 48, and 72 hours. The first result shows that the extracts did not present cytotoxicity and that there is a cell viability increase for all MIPs evaluated (**Figure 7**). Significant differences are observed; the highest proliferation occurs at 72 hours.

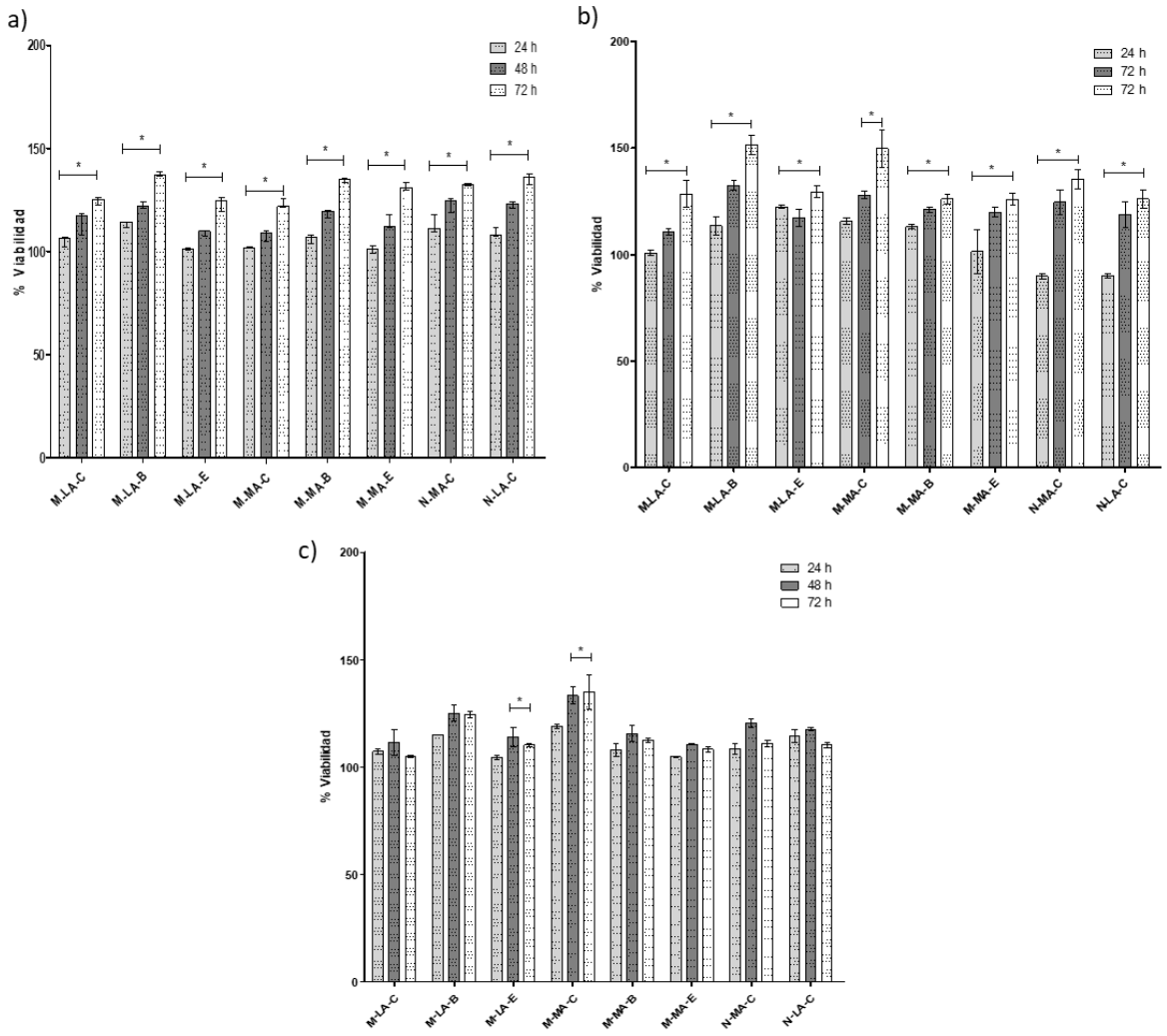

Fig. 7. Percentage of viability Dermal Fibroblast cells (nHDF) versus extracts obtained from 24, 28 and 72 h exposure of MIPs and NIPs in PBS at pH 5.4, using the AlamarBlue assay, percentage of viability for nHDF cells versus MIP extracts 7a) at 24 h, 7b) at 48 h and 7b) at 72 h. Each point represents the arithmetic mean ± SD of 5 independent experiments.

*M, Molecular imprinting polymer; N, non-imprinting polymer; MA, methacrylic acid; LA, lactic acid; B, bulk; C, co-precipitation; E, emulsion; * Statistically significant differences.*

According to the guideline of the International Organization for Standardization ISO (ISO 10993-5), the in-vitro cell viability of medical devices and materials after

exposure must be ≥ 70 % to be considered non-cytotoxic[44]. This organism recommends the biocompatibility evaluation as a mandatory requirement for the safe use of medical devices and materials. Therefore, cytotoxicity testing is paramount in biological evaluation[44]. Lactic acid is a widely used material approved by international institutions[45, 46]. Different therapeutical applications such as drug delivery have been explored[45]. On the other hand, MA presents high biocompatibility and low acute toxicity, which allows its use in medical applications[47]. Our results demonstrated acceptable viability in HDFn cell cultures and favored the growth of these cells. These data suggest that the developed materials may assist in the healing process. However, studies focused on this effect are needed to confirm this hypothesis.

García et al., synthesized a hydrogel with a dendritic monomer, tetramethylethylenediamine, ammonium persulfate, and CPX to evaluate their toxicity in fibroblasts through the MTT (3-[4,5-dimethylthiazol-2-yl]-2,5 diphenyl tetrazolium bromide) method for 24 hours; results demonstrated viabilities between 70 and 90% [34]. Conversely, viabilities in our study were higher than 100% from the first 24 hours of exposure, favoring cell growth.

Some limitations were considered when interpreting the results of this study. Morphological differences between synthesis methods were considered; however, the particle size and homogeneity need further investigation. The release profiles were performed for 8 hours in physiological pH and innocuous skin. Therefore, it is necessary to evaluate the release over a long period of time and at the pH characteristic of a wound. Also, the release study was performed using a PTFE membrane, so the evaluation on porcine skin could provide a broader perspective on the permeation ability of the drug after its release from the MIP. In addition, the antimicrobial activity assessment was performed only on ATCC strains, confirming that CPX release mediated by MIPs possesses acceptable characteristics for bacterial inhibition but its efficacy against isolated strains needs to be evaluated. Finally, the cytotoxicity study was performed by evaluating the metabolism of dermal fibroblasts, so studies that expand this information would be necessary. However, conventional topical products for wound treatment present disadvantages due to

inaccurate dosing, insufficient residence time, variable therapeutic performance, and removal from the skin [48], which represents therapeutic failure in the patient [49]. Other studies have demonstrated drug administration via oral, intravenous, transdermal, and ocular using MIPs synthesized by the co-precipitation method [11-13] [23, 25]. Our study developed a high-efficiency material with high CPX release without cytotoxicity risks to cell lines. The co-precipitation method presents advantages for drug administration compared to the bulk method due to the homogeneous solution obtained from the constant agitation and the uniformity of the particle size, meaning that grinding is not needed and avoiding damage to the bonding sites formed [25]. In addition, the IF for M-LA-C indicates high selectivity and specificity for CPX with a multilayer bond that allows an initial burst release, which is favorable for bactericidal antibiotics and a controlled release to eradicate the infection. Even when our results are promising, more investigation including the particle size and the interaction with coadjuvant materials (i.e., dermal patches) to assess the application of the model in animals and humans, is needed.

4. Conclusion

Different CPX MIPs were synthesized by a non-covalent method with two different functional monomers (LA y MA). The *in vitro* release studies demonstrated the ability of the MIPs to release the CPX in a controlled process in PBS at pH 5.4, with a release of up to 90.51 mg L^{-1} during the 8 hours of study, the method of synthesis and the use of different monomers were found to interfere with the release ability of the antibiotic. The Korsmeyer-Peppas model was the best fit for the release mechanism. CPX release mediated by MIPs showed effective antibacterial activity on *S. aureus* and *E. coli* with MIC of 0.016-0.125 mg L^{-1} and 0.004-0.028 mg L^{-1}, respectively. In addition, MIPs and NIPs exposure to fibroblasts confirmed their safety as materials and an increase in cell viability greater than 100%. Therefore, the results demonstrate that MIPs present promising properties in pharmaceutical delivery systems and their application in difficult-to-treat wounds.

Declaration of competing interest

The authors declare no conflict of interest.

Data availability

Not applicable

Acknowledgments

The authors acknowledge grants and fellowships from the National Council on Science and Technology- Sectoral Research Fund for Education Basic-Science # A1-S-28176.

References

[1] L.F.S. Gushiken, F.P. Beserra, J.K. Bastos, C.J. Jackson, C.H. Pellizzon, Cutaneous Wound Healing: An Update from Physiopathology to Current Therapies, Life (Basel, Switzerland), 11 (2021).
[2] A.J. Singer, Healing Mechanisms in Cutaneous Wounds: Tipping the Balance, Tissue Engineering Part B: Reviews, 28 (2021) 1151-1167.
[3] M.M. Mihai, M.B. Dima, B. Dima, A.M. Holban, Nanomaterials for Wound Healing and Infection Control, Materials, 12 (2019) 2176.
[4] K. Markakis, A.R. Faris, H. Sharaf, B. Faris, S. Rees, F.L. Bowling, Local Antibiotic Delivery Systems: Current and Future Applications for Diabetic Foot Infections, The International Journal of Lower Extremity Wounds, 17 (2018) 14-21.
[5] B.L. Price, R. Morley, F.L. Bowling, A.M. Lovering, C.B. Dobson, Susceptibility of monomicrobial or polymicrobial biofilms derived from infected diabetic foot ulcers to topical or systemic antibiotics in vitro, PLOS ONE, 15 (2020) e0228704.
[6] E.A. Madawi, A.R. Al Jayoush, M. Rawas-Qalaji, H.E. Thu, S. Khan, M. Sohail, A. Mahmood, Z. Hussain, Polymeric Nanoparticles as Tunable Nanocarriers for Targeted Delivery of Drugs to Skin Tissues for Treatment of Topical Skin Diseases, Pharmaceutics, 15 (2023) 657.
[7] I. Carayon, P. Szarlej, P. Gnatowski, E. Piłat, M. Sienkiewicz, M. Glinka, J. Karczewski, J. Kucińska-Lipka, Polyurethane based hybrid ciprofloxacin-releasing wound dressings designed for skin engineering purpose, Advances in Medical Sciences, 67 (2022) 269-282.
[8] T. Thai, B.H. Salisbury, P.M. Zito, Ciprofloxacin, in: StatPearls [Internet], StatPearls Publishing, 2021.
[9] M.R. Prausnitz, R. Langer, Transdermal drug delivery, Nature Biotechnology, 26 (2008) 1261-1268.
[10] N. Yuksel, S. Tektas, Molecularly imprinted polymers: preparation, characterisation, and application in drug delivery systems, Journal of Microencapsulation, 39 (2022) 176-196.
[11] J.J. BelBruno, Molecularly Imprinted Polymers, Chemical Reviews, 119 (2019) 94-119.
[12] A. Lusina, M. Cegłowski, Molecularly Imprinted Polymers as State-of-the-Art Drug Carriers in Hydrogel Transdermal Drug Delivery Applications, Polymers, 14 (2022) 640.
[13] K. Nishchaya, V.K. Rai, H. Bansode, Methacrylic acid as a potential monomer for molecular imprinting: A review of recent advances, Results in Materials, 18 (2023) 100379.
[14] S. Akgönüllü, M. Bakhshpour, A.A. Topçu, N. Bereli, A. Denizli, Chapter 5 - Molecularly imprinted polymeric carriers for controlled drug release, in: S. Das, S. Thomas, P.P. Das (Eds.) Novel Platforms for Drug Delivery Applications, Woodhead Publishing, 2023, pp. 85-103.
[15] B. Oktay, G.Ö. Eroğlu, S. Demir, S.E. Kuruca, N.K. Apohan, Poly(lactic acid) nanofibers containing phosphorylcholine grafts for transdermal drug delivery systems, Materials Today Sustainability, 18 (2022) 100132.

[16] Z. Ali, M. Sajid, M.M. Ahmed, M. Hanif, S. Manzoor, Synthesis of green fluorescent cross-linked molecularly imprinted polymer bound with anti-cancerous drug (docetaxel) for targeted drug delivery, Polymer Bulletin, (2023).
[17] L.D. de León-Martínez, M. Rodríguez-Aguilar, R. Ocampo-Pérez, J.M. Gutiérrez-Hernández, F. Díaz-Barriga, L. Batres-Esquivel, R. Flores-Ramírez, Synthesis and Evaluation of a Molecularly Imprinted Polymer for the Determination of Metronidazole in Water Samples, Bulletin of Environmental Contamination and Toxicology, 100 (2018) 395-401.
[18] Kuzin IA, Loskutov AI, USSR, j. Appl. Chem, 39 (1996) 85.
[19] M.L. Soto, A. Moure, H. Domínguez, J.C. Parajó, Recovery, concentration and purification of phenolic compounds by adsorption: A review, Journal of Food Engineering, 105 (2011) 1-27.
[20] S.-H. Kuo, C.-J. Shen, C.-F. Shen, C.-M. Cheng, Role of pH Value in Clinically Relevant Diagnosis, Diagnostics, 10 (2020) 107.
[21] H. Haidari, Z. Kopecki, A.T. Sutton, S. Garg, A.J. Cowin, K. Vasilev, pH-Responsive "Smart" Hydrogel for Controlled Delivery of Silver Nanoparticles to Infected Wounds, Antibiotics, 10 (2021) 49.
[22] Y. Wu, Y. Wang, L. Long, C. Hu, Q. Kong, Y. Wang, A spatiotemporal release platform based on pH/ROS stimuli-responsive hydrogel in wound repairing, Journal of Controlled Release, 341 (2022) 147-165.
[23] S. Kioomars, S. Heidari, B. Malaekeh-Nikouei, M. Shayani Rad, B. Khameneh, S.A. Mohajeri, Ciprofloxacin-imprinted hydrogels for drug sustained release in aqueous media, Pharmaceutical Development and Technology, 22 (2017) 122-129.
[24] M. Mabrouk, A.A. Mostafa, H. Oudadesse, A.A. Mahmoud, M.I. El-Gohary, Effect of ciprofloxacin incorporation in PVA and PVA bioactive glass composite scaffolds, Ceramics International, 40 (2014) 4833-4845.
[25] S. He, L. Zhang, S. Bai, H. Yang, Z. Cui, X. Zhang, Y. Li, Advances of molecularly imprinted polymers (MIP) and the application in drug delivery, European Polymer Journal, 143 (2021) 110179.
[26] S.A. Bhawani, T.S. Sen, M.N.M. Ibrahim, Synthesis of molecular imprinting polymers for extraction of gallic acid from urine, Chemistry Central Journal, 12 (2018) 19.
[27] J. Meléndez-Marmolejo, L. Díaz de León-Martínez, V. Galván-Romero, S. Villarreal-Lucio, R. Ocampo-Pérez, N.A. Medellín-Castillo, E. Padilla-Ortega, I. Rodríguez-Torres, R. Flores-Ramírez, Design and application of molecularly imprinted polymers for adsorption and environmental assessment of anti-inflammatory drugs in wastewater samples, Environmental science and pollution research international, 29 (2022) 45885-45902.
[28] R. Tabaraki, N. Sadeghinejad, Preparation and application of magnetic molecularly imprinted polymers for rutin determination in green tea, Chemical Papers, 74 (2020) 1937-1944.
[29] Y. Salguero, L. Valenti, R. Rojas, M.C. García, Ciprofloxacin-intercalated layered double hydroxide-in-hybrid films as composite dressings for controlled antimicrobial topical delivery, Materials Science and Engineering: C, 111 (2020) 110859.
[30] M. Humphries Romney, A. Hindler Janet, K. Shaffer, A. Campeau Shelley, Evaluation of Ciprofloxacin and Levofloxacin Disk Diffusion and Etest Using the 2019 Enterobacteriaceae CLSI Breakpoints, Journal of Clinical Microbiology, 57 (2019) e01797-01718.
[31] S.A. Zaidi, Molecular imprinted polymers as drug delivery vehicles, Drug Delivery, 23 (2016) 2262-2271.
[32] L. Li, Y. Aoki, Rheological Images of Poly(vinyl chloride) Gels. 1. The Dependence of Sol−Gel Transition on Concentation, Macromolecules, 30 (1997) 7835-7841.
[33] K. Dharmalingam, R. Anandalakshmi, Fabrication, characterization and drug loading efficiency of citric acid crosslinked NaCMC-HPMC hydrogel films for wound healing drug delivery applications, International Journal of Biological Macromolecules, 134 (2019) 815-829.
[34] M.C. García, J.C. Cuggino, C.I. Rosset, P.L. Páez, M.C. Strumia, R.H. Manzo, F.L. Alovero, C.I. Alvarez Igarzabal, A.F. Jimenez-Kairuz, A novel gel based on an ionic complex from a dendronized polymer and ciprofloxacin: Evaluation of its use for controlled topical drug release, Materials Science and Engineering: C, 69 (2016) 236-246.
[35] T. Madrakian, M. Ahmadi, A. Afkhami, M. Soleimani, Selective solid-phase extraction of naproxen drug from human urine samples using molecularly imprinted polymer-coated magnetic multi-walled carbon nanotubes prior to its spectrofluorometric determination, Analyst, 138 (2013) 4542-4549.
[36] E. Tamahkar, M. Bakhshpour, A. Denizli, Molecularly imprinted composite bacterial cellulose nanofibers for antibiotic release, Journal of Biomaterials Science, Polymer Edition, 30 (2019) 450-461.

[37] L.-P. Zhang, X.-X. Tan, Y.-P. Huang, Z.-S. Liu, Floating liquid crystalline molecularly imprinted polymer coated carbon nanotubes for levofloxacin delivery, European Journal of Pharmaceutics and Biopharmaceutics, 127 (2018) 150-158.
[38] S.A. Zaidi, Latest trends in molecular imprinted polymer based drug delivery systems, RSC advances, 6 (2016) 88807-88819.
[39] D. Pitocco, T. Spanu, M. Di Leo, R. Vitiello, A. Rizzi, L. Tartaglione, B. Fiori, S. Caputo, G. Tinelli, F. Zaccardi, Diabetic foot infections: a comprehensive overview, Eur Rev Med Pharmacol Sci, 23 (2019) 26-37.
[40] J.M. Ramirez-Acuña, S.A. Cardenas-Cadena, P.A. Marquez-Salas, I. Garza-Veloz, A. Perez-Favila, M.A. Cid-Baez, V. Flores-Morales, M.L. Martinez-Fierro, Diabetic Foot Ulcers: Current Advances in Antimicrobial Therapies and Emerging Treatments, Antibiotics (Basel, Switzerland), 8 (2019).
[41] L.L. Brunton, B.A. Chabner, B.C. Knollmann, Goodman & Gilman: Las bases farmacológicas de la terapéutica, McGraw hill, 2019.
[42] A. Hui, M. Willcox, L. Jones, In Vitro and In Vivo Evaluation of Novel Ciprofloxacin-Releasing Silicone Hydrogel Contact Lenses, Investigative Ophthalmology & Visual Science, 55 (2014) 4896-4904.
[43] S.L. Ortiz, V.R. Lugo, D. Salado-Leza, M.I. Reyes-Valderrama, L.E. Alcántara-Quintana, P. González-Martínez, D.M. Anaya, Dy2O3-unpurified hydroxyapatite: a promising thermoluminescent sensor and biomimetic nanotherapeutic, Applied Physics A, 127 (2021) 893.
[44] A. Ahmed, G. Getti, J. Boateng, Ciprofloxacin-loaded calcium alginate wafers prepared by freeze-drying technique for potential healing of chronic diabetic foot ulcers, Drug Delivery and Translational Research, 8 (2018) 1751-1768.
[45] J. Da Silva, S. Jesus, N. Bernardi, M. Colaço, O. Borges, Poly (D, L-Lactic Acid) nanoparticle size reduction increases its immunotoxicity, Frontiers in Bioengineering and Biotechnology, 7 (2019) 137.
[46] B. Tyler, D. Gullotti, A. Mangraviti, T. Utsuki, H. Brem, Polylactic acid (PLA) controlled delivery carriers for biomedical applications, Advanced drug delivery reviews, 107 (2016) 163-175.
[47] J. Lebeau, J.P. Efromson, M.D. Lynch, A review of the biotechnological production of methacrylic acid, Frontiers in Bioengineering and Biotechnology, 8 (2020) 207.
[48] P. Lam, K. Lee, R. Wong, G. Cheng, Z. Bian, C. Chui, R. Gambari, Recent advances on topical antimicrobials for skin and soft tissue infections and their safety concerns, Critical reviews in microbiology, 44 (2018) 40-78.
[49] K.Z. Vardakas, M. Horianopoulou, M.E. Falagas, Factors associated with treatment failure in patients with diabetic foot infections: an analysis of data from randomized controlled trials, Diabetes research and clinical practice, 80 (2008) 344-351.

Manuscrito 2. *Molecularly imprinted polymer systems for the controlled release of naphthoquinone*

El presente capítulo incluye la versión del manuscrito previa a la publicación del artículo titulado *"Molecularly imprinted polymer systems for the controlled release of naphthoquinone derivatives with antimicrobial activity"*, publicado en la revista *Reactive and Functional Polymers*.

Galván-Romero, V., Gonzalez-Salazar, F., Vargas-Berrones, K., Flores, F. C., Mendoza, B. N. Z., de Loera Carrera, D. A., ... & Flores-Ramírez, R. (2025). Molecularly imprinted polymer systems for the controlled release of naphthoquinone derivatives with antimicrobial activity. *Reactive and Functional Polymers*, *215*, 106388. doi.org/10.1016/j.reactfunctpolym.2025.106388.

Molecularly Imprinted Polymer Systems for the Controlled Release of Naphthoquinone Derivatives with Antimicrobial Activity

1. Introduction

In the last decades, antimicrobial resistance (AMR) has emerged as a significant challenge in public health, becoming a global concern threatening the effectiveness of preventing and treating infectious diseases [1]. AMR is a condition in which microorganisms can live and grow in the presence of antimicrobial agents that have proven effective against these microorganisms [2, 3]. The emergence of antimicrobial resistance is mainly driven by the misuse and overuse of antibiotics in clinical and agricultural settings, leading to persistent bacterial resistance and treatment failures [2]. Given these challenges, the development of novel antimicrobial compounds and innovative delivery systems is essential to mitigate antimicrobial resistance effectively. One example is naphthoquinone (NQ) and its derivatives, which have demonstrated significant antibacterial properties [4-7]. These properties are determined by the position and chemical composition of the side groups (R) attached to the naphthoquinone ring structure. Some examples of these groups include hydrogen, hydroxyl, methyl, nitrogen, sulfur, and halide, which stimulate oxidative stress and alkylation of cellular nucleophiles [8, 9]. In a study conducted by Lim [10], 5-hydroxy-1,4-naphthoquinone was isolated from *Caesalpinia sappan*, demonstrating its ability to inhibit the growth of different bacterial strains, including *Bifidobacterium bifidum, Bifidobacterium, Clostridium perfringens, Escherichia coli*, and *Lactobacillus casei*. Likewise, Choudhari [11] tested two derivatives of 1,4-naphthoquinone to establish their antibacterial potential against various pathogens; notable antibacterial activity was observed against *Staphylococcus aureus* and *Pseudomonas aeruginosa*. However, despite their potent antibacterial properties, the therapeutic application of naphthoquinones is limited by their solubility and stability. Therefore, an advanced drug delivery system (DDS) is required to ensure controlled and targeted release while minimizing side effects. Furthermore, the importance of control in the administration of antimicrobials has been highlighted to prevent the development of AMR, as their distribution in the

body allows them to reach areas such as the intestinal microbiome, resulting in dysbiosis and even the development of AMR [12]. In addition, the patient's physiopathological conditions can hinder the arrival of the therapeutic agent to the site of action, increasing the risk of developing AMR and even biofilms. Therefore, drug administration strategy offers significant advantages for preventing the emergence of AMR. DDS has been widely studied and has experienced rapid growth in recent decades [13, 14]. These materials offer controlled release rates over extended periods, are biocompatible, easily accessible, self-administered, and bypass first-pass metabolism [15, 16].

Molecularly Imprinted Polymers (MIPs) represent an approach for drug delivery and are synthetic receptors with specific recognition sites for template molecules used for drug administration in wounds due to their mechanical strength and biocompatibility [17-23]. Compared to conventional DDS, such as liposomes or polymeric nanoparticles [24, 25], MIPs offer superior molecular recognition, mechanical stability, and prolonged drug release [26-29]. These features make them particularly suitable for antimicrobial applications, as they enable targeted and sustained drug delivery while reducing the risk of bacterial resistance development [30, 31]. Therefore, this study aimed to synthesize, characterize, and evaluate molecularly imprinted polymers (MIPs) as an innovative delivery system for naphthoquinone derivatives, compounds known for their potent antimicrobial properties. The design of these MIPs focused on achieving specificity and controlled release capacity. MIPs efficiency was assessed through minimum inhibitory concentration (MIC) assays against bacterial strains (*Staphylococcus aureus* and *Escherichia coli*) to demonstrate their antimicrobial potential. In addition, MIPs' biocompatibility was evaluated by performing cytotoxicity tests using the MTT assay on human dermal fibroblast cells (HDFn) to confirm their safety.

2. Materials and Methods

2.1. Materials

All reagents, lactic acid (LA), methacrylic acid (MA), ethylene glycol dimethacrylate (EDGMA), and azobisisobutyronitrile (AIBN) were purchased from

Sigma-Aldrich (Darmstadt, Germany). Hydrochloric acid (HCl) and sodium hydroxide (NaOH) were supplied by Merck (State of Mexico). 3-chloro-2-tyrosine-1,4- naphthoquinone and 2-tyrosine-1,4-naphthoquinone were obtained through organic synthesis in the research group [32].

2.2. Molecularly imprinted polymers synthesis

The polymer synthesis was performed with minor modifications based on previous work performed by our research group [17] using two non-covalent polymerization methods.

(i) Bulk polymerization. First, the template (Cl-NQ-TYR 1mmol, NQ-TYR 1 mmol) and the functional monomer (LA and MA) were mixed in a 1:4 rate (template: monomer), 3 mL of methanol and 3 mL of acetonitrile were used as porogen, EDGMA as crosslinker, and AIBN as initiator. The reaction was carried out under a nitrogen atmosphere without stirring and in a glycerin bath at 70°C for 24 h.

(ii) Co-precipitation polymerization. The procedure and conditions used were the same as those in bulk polymerization. Nevertheless, a porogen excess (15 mL of methanol and 15 mL of acetonitrile) and magnetic stirring (100 rpm) were added in a glycerin bath at 70°C for 24 h. NIPs for each synthesized polymer were prepared under similar conditions to their respective MIPs but without the template. The polymers were crushed in a mortar, sieved into 250μm (particle size), and weighed to establish the reaction yield. The MIPs cleaning was achieved by performing ten washing cycles with 10 mL of methanol and HCl (0.1 N). Each cycle was sonicated for 15 minutes and centrifuged at 2500 rpm for 5 minutes.

2.3. Cl-NQ-TYR and NQ-TYR determination by HPLC-DAD

The analysis of Cl-NQ-TYR and NQ-TYR in the samples was carried out using high-performance liquid chromatography (HPLC) equipped with a diode array detector (DAD) (Agilent® 1260 Infinity Series) and a Zorbax SB C18 column (4.6 × 150 mm, 5 μm). The mobile phase consisted of 30:70 formic acid and acetonitrile at an isocratic flow rate of 1 mL min^{-1}. The sample volume was 10 μL, the DAD wavelength was 235 nm of excitation, and the method duration was 10 min.

The analytical method validation was performed following the guidelines for the validation of analytical methods for the determination of organic compounds at trace level (AOAC/FAO/IAEA/IUPAC 2000). The evaluation included the detection limit (LOD), quantification limit (LOQ), linearity (R^2), sensitivity, and precision. The linearity was expressed by the correlation coefficient (R^2), sensitivity by the slope of the curve, and precision considering the average of seven curves carried out for three days (3 for repeatability and 4 for reproducibility). The LOD was calculated using the equation:

$$LOD = X + 3SD_{blank} \quad (1)$$

Where X is represents the concentration and SD is the standard deviation of the blank. The LOQ was determined as follows:

$$LOQ = X + 10SD_{blank}. \quad (2)$$

2.4. Determination of retention percentages

The retention percentages of MIP for each template (Cl-NQ-TYR and NQ-TYR) were determined by packing 10 mg of each MIP into 5 mL solid-phase extraction cartridges. Then, a 2 mg L^{-1} solution of each template was added to the corresponding imprinted polymer. The solution was stirred for 1 hour, followed by centrifugation, and the eluent was analyzed using HPLC-DAD. The retention percentage (%R) was calculated using the following equation:

$$\%R = [(C_0 - C_f)/C_0)] * 100\% \quad (3)$$

Where C_0 represents the initial concentration of each template (mg L^{-1}), and C_f is the eluent concentration (mgL^{-1}).

2.5. Morphological characterization of MIPs/NIPs by Field Emission Scanning Electron Microscopy (FE-SEM)

Micrographs of MIPs and NIPs were obtained using a field emission scanning electron microscope (FE-SEM), FEI model Inspect F50, to evaluate their surface and morphology. The analysis was performed using an Everhart-Thornley (ETD)

detector in secondary electron (SE) mode, with an accelerating voltage of 30 kV, a beam current of 0.17 nA, and a probe current of 85 pA. The parameters considered included magnification (x), horizontal field width (HFW), and working distance (WD).

2.6. Infrared Spectroscopy

The analysis of functional groups was carried out using Attenuated Total Reflection Fourier-transform Infrared Spectroscopy (ATR-FTIR) with a Thermo Scientific® Nicolet iS10 spectrometer. Infrared spectra were recorded within a wavelength range of 500 to 4000 cm^{-1} to identify the characteristic vibrational modes of the chemical bonds present in the samples.

2.7. Surface charge distribution and zero charge point

The surface charge of MIPs and NIPs was determined using the acid-base titration method proposed by Kuzin & Loskutov [33]. A neutralizing solution (pH 2-12) was prepared, with 50 mL in total. Of this, 25 mL was added to 0.1 mg of MIP or NIP in a centrifuge tube, and the remaining 25 mL served as a blank. The solutions were stirred, and pH measurements were taken every 30 minutes for two hours to generate the potentiometric curves for both the blank and the adsorbent. The Zero Charge Point (ZCP) was determined by identifying the intersection between the MIP or NIP solution curve and the blank curve. Subsequently, the surface charge

distribution was established by plotting the potentiometric curves for the adsorbent and the blank (the volume of HCl was considered negative, and the volume of NaOH was considered positive). The volumes of both the blank and adsorbent were plotted against different pH values. The surface charge was calculated using the following equation:

$$C_S = [C_N(V_B - V_A) / m] F \quad (4)$$

Where C_S is the surface charge (C g^{-1}), C_N is the concentration of the neutralizing solution (mol L^{-1}), V_B and V_A are the volumes of the base and acid required for neutralization (L), m is the mass of the adsorbent (g), and F is the Faraday constant (96485 C mol^{-1}).

2.8. Adsorption isotherms of MIPs

The Freundlich, Langmuir, and SIPS isotherms models have been widely used to describe the interaction between adsorbent and adsorbate using concentrations between 1–310 mg L^{-1} of Cl-NQ-TYR and NQ-TYR, with a dissolution volume of 2 mL, at 24 °C, 50 rpm, and a contact time of 2 hours. The equilibrium adsorption capacity q (mg g^{-1}), was calculated using the following equation:

$q_e = [(C_0 - C_e)V]/W$ (5)

Where Co (mg L^{-1}) is the initial concentration of the adsorbent and Ce (mg L^{-1}) is the equilibrium concentrations of the adsorbent. V (L) is the volume of stock solution, and W (g) is the weight of the polymer used.

The Langmuir isotherm (6), Freundlich isotherm (7) and SIPs isotherms (8) models are shown in the following equations:

$q = (Kq_mC)/(1 + KC)$ (6)

$1\_q = kCn$ (7)

$q = (N_taC^m)/(1 + aC^m)$ (8)

Where *C* (mg L^{-1}) is the concentration of the adsorbate at equilibrium, qm (mg L^{-1}) is the maximum adsorption capacity, *K* (L mg^{-1}) is the affinity constant, which is related to the adsorption energy. k ($mg^{1-1/n}$ $L^{1/n}$ g^{-1}) is the adsorption capacity of the adsorbent and the constant n indicates the adsorption intensity, a value of n > 1.0 represents a favorable adsorption condition. SIPs model includes the characteristics of the Langmuir and Freundlich models, where a is the isotherm constant [34-36].

The software Origin® (version 8.5) was used to fit the experimental data to the math models. The following analysis was performed according to the model with the best correlation coefficient (R^2).

2.9. Imprinting factor

The selectivity of the MIPs towards the template, using various monomers, was verified by preparing a 2 mg L^{-1} solution of each template in Milli-Q water. One mL of this solution was passed through each MIP using the isothermal assay method. In the same way, NIPs were examined for comparison with their respective MIPs. The selectivity of both MIPs and NIPs was assessed based on the partition coefficient between the polymer (Cl- NQ-TYR and NQ-TYR) and the solution. The partition coefficient was determined using the following equations:

$$K = q_e/C_0 = q_e/\{C\ [1 - (\%R/100)]\} \quad (9)$$

$$\%R = [(C_0 - C)/C_0]100\%] \quad (10)$$

Where C_0 (mg L^{-1}) represents the amount of analyte bound to the MIP or NIP, C (mg L^{-1}) is the concentration of each analyte remaining in the eluting solution, q_e is the amount of adsorbate bound to the adsorbent at equilibrium, and $\%R$ is the retention percentage. Furthermore, the imprinting factor (IF) was used to evaluate the selectivity of each MIP for the template in the presence of other NIPs with similar structural features. The IF was calculated with the following equation:

$$IF = K_{MIP}/K_{NIP} \quad (11)$$

where K_{MIP} and K_{NIP} represent the partition coefficients of each compound.

2.10. Release Profile and Kinetics of Cl-NQ-TYR and NQ-TYR by MIPs

In vitro diffusion assays were performed at 37°C ± 0.5 °C using a Franz diffusion cell, with polyvinyl difluoride (PVDF) filter paper to determine the release kinetics. The filter paper was positioned between the donor and the receptor cell compartments, and the receptor compartment was filled with 20 mL of phosphate buffer (pH 5.4) to mimic physiological skin conditions [37-39]. Finally, the samples were collected from the receptor compartment at different times (0, 0.25, 0.5, 1, 2, 3, 4, 5, 6, 7, 8, 12, and 24 h), and phosphate buffer was added for further analysis (HPLC-DAD). Experiments were conducted in quintuplicate for each synthesized MIP. The release profiles were fitted according to the zero-order (12), first-order (13), Higuchi (14), and Korsmeyer- Peppas (15). equation:

$Q_t = Q_0 - K_0 t$ (12)

$\ln (Q_t/Q_0) = -K_1 t$ (13)

$Q_t = K_H t^{1/2}$ (14)

$Q_t / Q_\infty = k t^n$ (15)

Where Q_t is the fraction of the released drug at a time t, K_0 constant of zero-order, K_1 constant of first-order, K_H and k is the diffusion constant of Korsmeyer-Peppas Q_∞, and n is the release exponent. The exponent n indicates the drug release mechanism from a polymeric matrix system. If $n \leq 0.45$, the drug release mechanism is considered Fickian; if $0.45 < n < 0.89$, the mechanism is considered non-Fickian (anomalous transport); if $n = 0.89$, the mechanism is case II transport; and if $n > 0.89$ the mechanism is super case II transport [40, 41].

The software Origin® (version 8.5) was used to fit the experimental data to the math models. The following analysis was performed according to the model with the best correlation coefficient (R^2).

2.11. Antimicrobial activity

The minimum inhibitory concentration (MIC) was determined using the microdilution method, with the assay previously validated using reference strains supplied by the American Type Culture Collection (ATCC). The polymers were tested against Gram-positive *S. aureus* (ATCC 25923) and Gram-negative *E. coli* (ATCC 25922) to determine their antimicrobial activity. The microorganism strains were cultured on Mueller Hinton solid medium (211443, BBL™) and incubated in a 96-well microplate in a humidified atmosphere containing 5% CO2 for 24 hours. The microorganisms were exposed to varying concentrations of MIPs and NIPs, and the absence of turbidity in the wells indicated the endpoint. All assays were conducted in triplicate to ensure reproducibility.

2.12. Cytotoxicity

The cytotoxicity of the polymers in dermal fibroblasts (NIH/3T3) was evaluated. The cells were maintained in Dulbecco's modified Eagle's medium (DMEM, 30-2002 ATCC) supplemented with 10% (v/v) fetal bovine serum (1600.036, Gibco) and 1% (v/v) penicillin-streptomycin (13377820, ROCHE). This solution was incubated at 37°C in a humified atmosphere of 5% CO_2 for 24 hours. The cells ($1x10^4$ cells/well) were cultured in 96-well microplates. Cell viability assays were carried out using 3-(4,5-dimethylthiazol-2-yl)-2,5-diphenyl tetrazolium bromide (MTT,11465007001, ROCHE) to estimate the number of viable cells. The cells were exposed to polymeric extract (in PBS) for 24 hours, and after incubation, 100 µL of MTT was added to each well. After 4 hours, the absorbance was measured at 570 nm using a microplate reader (Multiskan FC, Thermo Scientific). Cells with DMEM medium were used as a negative control, while cells treated with hydrogen peroxide were used as a positive control. All experiments were performed in quintuplicate, and the viability percentage was calculated with the positive control set as 100% [42].

2.13. Statistical analysis

Data normality tests were performed using Shapiro-Wilk, and parametric tests of inferential statistics were applied using analysis of variance (ANOVA) and Dunn's post hoc test.

3. Results and discusión

3.1. Molecularly imprinted polymers synthesis Cl-NQ-TYR and NQ-TYR determination by HPLC-DAD

A total of eight MIPs and four NIPs were synthesized, yielding approximately 3 g of polymer (**Table 1**). The analytical method validation was carried out for Cl-NQ-TYR and NQ-TYR, achieving a linearity of 0.99 for each template within the working range of 0.5 - 10 mg L^{-1}. The sensitivity was found to be 52.20 (95% CI: 48.04-58.48 mg L^{-1}) for Cl-NQ-TYR and 49.84 (95% CI: 45.58-55.55 mg L^{-1}) for NQ-TYR (**Table 2**). The retention times for the templates were 6.26 min for Cl-NQ-TYR and 6.29 min for NQ-TYR (**Figure 1**). The limits of detection (LOD) and quantification (LOQ) were determined using the slope method, with values of 0.73 and 0.86 mg

L^{-1} for Cl-NQ-TYR, and 0.71 and 0.86 mg L^{-1} for NQ-TYR, respectively. Precision was evaluated in terms of repeatability and reproducibility, with each point in the calibration curve assessed for the coefficient of variation (CV). Both Cl-NQ-TYR and NQ-TYR exhibited an acceptable CV, confirming the reliability of the methods across different workdays [43].

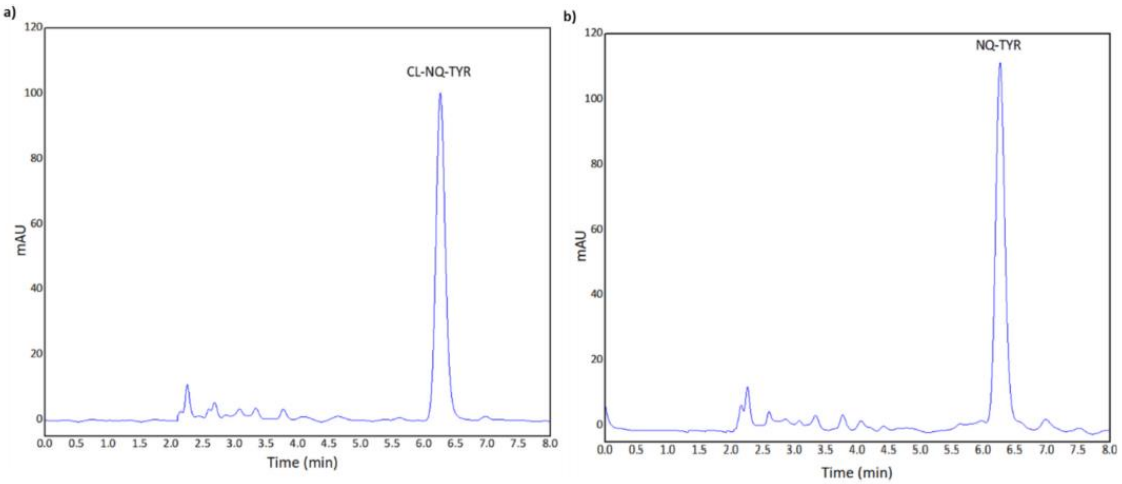

Figure 1. Chromatograms of a) CL-NQ-TYR (2 mg L^{-1}) with a retention time of 6.26 min and b) NQ-TYR (2 mg L^{-1}) with a retention time of 6.29 min.

Table 1. Code of the synthesized polymers for both templates.

Code	Template	MIP	NIP	Monomer	Method
CNT-MA-B	Cl-NQ-TYR	X		Methacrylic acid	Bulk
CNT-MA-C	Cl-NQ-TYR	X		Methacrylic acid	Co-precipitation
CNT-LA-B	Cl-NQ-TYR	X		Lactic acid	Bulk
CNT-LA-C	Cl-NQ-TYR	X		Lactic acid	Co-precipitation
NT-MA-B	NQ-TYR	X		Methacrylic acid	Bulk
NT-MA-C	NQ-TYR	X		Methacrylic acid	Co-precipitation
NT-LA-B	NQ-TYR	X		Lactic acid	Bulk
NT-LA-C	NQ-TYR		X	Lactic acid	Co-precipitation
N-MA-B	-		X	Methacrylic acid	Bulk
N-MA-C	-		X	Methacrylic acid	Co-precipitation
N-LA-B	-		X	Lactic acid	Bulk
N-LA-C	-		X	Lactic acid	Co-precipitation

Table 2. Parameters for the validation of the analytical method for both templates.

Template	LOD (mg L^{-1})	LOQ (mg L^{-1})	Sensibility	Linearity

Cl-NQ-TYR	0.732	0.86	52.20 (IC 95% 48.04 - 58.48)	0.9980
NQ-TYR	0.715	0.864	49.84 (IC 95%: 45.58-55.55)	0.9970

LOD, Limit of detection; LOQ, Limit of quantification

3.2. Determination of retention percentages

The selective recognition ability of MIPs is established during polymer preparation by using suitable monomers specific to the target molecule [18, 44-46]. The molecular imprinting technique involves a template molecule, functional monomer, and a cross-linker dissolved in an appropriate solvent, resulting in a highly cross-linked polymer due to the formation of non-covalent bonds between the template and the monomer during the synthesis process [47]. Monomers, such as methacrylic acid and lactic acid, have been widely used for DDS development due to their biocompatibility [47, 48]. **Table 3** presents the retention percentages of the MIPs and their respective NIPs. All MIPs exhibited high retention percentages (>90%), with MIPs synthesized using MA by both synthesis methods showing the highest retention percentages (99.53% and 98.58%). Contrarily, the highest retention percentage for the NIPs was 63.43%. These results demonstrate the MIPs' capability to retain the NQ- TYR template, highlighting the influence of the synthesis method and the polymer type. The retention percentages of the polymers synthesized using the Cl-NQ-TYR template also showed high retention (>90%). Two MIPs presented excellent performance: the MIP synthesized with lactic acid as monomer and using the coprecipitation method (98.3%), and the MIP with methacrylic acid as monomer and using the bulk polymerization method (96.6%). These results were compared with their corresponding NIPs, which showed retention values of 78.83% and 68.95%, respectively. Furthermore, a direct correlation was observed between the retention capacity and the active sites in the structure of the imprinted polymers. This behavior was evident in the NIP results, where lower retention capacities were seen due to the absence of specific active sites. These results confirm the importance of molecular imprinting in generating sites for selective recognition in MIPs, which confers upon them their unique ability to effectively retain and adsorb target

molecules, as reflected in their ability to release template molecules in a controlled manner.

Table 3. Textural properties of MIPs.

Parameters	CNT-MA-C	CNT-MA-B	CNT-LA-C	CNT-LA-B
S_{BET} (m^2 g^{-1})	127	401	155	244
V_p (cm^3 g^{-1})	0.145	0.922	0.491	0.352
D_p (nm)	10.118	12.714	11.507	9.567

S_{BET}, Surface area; V_P, pore volumen; D_p, pore diameter.

3.3. Morphological characterization of MIPs/NIPs by Field Emission Scanning Electron Microscopy (FE-SEM)

The morphological characteristics of the synthesized MIPs were examined using scanning electron microscopy (SEM); the surface of spherical particles comprises a polymeric network formed by the functional monomer and the cross-linker in the synthesized MIPs [17]. Polymers synthesized through the coprecipitation method exhibited heterogeneous and irregular aggregates (**Figure 2**), which can be attributed to the excess of porogen used during synthesis. This excess of porogen promotes the formation of reaction nuclei, allowing independent polymer growth and creating a larger reaction space. Although this behavior enhances a greater separation between the monomer and the template, which may facilitate subsequent release, it can also lead to independent growth of each particle, causing differences in size and morphology. Likewise, amorphous agglomerated particles were observed in the polymers synthesized using the bulk method (**Figure 3**). However, the particle size of the NIPs was smaller, and larger structures were formed since no agitation was employed during the synthesis. As a result, mechanical grinding was necessary, leading to unintended modifications in the structure, morphology, and size of the MIPs [17]. Results suggest that the difference between the templates (Cl-NQ-TYR and NQ-TYR) in the polymeric matrix does not affect the resulting polymer morphology, as MIPs and NIPs synthesized under identical conditions exhibited similar structural characteristics [49].

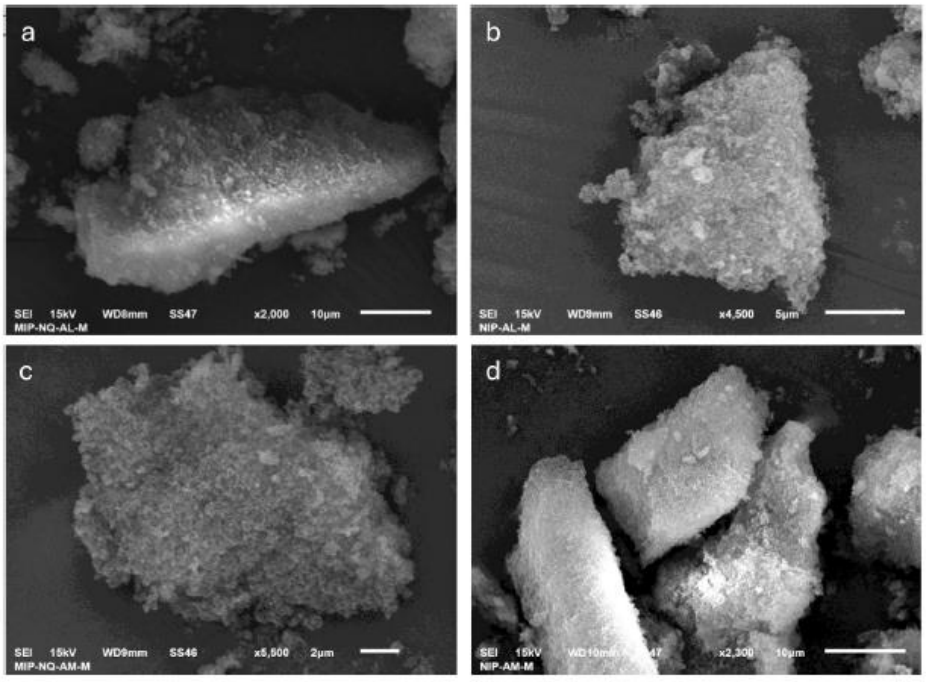

Fig. 2. Scanning electron microscope images for polymers made by the co-precipitation method a) NT-LA-C, b) NT-MA-C, c) N-LA-C and d) N-MA-C. MA, methacrylic acid; LA, lactic acid; C, co-precipitation

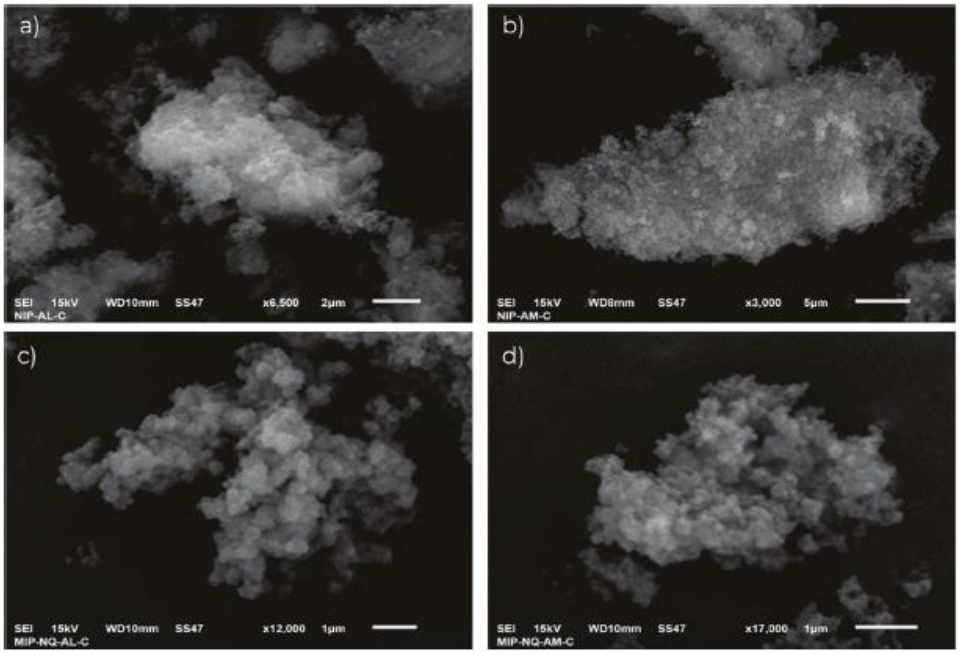

3.4. Infrared Spectroscopy

The presence of the templates in the synthesized MIPs was confirmed through ATR-FTIR analysis, with infrared spectra comparisons between MIPs, template-free MIPs, and NIPs presented in **Figure 4**. Characteristic peaks observed in the 1350–1250 cm^{-1} range correspond to C-N stretching vibrations, while peaks at 750 cm^{-1} were associated with N-H wag vibrations. Additionally, peaks at 804 cm^{-1} and 812 cm^{-1} were attributed to C- Cl stretching vibrations corresponding to the naphthoquinone structure (**Figure 4a** and **4c**). In comparison with **Figures 4b** and **4d**, the spectrum did not significantly change with peaks attributed to vibration of amine groups, which proved that templates were successfully imprinted [50, 51].

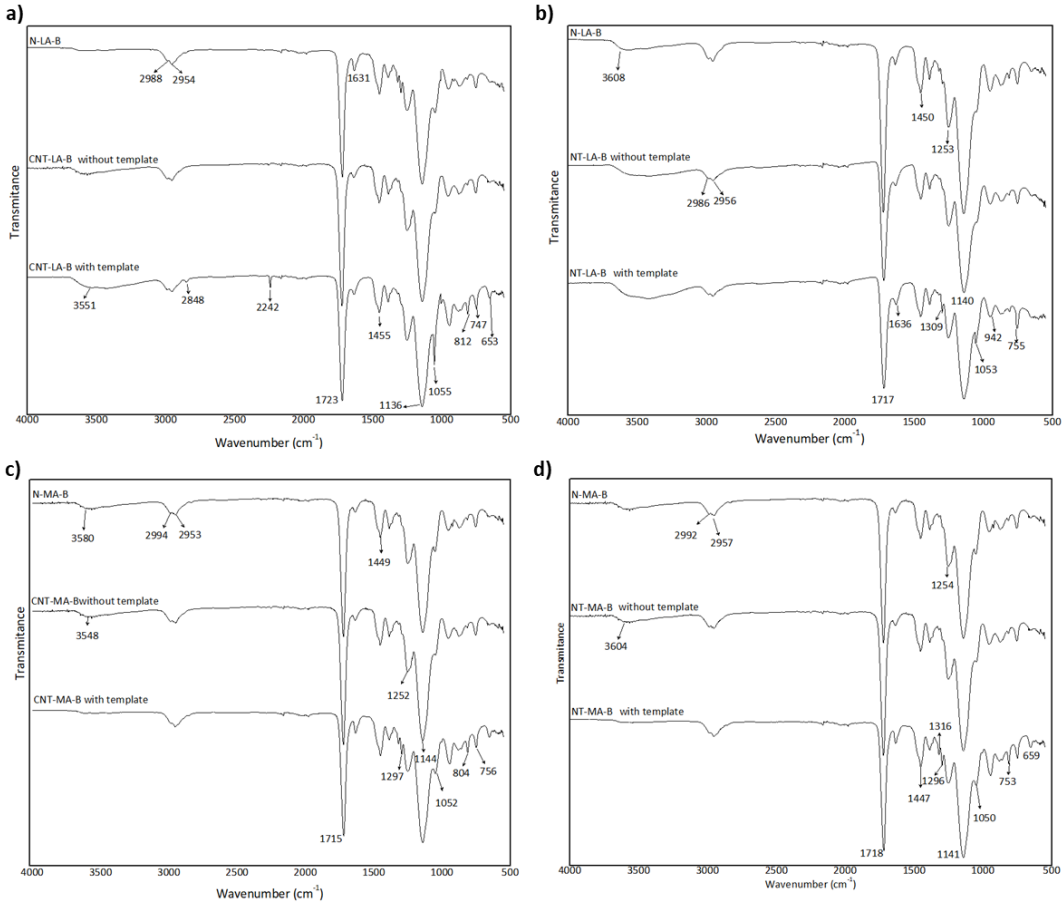

Figure 4. Spectral ATR-FTIR spectrum, NIP, MIP before and after extraction of the template: a) CNT-LA-B, b) NT-LA-B c) CNT-MA-B and d) NT-MA-B. *M, Molecular imprinting polymer; N, nonimprinting polymer; MA, methacrylic acid; LA, lactic acid; B, bulk; C, co-precipitation.*

On the other hand, two distinct bands corresponding to carboxylic acid groups were identified within the working spectral range (1720–1250 cm^{-1}), corresponding to *v*(C=O) and *v*(C-O) vibrations. Peaks at 1450 cm^{-1} and 1140 cm^{-1} correspond to symmetric stretching vibrations of COO^- and -C-O-C- of carboxylic acid. In addition, a broad peak between 3300 and 3600 cm^{-1} was associated with the C-H elongation (COOH groups), while the peak at 1630 cm^{-1} was attributed to the C=C bond, formed by the cross-linker (EDGMA) and functional monomers (LA and MA). Even when the ATR-FTIR spectra of the MIPs and NIPs show a similar pattern, it is because of the structure of the polymeric base; however, distinctive signals of the functional groups corresponding to the template molecules (Cl-NQ-TYR and NQ-TYR) were observed in the charged MIPs. These signals were not detected in the MIPs and NIPs after extraction, indicating that the presence of the analyte was due to its incorporation during polymerization. The disappearance of these bands after the washing process confirms a successful extraction without affecting the structural integrity of the polymer. This observation and the difference in retention percentages between MIPs and NIPs (**Table 3**) represent solid evidence of the imprinting molecular process. According to the literature, infrared spectroscopy is widely employed because it identifies the initial interaction between the functional monomer, the template, and the template removal [50, 51]. The structural stability of the polymer plays a fundamental role in its interaction with the analyte. In this study, MA and LA remained in their non-ionized forms due to their acidic nature in aqueous media and under acidic conditions (**Figure S1**). The carboxyl group (-COOH) facilitates strong interactions with hydrogen bond donors and acceptors, as well as electrostatic interactions within the naphthoquinone derivative structure. Specifically, the oxygen within the carboxyl group functions as a hydrogen bond acceptor, forming bonds with hydrogen donors. The structural composition of naphthoquinone derivatives includes an amino group, three carbonyl groups, and a carboxyl group, all of which provide a robust foundation for these interactions [17, 40].

3.5. Surface charge distribution and zero charge point

One of the defining characteristics of molecularly imprinted materials designed for drug release is the interaction between the template molecule and the electrostatic charges of the functional groups introduced by the functional monomer. These interactions play a critical role in determining the zero point of charge (ZPC) [17, 52]. **Figure 5** illustrates the potentiometric curves for the MIPs CNT-LA-B and CNT-LA-B, and its respective blank. As shown in **Figure 5a.** for the MIP with MA, the intersection of these curves at a pH of 4.8 confirms its acidic nature, which aligns with the pKa value (4.7) of the employed monomer (MA). Additionally, **Figure 5b** presents the ZPC (3.8) of the polymers synthesized with lactic acid as the functional monomer, emphasizing the significant impact of lactic acid on the polymer's acidic properties concerning pH. These results underscore the necessity of careful monomer selection during polymer synthesis, as it directly influences the physicochemical properties of the resulting MIPs. Based on these results, the release behavior of naphthoquinones through the MIPs at a pH higher than the ZPC is expected; the polymeric matrix will be ionized, thereby promoting drug release. The surface charge of a material immersed in an aqueous solution arises from its interactions with surrounding ions (H^+ and OH^-). Consequently, the surface charge potential is closely associated with the density of functional groups in the polymer structure and the pH of the medium [49]. To further understand this phenomenon, the surface charge of the MIPs was evaluated over a broad pH range. Figures 5c and 5d illustrate the charge distribution of CNT-MA-B and CNT-LA-B MIPs as a function of pH, revealing distinct material charge characteristics across different pH values. For CNT-MA-B, a negative charge predominates above the ZPC, suggesting a strong tendency for lectrostatic interactions with positively charged species in solution. Contrarily, below the ZPC, the material shows a positive charge, suggesting a greater affinity for negatively charged species. These results show the acid-base properties of CNT-MA-B and its ability to adjust its charge in response to the pH of the environment. In contrast, CNT-LA-B displays a slightly positive surface charge across a pH range of 2 to 9, with a marked increase in charge at higher pH values, indicating greater positivity. This behavior suggests that CNT-LA-B may demonstrate a stronger affinity for negatively charged species

in alkaline conditions. The detailed analysis of surface charge distribution as a function of pH provides valuable insights into the electrostatic interactions and the MIPs' selectivity toward different charged species.

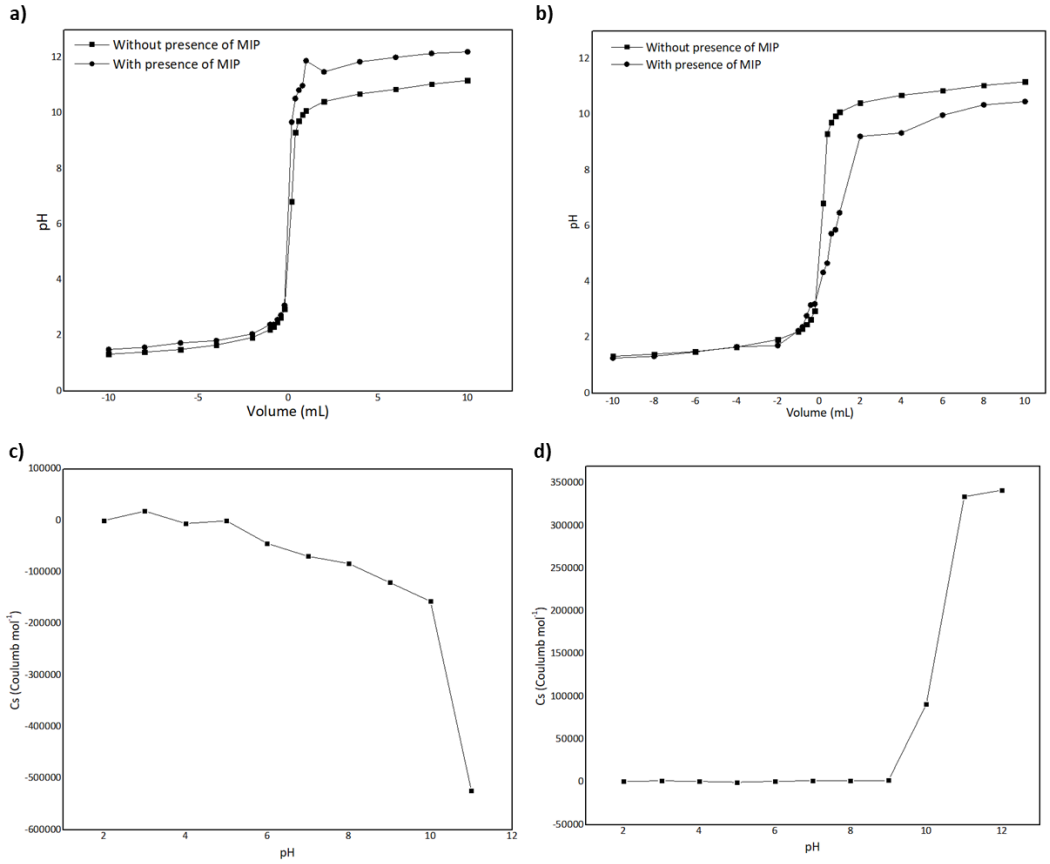

Figure 5. Potentiometric curves: a) blank and CNT-MA-B solution, and b) blank and CNT-LA-M solution. Surface charge distribution of c) CNT-MA-B and d) CNT-LA-B.

3.6. Adsorption isotherms of MIPs

Adsorption experiments were conducted to determine the most suitable model for describing the adsorption behavior of the synthesized MIPs. The equilibrium data were analyzed using the Freundlich, Langmuir, and SIPS models, with the selection based on the correlation coefficient (R^2), prioritizing values closest to 1. The adsorption isotherm parameters for the studied MIPs are summarized in **Table 4** considering the maximum adsorption capacity (Q_m o N_t), the analyte affinity (*kL, kF, a*) and the system heterogeneity (*n, m*). The MIPs CNT-LA-C and CNT-LA-B exhibited a better fit to the Freundlich model, suggesting the presence of multiple

adsorption layers within their polymeric structures. This model is particularly appropriate for systems with heterogeneous adsorption surfaces, indicating the existence of adsorption sites with varying affinities and retention capacities. The adoption of the Freundlich model highlights the structural complexity and interactive nature of these MIPs, underscoring their potential for selective adsorption of target molecules. In this model, unfavorable adsorption occurs when $0 < n < 1$, while $n > 1$ indicates favorable adsorption, and $n = 1$ represents a linear adsorption process [53]. The application of the Freundlich model emphasizes the diversity and heterogeneity of the MIP surfaces. Contrarily, NT-LA-C, NT-LA-B, CNT-MA-B, and NT-MA-B were best described by Langmuir model, suggesting a monolayer adsorption mechanism. This result implies that these polymers possess a homogeneous surface with a finite and specific number of binding sites for molecule adsorption. The Langmuir model assumes that each binding site is independent and exhibits a constant affinity for target molecules. Consequently, the adsorption capacity of these MIPs depends on the saturation of individual binding sites, suggesting a uniform distribution of active sites across the polymeric surface [36]. Meanwhile, the experimental data for CNT-MA-C and CNT-MA-C showed an optimal fit to the SIPS model. The SIPS model indicates that the binding sites may exhibit homogeneous and heterogeneous characteristics. Therefore, the polymer surface may contain different types of adsorption sites with diverse affinities and retention capacities. This heterogeneity enhances the selectivity and specificity of the MIPs for the target molecule [54]. CNT-LA-C and NT-MA-C showed a higher adsorption capacity among the evaluated MIPs. The Langmuir model presented values for Q_m of 13,204.5 mg g^{-1} and 859,770.1 mg g^{-1}, respectively. Even when the last value is unusually high, it could indicate the model's limitation in heterogeneous systems. Results of the Sips model (N_t de 201.4 y 156.7 mg g^{-1}, respectively) with high correlation coefficients ($R^2 > 0.939$) support the high adsorbent capacity of the materials. The Freundlich model also showed adequate adsorption with values of n > 1 (1.063 y 1.127, respectively), indicating a heterogeneous surface with active sites. These results suggest that the functional monomer (lactic acid or methacrylic acid) and the polymerization method (bulk or co-precipitation) significantly affect

the formation and efficiency of the recognition sites. Other MIPs like CNT- MA-C and NT-LA-C also presented adequate adsorption capacity (Q_m = 203 - 356 mg g^{-1}), confirming that the molecular imprinting was effective with different efficiencies depending on the formulation and synthesis method. Overall, adsorption data indicates that the evaluated MIPs possess specific recognition sites to naphthoquinone derivatives, where the more efficient materials were synthesized by the co-precipitation method and using lactic acid or methacrylic acid as functional monomers.

Table 4. Adsorption isotherm constants of MIPs (10 mg of MIP, 1 hour of contact, 5 mL of solution, medium temperature: 24°C, medium pH: 6).

MIP	Langmuir			Freundlich			Sips			
	Qm (mg g^{-1})	k_L	R^2	k_F (L mg^{-1})	n	R^2	N_t (mg g^{-1})	a (L g^{-1})	m	R^2
CNT-LA-C	13204.50	2.12E-06	0.9193	2.2849	1.0626	0.9703	201.3524	5.2945	136.1671	0.9387
CNT-LA-B	240.5377	0.0193	0.9093	7.7192	0.7157	0.9858	30470.7302	9.48E-06	0.7160	0.9629
NT-LA-C	203.8504	0.0280	0.9892	8.4105	0.7134	0.9838	192.8135	0.0338	1.0628	0.9876
NT-LA-B	179.5702	0.0292	0.9772	8.1688	0.6845	0.9675	122.9221	10.3528	118.5963	0.9511
CNT-MA-C	355.9430	0.0066	0.9415	2.7195	0.8959	0.9298	134.6689	5.5318	123.4485	0.9846
CNT-MA-B	129.8040	0.0235	0.9447	149.8840	0.0235	0.9047	109.0470	6.0696	144.4540	0.9251
NT-MA-B	249.8820	0.0251	0.9557	8.2264	0.5836	0.9309	119.7071	5.0611	114.5440	0.9050
NT-MA-C	859770.08	3.25E-06	0.9459	1.8656	1.1271	0.9337	156.6817	6.9875	131.1907	0.9964

Qm is the maximum amount of adsorbate on adsorbent at equilibrium. k_L is Langmuir's constant, k_F is Freundlich's constant, n is the exponent of the Freundlich isotherm, a and m are the SIPS isotherm constants, and R^2 is the correlation coefficient.

3.7. Imprinting factor

The selectivity of the MIPs was evaluated based on the imprinting factor (IF). which quantifies the relative ability of the MIPs to adsorb their target molecule compared to their corresponding NIP. The IF values for each MIP are summarized in **Table 5.** This factor is calculated by dividing the adsorption capacity of the MIP by that of the NIP for the target molecule. An IF greater than one indicates a higher affinity and selectivity toward the target molecule, whereas an IF less than one suggests low selectivity and similar adsorption performance to the NIP [55, 56]. Results revealed that all MIPs exhibited IF values greater than one, confirming their selective recognition ability. Notably, the MIPs synthesized with the Cl-NQ-TYR template displayed slightly higher IF values than those synthesized with the NQ-TYR

template. These values quantitatively demonstrate the selectivity of each MIP, which is crucial for determining their applicability in controlled drug release systems. These findings align with the retention capacities reported for the MIPs compared to their NIPs, where the latter exhibited lower adsorption capacity (**Table 3**).

Table 5. Partition coefficients and printing factors of Cl-NQ-TYR and NQ-TYR on the corresponding MIP and NIP.

MIP/NIP	Q_{MIP}	Q_{NIP}	IF
CNT-MA-B/N-MA-B	1.99	1.26	1.56
CNT-MA-C/N-MA-C	1.97	1.04	1.89
CNT-LA-B/N-LA-B	1.97	1.15	1.7
CNT-LA-C/N-LA-C	1.83	1.05	1.73
NT-MA-B/N-MA-B	1.87	1.57	1.18
NT-MA-C/N-MA-C	1.87	1.53	1.21
NT-LA-B/N-LA-B	1.85	1.33	1.38
NT-LA-C/N-LA-C	1.89	1.37	1.35

3.8. Release Profile and Kinetics of Cl-NQ-TYR and NQ-TYR by MIPs

The *in vitro* release behavior of NQ-TYR and Cl-NQ-TYR was carried out in phosphate buffer at pH 5.4, natural pH of healthy skin, over a 24-hour period. Most MIPs display a similar release profile, characterized by an initial burst release followed by a sustained and controlled release over time (**Figure 6**). **Figure 6a** illustrates the NQ-TYR release profile over 24 hours. In the initial phase, a burst release was observed for all MIPs, except for NT-MA-B, which the release rate decreased during the first 8 hours. In contrast, the other three MIPs demonstrated a continuous decrease in the release rate after the initial burst phase, indicating better control over NQ-TYR release. Notably, the NT-MA-C MIP exhibited the highest release capacity. A similar behavior was observed for the Cl-NQ-TYR, CNT-LA-B, and CNT-LA-C, where an initial burst release was followed by a gradual decline in the release rate, indicating a controlled and sustained release. These results highlight the influence of polymer composition and synthesis method on the release profile of the template molecules, further emphasizing the role of molecular imprinting in controlling drug release behavior. The CNT-MA-B polymer exhibited a distinct release profile, maintaining a constant release from the beginning, with a slight increase at 2 hours and

stabilization throughout the 24-hour evaluation period. This behavior highlights differences between the interactions of every template, the functional monomers, and the synthesis method. Our results suggest that NQ-TYR and Cl-NQ-TYR MIPs can control the target molecule release, offering different profiles depending on specific conditions. Moreover, the molecule release can be adjusted according to therapeutic needs or specific requirements, highlighting their application potential in controlled and targeted release systems. These results provide a deeper understanding of the release kinetics and mechanisms essential for device design optimization and therapeutic applications. The Langmuir model predicted a higher adsorption capacity for the MIP NT-A-C, suggesting a great affinity between the polymeric matrix and the naphthoquinone, according to the correlation factor in the Sips model (R^2= 0.996). However, this material presented a moderate release (35.35 mg L^{-1} in 24h), suggesting a strong retention of the template, consistent with the high adsorption capacity and the observed retention percentage (95%). On the contrary, MIPs like CNT-MA-B, even when they present lower adsorption capacity (Q_m = 129.8 mg g^{-1}), higher antibiotic release was observed (66.88 mg L^{-1} in 24 h), probably due to the weaker interactions or lower specificity of the system. This behavior was also observed in the low n parameter of the Freundlich model (n = 0.023), indicating a least favorable adsorption process. Overall, results suggest that even when the antibiotic was efficiently charged, the interactions with the matrix were not strong enough to prolong the release in physiological conditions.

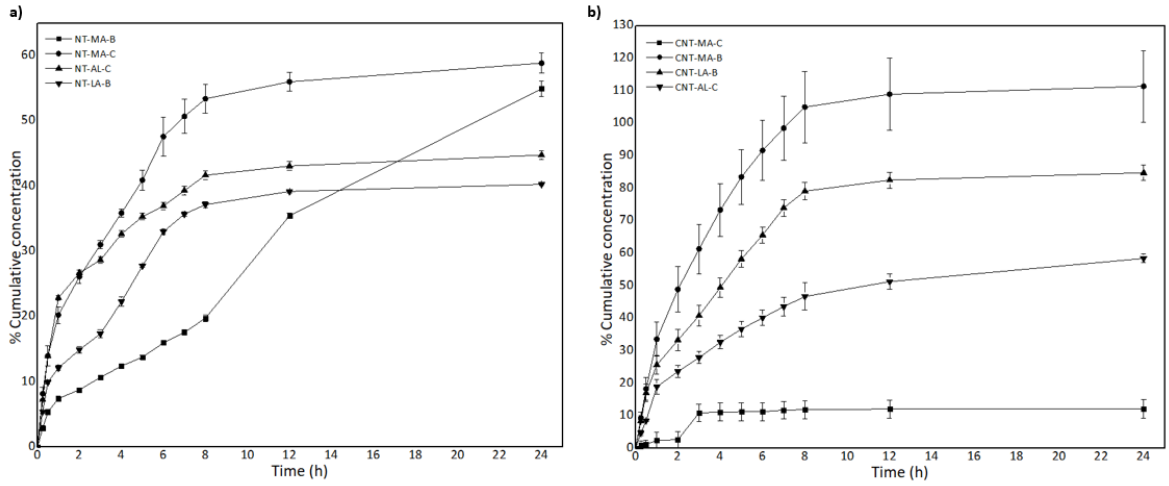

Figure 6. Cumulative concentration release of a) NQ-TYR and b) Cl-NQ-TYR present in each of the MIPs. Each point represents the arithmetic mean ± SD of 3 independent experiments. *M, Molecular imprinting polymer; N, non-imprinting polymer; MA, methacrylic acid; LA, lactic acid; B, bulk; C, co-precipitation.*

The influence of the monomer type was evident. Materials synthesized with MA, with PZC of 4.8-5.4, will present partially ionized carbonyls, generating a slightly negative surface, favoring the electrostatic interaction with protonated template molecules, promoting their retention, allowing a more controlled release, and causing a light ionic repulsion to negatively charged molecules. On the other hand, LA (PZC = 3.8) forms a more negative surface at the same pH, which could improve the ionic repulsion with the drug if it also presents negative charges, favoring a quick release and being less controlled. On the other hand, the chemical structure of the templates used also influences the release profile. Both molecules share a naphthoquinone and tyrosine nucleus; however, CNT has a Cl atom in the third position, increasing its polarity and the capacity to form dipole-dipole interactions and stronger hydrogen bonds with the functional monomer. This structural difference may explain the more controlled release observed in some systems, like CNT-MA-C (7.32 mg L-*1* in 24 h) and NT-MA-C (35.35 mg L-*1* in 24 h), compared with their counterparts based on LA, which PZC is lower (3.8), generating a more negative surface inducing higher repulsion.

Finally, the synthesis method was decisive. The synthesized MIPs using the co-precipitation method presented lower cumulated release values, indicating higher structural stability of the polymeric matrixes and specific cavities, like CNT-MA-C, NT-MA-C, and NT-LA-C with total release values between 7.32 and 35.35 mg L^{-1}. On the contrary, synthesized MIPs with the bulk process presented a release of higher concentrations, like the one observed in CNT-MA-B (66.88 mg L^{-1}) and NT-MA-B (33.00 mg L^{-1}), which could be due to lower reticulation density and less specific cavities formation. Our controlled release results through MIPs are similar to systems previously reported. For example, Alhuwaila et al. [57] valuated amoxicillin (AMOX) release from poly (vinyl sulfone) (PVS) electrophile matrixes showing rapid release in the fibers without MIP (731% in 90 min), an average release in the NIP system

(~53.9 % in 24 h) and a controlled release in the PVS-AMOX-MIP (43.6 % after 48 h, with 36 % release in 180 min). The kinetics of the MIP was adjusted to the Korsmeyer–Peppas model (R^2 = 0.9985, n = 0.53), indicating a non-Fickian mechanism, meaning a combined control (diffusion and swallowing), mechanisms also observed in the naphthoquinones MIPs (n≥ 0.5). Likewise, Elhabal et al. [58] studied clindamycin release from MIP nanoparticles and polyurethane nanofibers charged with MIP, showing a prolonged release of ~77 % y ~50 % in 30 h, respectively in 30 h, compared to the 98% in 4 h in a MIP-free solution. Even when a kinetic model was not reported, a biphasic profile with a rapid initial release followed by a sustained phase was observed, similar to the naphthoquinones MIPs. In contrast, other non-imprinted systems like the contribution of Alavarse et al., which uses PVA/quinine nanofibers with tetracycline (TCH), showed a biphasic liberation (~80 % in 24 h) adjusted to a first-order Fickian kinetic (R^2 = 0.991, n = 0.179), where no specific interactions between the drug and the polymer are observed [59]. Differently, MIPs allow a more controlled release because of their specific recognition sites, which decreases the initial burs effect and prolongs drug availability. The naphthoquinone release was evaluated in Franz cells with a PVDF membrane at pH 5.4 and 7.4, which simulate healthy and infected skin conditions, respectively. Also, bi-component and non-electrospinning (lactic acid and EGDMA) polymeric matrixes were considered. Finally, Rukavina et al. reported liposomes charged with azithromycin (AZT), which were evaluated also in Franz cells, where deformable liposomes released up to 70% of the drug in 6 h, against 52% of conventional liposomes [60]. In these cases, the release is determined by the fluency and elasticity of the bilayer. Therefore, the kinetic of the MIPs depends on the molecular affinity and the polymeric network design, providing better control and selectivity in the release.

To further analyze the release profiles of NQ-TYR and Cl-NQ-TYR from the MIPs, the experimental data were fitted to mathematical models describing different release kinetics. The following models were employed: zero- order, first-order, Higuchi, and Korsmeyer-Peppas. The model parameters for the release kinetics are summarized in **Table 6**. The correlation coefficient (R^2) was used to determine the

best fit, with values closer to 1 indicating better correlation. For all MIPs, except NT-MA-B, the release of NQ-TYR and Cl-NQ-TYR was best described by the Korsmeyer-Peppas model. This model provides insights into the drug release mechanism from polymeric matri base for developing new materials to control the release of naphthoquinone derivatives molecules ces. According to the model, the release mechanism could be considered Fickian, non- Fickian (anomalous transport), case II transport, or super case II transport, depending on the n value. If $n \leq 0.45$, the mechanism is Fickian; if $0.45 < n < 0.89$, the mechanism is non-Fickian; if $n = 0.89$, the mechanism is case II transport; and if $n > 0.89$, the mechanism is super case II transport [61, 62]. The obtained values indicated that the drug release mechanism followed a non-Fickian diffusion, suggesting that the release follows an anomalous diffusion and implying a complex release involving processes like polymer swelling, chain relaxation, and pores formation in the release matrix system. In contrast, NT-LA-C exhibited a Fickian drug release mechanism, meaning that the release process was primarily diffusion-controlled [63, 64]. Finally, NT- MA-B was fitted with zero order model, indicating a release rate independent of drug concentration.

Table 6. Comparison of kinetic parameters for MIP.

MIP	Zero order			First Order			Higuchi			Korsmeyer-peppas		
	Q_0	K_0	R^2	$LogQ_0$	K_1	R^2	$\%Q_t$	K_H	R^2	k	*n*	R^2
CNT-LA-C	10.356	1.4008	0.6672	2.3221	0.0767	0.3981	5.0783	12.8799	0.9109	2.6453	*0.5522*	**0.9366**
CNT-LA-B	19.4714	1.9017	0.5893	2.8056	0.0734	0.4056	8.9656	19.803	0.8439	3.1392	*0.526*	**0.9447**
CNT-MA-C	2.9301	0.3072	0.3725	0.8111	0.084	0.2811	1.7516	3.0806	0.5964	1.0603	*0.652*	**0.8225**
CNT-MA-B	27.3192	2.461	0.5332	3.0805	0.0753	0.3443	13.7156	26.2862	0.8123	3.3736	*0.5704*	**0.9239**
NT-LA-C	13.8906	0.7915	0.5078	2.5202	0.0503	0.3234	12.7907	8.5135	0.7879	2.8831	*0.3832*	**0.8862**
NT-LA-B	9.3533	0.896	0.5920	2.1172	0.0689	0.4551	4.69	9.2529	0.8319	2.4893	*0.4704*	**0.9411**
NT-MA-C	14.7145	1.2299	0.5930	2.57	0.0639	0.4204	9.3057	12.8203	0.851	2.9318	*0.4538*	**0.9537**
NT-MA-B	2.3198	1.3131	0.**9800**	1.3987	0.1066	0.7725	-7.1266	11.2506	0.9013	1.8678	*0.5819*	0.9448

Q_0 is the cumulative amount of drug released at time t, Q_t is the initial amount of drug in solution and K_0 is the zero-order release constant. Q_t/Q_∞ is the rate of change in drug concentration in solution with respect to time and the value K_1 is the first order release rate constant, K_H is the Higuchi release constant, k is the constant and n is the release exponent, n is the diffusion or release exponent. M, Molecular imprinting polymer; N, non-imprinting polymer; MA, methacrylic acid; LA, lactic acid; B, bulk; C, co-precipitation.

3.9. Antimicrobial activity

Table 7 shows the antimicrobial activity of NQ derivatives released through their respective MIP. All synthesized MIPs presented a Minimum Inhibitory Concentration (MIC) of 12.5 μg mL $^{-1}$ against *E. coli*, and 3.12 μg mL $^{-1}$ against *S. aureus*. These results emphasize the antimicrobial effectiveness of Cl-NQ-TYR and NQ-TYR MIPs. On the other hand, NIPs showed no antibacterial activity, indicating that the synthesis components lack antibacterial activity against the evaluated bacteria. Therefore, the antimicrobial activity is exclusively related to the naphthoquinone derivatives released through the MIPs. Pathogenic bacteria commonly found in infected wounds include *S. aureus* and *E. coli*, requiring broad-spectrum antibiotics for effective treatment [65]. Recently, naphthoquinone derivatives represented an opportunity to find efficient solutions against bacterial resistance and safeguard public health [66] since their antimicrobial activity is improved by modifying their base structure [67]. However, to ensure safe administration and improve functionality, a controlled release vehicle is essential. This strategy not only enhances therapeutic efficacy but also reduces bacterial resistance by directly delivering the antimicrobial agent to the infection site. As a result, research efforts have increasingly focused on developing materials with improved functionality, controlled release properties, and high biocompatibility. The antimicrobial release efficiency through molecular imprinting techniques of ciprofloxacin (CPX) has been confirmed by our research group before [17]. Results showed MICs within the ranges established by the Clinical and Laboratory Standards Institute, confirming the effectiveness of MIPs in their antimicrobial activity against *S. aureus* (ATCC 25923) and *E. coli* (ATCC 25922). Also, other studies using vancomycin-controlled release through MIPs were demonstrated through a non-Fickian transport [68]. Likewise, chitosan nanocapsules loaded with 2,3-dichloro-1,4-naphthoquinone were developed and evaluated for their antimicrobial activity against *S. aureus* (ATCC 14458 and ATCC 29213), *S. epidermidis*, and *S. pyrogenes* (ATCC 19615). Minimum inhibitory concentrations (MICs) of 1.2-2.5 mg mL^{-1} and 0.3-5 mg mL^{-1} were obtained for *S. aureus* (ATCC 14458) and *S. aureus* (ATCC 29213), respectively [69]. These values are higher than those obtained in our study, possibly due to the release

capacity of MIPs that allows for an initial burst release, as observed in our initial evaluation tests. The increasing prevalence of antibiotic resistance and the limitations of conventional drug administration are critical issues that must be addressed. Inadequate antibiotic concentrations at infection sites and the need for frequent dosing have significantly contributed to the global crisis of bacterial resistance, posing a major challenge for modern medicine. Therefore, the development of innovative materials with antimicrobial properties and efficient DDS is crucial. MIPs stand out as promising drug delivery platforms, enabling precise and sustained release while offering significant advantages for enhancing therapeutic outcomes and mitigating bacterial resistance.

Table 7. Antimicrobial activity of MIPs and NIPs shown against the planktonic form of *Escherichia coli* (ATCC 25922) and *Staphylococcus aureus* (ATCC 25923).

Antimicrobial activity	Lactic acid				Methacrylic acid			
	CNT-LA-B	CNT-LA-C	NT-LA-B	NT-LA-C	CNT-MA-B	CNT-MA-C	NT-MA-B	NT-MA-C
MIC (µg ml^{-1}) *E. coli*	12.5	12.5	-	-	12.5	12.5	-	-
CMB (µg ml^{-1}) *E. coli*	25	25	-	-	25	25	-	-
MIC (µg ml^{-1}) *S. aureus*	3.12	3.12	-	-	3.12	3.12	-	-
CMB (µg ml^{-1}) *S. aureus*	3.12	3.12	-	-	3.12	3.12	-	-

3.10. Cytotoxicity

Biocompatibility testing is essential to guarantee the safe application of MIPs in medical devices. The International Organization for Standardization (ISO) recommends cytotoxicity testing as an essential part of biological assessment, enabling the detection of potential adverse effects and improvements in biological functionality. Compliance with ISO guidelines on cell viability and cytotoxicity is crucial to ensure medical device safety, safeguarding patient health and ensuring reliable, high-quality treatments. specifies the criteria for in vitro cell viability testing in medical materials and devices, establishing that a cell viability of 70% or higher is considered acceptable for ensuring compatibility with human tissues. In this study, cell viability was evaluated using the MTT assay with human dermal fibroblasts

(HDFn). Untreated cells served as positive control, representing normal cell viability, while hydrogen peroxide-exposed cells were used as a negative control to induce cellular stress. The viability data (**Figure 7**) depict HDFn cell responses after 24 hours of exposure. None of the evaluated MIPs exhibited cytotoxic effects throughout the study, and a notable increase in cell viability was observed across all MIPs, particularly in the CNT-AL-M MIP. These findings suggest that the synthesized MIPs are non-hazardous to HDFn cells and may even improve their viability compared to the control group. These results indicate that the synthesized MIPs are not harmful to HDFn cells and may even enhance cell viability compared to the control group. This study supports the biocompatibility and safety of MIPs synthesized using lactic acid (LA) and methacrylic acid (MA) loaded with naphthoquinone derivatives.

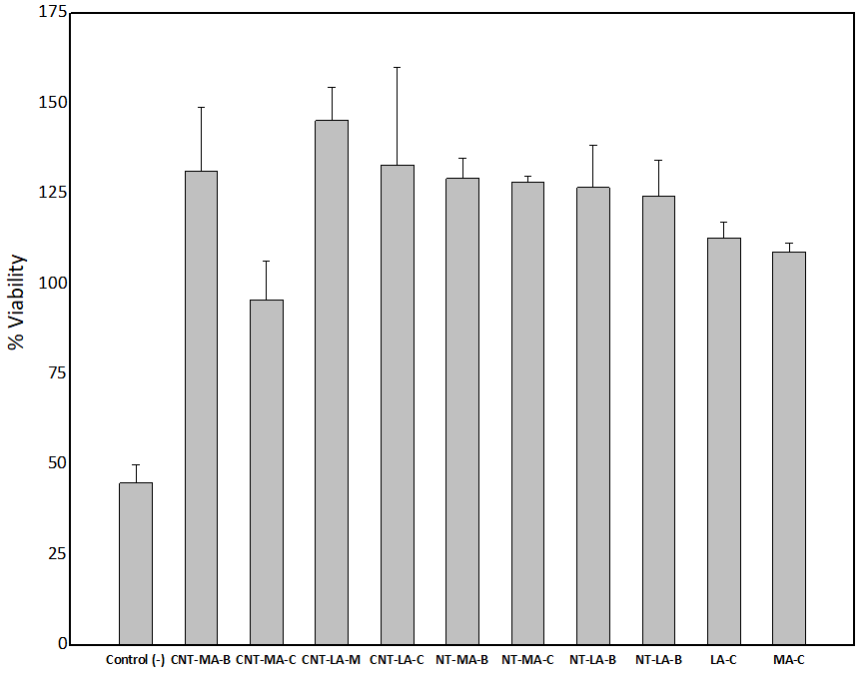

Figure 8. Percentage of viability Dermal Fibroblast cells (nHDF) versus extracts obtained from 24 h exposure of MIPs and NIPs in PBS at pH 5.4, using the MTT assay, each point represents the arithmetic mean ± SD of 3 independent experiments.

M, Molecular imprinting polymer; N, non-imprinting polymer; MA, methacrylic acid; LA, lactic acid; B, bulk; C, co-precipitation.

The findings surpassed the ISO-established viability threshold, confirming the suitability of these polymers for biomedical and environmental applications. Moreover, the absence of cytotoxicity in HDFn cells reinforces the potential of MIPs as safe and effective materials for medical devices. These outcomes further validate the therapeutic promise of naphthoquinone-loaded MIPs in biomedical applications.

Some limitations are considered when interpreting the results of this study. The release assay was performed using a PVDF membrane; however, the evaluation in skin tissues may offer a more realistic perspective on NQ release through MIPs. Even when *in vitro* assays give helpful information, *in vivo* assays would allow us to extrapolate results in a more complex and representative biological scenery. On the other hand, the exclusive use of ATCC strains confirms that the MIPs release NQ with antimicrobial properties; however, efficacy assessment against multiresistant or clinically isolated infection strains would offer a broader vision of their antimicrobial potential. Finally, cytotoxicity was assessed in dermal fibroblasts; nevertheless, studies in other cell lines like keratinocytes or immune cells would contribute to a more integral understanding of their safety and potential secondary effects in related tissues with wound healing. These areas represent critical opportunities for future research that could enhance experimental design and improve the relevance of the reported results. Currently, topic administration products for infection treatments in wounds face diverse limitations, for example, the need for frequent applications, a limited capacity to control the drug release, and inefficacy against antimicrobial resistance. However, previous studies have demonstrated that the use of MIPs in controlled drug release, applied in different disease treatments through diverse administration routes, is promising under a security profile [20, 21, 40, 70, 71]. A material with local and controlled drug release and antimicrobial activity was developed, demonstrating their safety against dermal fibroblasts. Even when results are promising, additional research is needed to evaluate their efficacy and effectiveness in animal models and, further, in humans.

4. Conclusions

Several MIPs were synthesized using two functional monomers (LA and MA) and were evaluated as release systems of NQ derivatives with antimicrobial activity. Retention studies demonstrated that all MIPs presented high retention percentages (>90%), compared to a maximum of 63.43% of their non-imprinting homologs (NIPs), which confirm the MIPs' capacity to adsorb molecules by forming specific cavities for each template. The NQ release behavior was influenced by the surface charge potential and the pH. Higher pH than the zero charge point of each MIP (3.8 for MIPs with LA and 4.7 for MIPs with MA) favored the template release. The drug release mechanisms were complex, involving processes like polymer swallowing, chain relaxation, and pores formation, resulting in a burst initial release, followed by a decrease in the release velocity and ending with a constant drug release after 2 hours. Antimicrobial assays confirmed the antimicrobial activity of NQ derivatives released by the MIPs, demonstrating an effective activity against strains like *S. aureus* and *E. coli.* In addition, cytotoxicity assays in dermal fibroblasts demonstrated the MIPs' security. These findings suggest that MIPs possess promising properties for the controlled release of antimicrobial activity molecules, like NQ.

Even when further studies are needed for their application as drug-release devices, this study presents a solid base for developing new materials to control the release of naphthoquinone derivatives molecules.

Ethics approval and consent to participate.

The paper reflects the authors' own research and analysis in a truthful and complete manner.

Consent for publication

All people who meet authorship criteria are listed as authors, and all authors consent to participate and publish in the work to take public responsibility for the content.

Availability of data and materials

Data available on request from the authors.

Competing interest

The authors declare that they have no known competing financial interests or personal relationships that could have appeared to influence the work reported in this paper.

Funding

The authors acknowledge grants and fellowships from the Secretaría de Ciencia, Humanidades, Tecnología e Innovación (SECIHTI) Academic Doctoral Research CVU 1078903 and Sectoral Research Fund for Education Basic-Science # A1-S-28176.

Authorship contributions statement

Vanessa Sarahí Galván-Romero: Conceptualization, Methodology, Investigation, Formal analysis, Writing original draft. **Rogelio Flores-Ramírez**: Conceptualization, Investigation, Funding acquisition, Data curation, Validation, Writing – review & editing. **Fernando González-Salazar**: Methodology, Writing – review & editing. **Karla Ximena Vargas-Berrones**: Investigation, Data curation. **Blanca Nohemí Zamora Mendoza**: Investigation, Formal analysis. **Fidel Martínez-Gutiérrez**: Supervision, Writing – review & editing. **Denisse Atenea de Loera Carrera**: Resources, Project administration. **Luz Eugenia Alcántara-Quintana**: Supervision, Conceptualization, Writing – review & editing.

References

[1] T.-N. Pham, P. Loupias, A. Dassonville-Klimpt, P. Sonnet, Drug delivery systems designed to overcome antimicrobial resistance, Medicinal Research Reviews 39(6) (2019) 2343-2396.

[2] F. Nainu, A.D. Permana, N.J.N. Djide, Q.K. Anjani, R.N. Utami, N.R. Rumata, J. Zhang, T.B. Emran, J. Simal-Gandara, Pharmaceutical Approaches on Antimicrobial Resistance: Prospects and Challenges, Antibiotics 10(8) (2021) 981.

[3] V. Puca, R.Z. Marulli, R. Grande, I. Vitale, A. Niro, G. Molinaro, S. Prezioso, R. Muraro, P. Di Giovanni, Microbial species isolated from infected wounds and antimicrobial resistance analysis: Data emerging from a three-years retrospective study, Antibiotics 10(10) (2021) 1162.

[4] P.K. Mantravadi, K.A. Kalesh, R.C.J. Dobson, A.O. Hudson, A. Parthasarathy, The Quest for Novel Antimicrobial Compounds: Emerging Trends in Research, Development, and Technologies, Antibiotics 8(1) (2019) 8.

[5] B.R. Jali, R. Behura, S.R. Barik, S. Parveen, S.P. Mohanty, R. Das, A brief review: biological implications of naphthoquinone derivatives, Research Journal of Pharmacy and Technology 11(8) (2018) 3698-3702.

[6] N.S. Mone, S. Syed, P. Ravichandiran, E.E. Kamble, K.R. Pardesi, S. Salunke-Gawali, M. Rai, A. Vikram Singh, S. Prasad Dakua, B.H. Park, Synergistic and Additive Effects of Menadione in Combination with Antibiotics on Multidrug-Resistant Staphylococcus aureus: Insights from Structure-Function Analysis of Naphthoquinones, ChemMedChem 18(24) (2023) e202300328.

[7] L. Xu, Y. Zhou, D. Ou, H. Yang, H. Feng, H. Song, N. Xie, X. Niu, X. Deng, M. Sun, Potent synergistic efficacy of 2-methoxy-1, 4-naphthoquinone derived from quinones against drug-resistant bacteria, One Health Advances 2(1) (2024) 1.

[8] E. Leyva, S. Loredo-Carrillo, L. López, E. Escobedo-Avellaneda, G. Navarro-Tovar, Importancia química y biológica de naftoquinonas. Revisión bibliográfica, Afinidad 74(577) (2017).

[9] C.E. Pereyra, R.F. Dantas, S.B. Ferreira, L.P. Gomes, F.P. Silva-Jr, The diverse mechanisms and anticancer potential of naphthoquinones, Cancer Cell International 19 (2019) 1-20.

[10] M.-Y. Lim, J.-H. Jeon, E.-Y. Jeong, C.-H. Lee, H.-S. Lee, Antimicrobial activity of 5-hydroxy-1, 4-naphthoquinone isolated from Caesalpinia sappan toward intestinal bacteria, Food chemistry 100(3) (2007) 1254-1258.

[11] D. Choudhari, D.N. Lande, D. Chakravarty, S.P. Gejji, P. Das, K.R. Pardesi, S. Satpute, S. Salunke-Gawali, Reactions of 2, 3-dichloro-1, 4-naphthoquinone with aminophenols: evidence for hydroxy benzophenoxazine intermediate and antibacterial activity, Journal of Molecular Structure 1176 (2019) 194-206.

[12] S.A. Kelly, A.M. Rodgers, S.C. O'Brien, R.F. Donnelly, B.F. Gilmore, Gut Check Time: Antibiotic Delivery Strategies to Reduce Antimicrobial Resistance, Trends in Biotechnology 38(4) (2020) 447-462.

[13] M. Dallo, K. Patel, A.A. Hebert, Topical Antibiotic Treatment in Dermatology, Antibiotics 12(2) (2023) 188.

[14] K. Razdan, V.R. Sinha, K.K. Singh, New Paradigms in the Treatment of Skin Infections: Lipid Nanocarriers to the Rescue, in: M. Rahman, S. Beg, V. Kumar, F.J. Ahmad (Eds.), Nanomedicine for Bioactives : Healthcare applications, Springer Singapore, Singapore, 2020, pp. 317-339.

[15] K. Razdan, J. Garcia-Lara, V. Sinha, K.K. Singh, Pharmaceutical strategies for the treatment of bacterial biofilms in chronic wounds, Drug Discovery Today 27(8) (2022) 2137-2150.

[16] E. Eriksson, P.Y. Liu, G.S. Schultz, M.M. Martins-Green, R. Tanaka, D. Weir, L.J. Gould, D.G. Armstrong, G.W. Gibbons, R. Wolcott, O.O. Olutoye, R.S. Kirsner, G.C. Gurtner, Chronic wounds: Treatment consensus, Wound Repair and Regeneration 30(2) (2022) 156-171.

[17] V. Galván-Romero, F. Gonzalez-Salazar, K. Vargas-Berrones, L.E. Alcantara-Quintana, F. Martinez-Gutierrez, S. Zarazua-Guzman, R. Flores-Ramírez, Development and evaluation of ciprofloxacin local controlled release materials based on molecularly imprinted polymers, European Journal of Pharmaceutics and Biopharmaceutics 195 (2024) 114178.

[18] A. Lusina, M. Cegłowski, Molecularly Imprinted Polymers as State-of-the-Art Drug Carriers in Hydrogel Transdermal Drug Delivery Applications, Polymers 14(3) (2022) 640.

[19] M. Ovezova, F. Yılmaz, I. Göktürk, K.Ç. Güler, A. Denizli, Molecularly imprinted polymers for pharmaceutical and biomedical analysis, Journal of Pharmaceutical and Biomedical Analysis Open 4 (2024) 100038.

[20] S.F. Elhabal, R. Abdelmonem, R.M. El Nashar, M.F.M. Elrefai, A.M.E. Hamdan, N.A. Safwat, M.S. Shoela, F.E. Hassan, A. Rizk, S.L. Kabil, N.A. El-Nabarawy, A.A. Taha, M. El-Nabarawi, Enhanced Antibacterial Activity of Clindamycin Using Molecularly Imprinted Polymer Nanoparticles Loaded with Polyurethane Nanofibrous Scaffolds for the Treatment of Acne Vulgaris, Pharmaceutics 16(7) (2024) 947.

[21] H. Kempe, A. Parareda Pujolràs, M. Kempe, Molecularly Imprinted Polymer Nanocarriers for Sustained Release of Erythromycin, Pharmaceutical Research 32(2) (2015) 375-388.

[22] L.-P. Zhang, X.-X. Tan, Y.-P. Huang, Z.-S. Liu, Floating liquid crystalline molecularly imprinted polymer coated carbon nanotubes for levofloxacin delivery, European Journal of Pharmaceutics and Biopharmaceutics 127 (2018) 150-158.

[23] M. Shadabfar, M. Abdouss, H.A. Khonakdar, Synthesis, characterization, and evaluation of a magnetic molecular imprinted polymer for 5-fluorouracil as an intelligent drug delivery system for breast cancer treatment, Journal of Materials Science 55(26) (2020) 12287-12304.

[24] P. Kaiser, J. Wächter, M. Windbergs, Therapy of infected wounds: overcoming clinical challenges by advanced drug delivery systems, Drug Delivery and Translational Research 11(4) (2021) 1545-1567.

[25] R. Tiwari, K. Pathak, Local Drug Delivery Strategies towards Wound Healing, Pharmaceutics 15(2) (2023) 634.

[26] R. Liu, A. Poma, Advances in Molecularly Imprinted Polymers as Drug Delivery Systems, Molecules 26(12) (2021) 3589.

[27] J. Kupai, M. Razali, S. Buyuktiryaki, R. Kecili, G. Szekely, Long-term stability and reusability of molecularly imprinted polymers, Polymer chemistry 8(4) (2017) 666-673.

[28] N. Ezati, M. Abdouss, M. Rouhani, P.G. Kerr, E. Kowsari, Novel serotonin decorated molecularly imprinted polymer nanoparticles based on biodegradable materials; A potential self-targeted delivery system for Irinotecan, Reactive and Functional Polymers 181 (2022) 105437.

[29] N.E. Valderruten, J. García, Interpenetrating polymer networks of poly (2-hydroxyethyl methacrylate co-itaconic acid) and chitosan as a controlled release matrix, Reactive and Functional Polymers 210 (2025) 106192.

[30] S. Dhanashree, M. Priyanka, K. Manisha, K. Vilasrao, Molecularly imprinted polymers: Novel discovery for drug delivery, Current Drug Delivery 13(5) (2016) 632-645.

[31] S.A. Zaidi, Molecular imprinted polymers as drug delivery vehicles, Drug delivery 23(7) (2016) 2262-2271.

[32] L.I. López-López, E. Rivera-Ávalos, C. Villarreal-Reyes, F. Martínez-Gutiérrez, D. de Loera, Synthesis and Antimicrobial Evaluation of Amino Acid Naphthoquinone Derivatives as Potential Antibacterial Agents, Chemotherapy 67(2) (2021) 102-109.

[33] Kuzin IA, Loskutov AI, USSR, j. Appl. Chem 39(1) (1996) 85.

[34] M. Musah, Y. Azeh, J.T. Mathew, M.T. Umar, Z. Abdulhamid, A.I. Muhammad, Adsorption kinetics and isotherm models: a review, CaJoST 4(1) (2022) 20-26.

[35] M.L. Soto, A. Moure, H. Domínguez, J.C. Parajó, Recovery, concentration and purification of phenolic compounds by adsorption: A review, Journal of Food Engineering 105(1) (2011) 1-27.

[36] S. Azizian, S. Eris, Chapter 6 - Adsorption isotherms and kinetics, in: M. Ghaedi (Ed.), Interface Science and Technology, Elsevier2021, pp. 445-509.

[37] H. Haidari, Z. Kopecki, A.T. Sutton, S. Garg, A.J. Cowin, K. Vasilev, pH-responsive “smart” hydrogel for controlled delivery of silver nanoparticles to infected wounds, Antibiotics 10(1) (2021) 49.

[38] S.-H. Kuo, C.-J. Shen, C.-F. Shen, C.-M. Cheng, Role of pH value in clinically relevant diagnosis, Diagnostics 10(2) (2020) 107.

[39] Y. Wu, Y. Wang, L. Long, C. Hu, Q. Kong, Y. Wang, A spatiotemporal release platform based on pH/ROS stimuli-responsive hydrogel in wound repairing, Journal of Controlled Release 341 (2022) 147-165.

[40] S. Kioomars, S. Heidari, B. Malaekeh-Nikouei, M. Shayani Rad, B. Khameneh, S.A. Mohajeri, Ciprofloxacin-imprinted hydrogels for drug sustained release in aqueous media, Pharmaceutical Development and Technology 22(1) (2017) 122-129.

[41] M. Mabrouk, A. Mostafa, H. Oudadesse, A.A. Mahmoud, M.I. El-Gohary, Effect of ciprofloxacin incorporation in PVA and PVA bioactive glass composite scaffolds, Ceramics International 40(3) (2014) 4833-4845.

[42] I. ISO, 10993–18: 2020 Biological evaluation of medical devices-Part 18: Chemical characterization of medical device materials within a risk management process, International Organization for Standardization (ISO): Geneva, Switzerland (2020).

[43] W. Horwitz, Evaluation of Analytical Methods Used for Regulation, Journal of Association of Official Analytical Chemists 65(3) (2020) 525-530.

[44] Z. Soosani, B. Rezaei, E. Heydari-Bafrooei, A.A. Ensafi, Chemical sensors based on molecularly imprinted polymers can determine drug release kinetics from nanocarriers without filtration, centrifugation, and dialysis steps, ACS sensors 8(5) (2023) 1891-1900.

[45] R. Keçili, Ö.B. Ünlüer, A. Ersöz, R. Say, Molecularly imprinted polymers (MIPs) for biomedical applications, Advances in Biomedical Polymers and Composites, Elsevier2023, pp. 745-768.

[46] Z. Ali, M. Sajid, M.M. Ahmed, M. Hanif, S. Manzoor, Synthesis of green fluorescent cross-linked molecularly imprinted polymer bound with anti-cancerous drug (docetaxel) for targeted drug delivery, Polymer Bulletin 81(1) (2024) 679-696.

[47] K. Nishchaya, V.K. Rai, H. Bansode, Methacrylic acid as a potential monomer for molecular imprinting: A review of recent advances, Results in Materials 18 (2023) 100379.

[48] B. Oktay, G.Ö. Eroğlu, S. Demir, S.E. Kuruca, N.K. Apohan, Poly(lactic acid) nanofibers containing phosphorylcholine grafts for transdermal drug delivery systems, Materials Today Sustainability 18 (2022) 100132.

[49] J. Meléndez-Marmolejo, L. Díaz de León-Martínez, V. Galván-Romero, S. Villarreal-Lucio, R. Ocampo-Pérez, N.A. Medellín-Castillo, E. Padilla-Ortega, I. Rodríguez-Torres, R. Flores-Ramírez, Design and application of molecularly imprinted polymers for adsorption and environmental assessment of anti-inflammatory drugs in wastewater samples, Environmental Science and Pollution Research 29(30) (2022) 45885-45902.

[50] N. Agarwala, D. Ranke, L. Rohani, G. Hastings, Calculated and experimental infrared spectra of substituted naphthoquinones, Frontiers in Science, Technology, Engineering and Mathematics (FSTEM) 3(2) (2019) 71-80.

[51] N. Agarwala, L. Rohani, G. Hastings, Experimental and calculated infrared spectra of disubstituted naphthoquinones, Spectrochimica Acta Part A: Molecular and Biomolecular Spectroscopy 268 (2022) 120674.

[52] L. Torn, A. De Keizer, L. Koopal, J. Lyklema, W. Blokzijl, Polymer adsorption on a patchwise heterogeneous surface, Horizons 2000–aspects of colloid and interface science at the turn of the millenium, Springer, 1998, pp. 153-160.

[53] K.Y. Foo, B.H. Hameed, Insights into the modeling of adsorption isotherm systems, Chemical engineering journal 156(1) (2010) 2-10.

[54] G.P. Jeppu, T.P. Clement, A modified Langmuir-Freundlich isotherm model for simulating pH-dependent adsorption effects, Journal of Contaminant Hydrology 129-130 (2012) 46-53.

[55] A.N. Stephen, S.R. Dennison, M.A. Holden, S.M. Reddy, Rapid sub-nanomolar protein determination in serum using electropolymerized molecularly imprinted polymers (E-MIPs), Analyst 148(21) (2023) 5476-5485.

[56] E.N. Ndunda, Molecularly imprinted polymers—A closer look at the control polymer used in determining the imprinting effect: A mini review, Journal of Molecular Recognition 33(11) (2020) e2855.

[57] A. Çerçi, O. Akgün, E. Karaca, M. Bakhshpour-Yücel, F. Arı, A. Yiğit Çınar, Ç. Bozkurt Güzel, B. Osman, Molecularly Imprinted Nanoparticle-Embedded Electrospun Mat as an Antibacterial Wound Dressing, Polymers for Advanced Technologies 36(2) (2025) e70100.

[58] Q. Zhang, M. Zhang, Z. Huang, Y. Sun, L. Ye, Molecularly imprinted polymers for targeting lipopolysaccharides and photothermal inactivation of pseudomonas aeruginosa, ACS Applied Polymer Materials 5(4) (2023) 3055-3064.

[59] A.C. Alavarse, F.W. de Oliveira Silva, J.T. Colque, V.M. da Silva, T. Prieto, E.C. Venancio, J.-J. Bonvent, Tetracycline hydrochloride-loaded electrospun nanofibers mats based on PVA and chitosan for wound dressing, Materials Science and Engineering: C 77 (2017) 271-281.

[60] Z. Rukavina, M.Š. Klarić, J. Filipović-Grčić, J. Lovrić, Ž. Vanić, Azithromycin-loaded liposomes for enhanced topical treatment of methicillin-resistant Staphyloccocus aureus (MRSA) infections, International journal of pharmaceutics 553(1-2) (2018) 109-119.

[61] P.L. Ritger, N.A. Peppas, A simple equation for description of solute release I. Fickian and non-fickian release from non-swellable devices in the form of slabs, spheres, cylinders or discs, Journal of Controlled Release 5(1) (1987) 23-36.

[62] R.W. Korsmeyer, R. Gurny, E. Doelker, P. Buri, N.A. Peppas, Mechanisms of solute release from porous hydrophilic polymers, International Journal of Pharmaceutics 15(1) (1983) 25-35.

[63] Y. Shi, Y. Wang, J. Zhu, W. Liu, M.Z.H. Khan, X. Liu, Molecularly imprinting polymers (MIP) based on nitrogen doped carbon dots and MIL-101 (Fe) for doxorubicin hydrochloride delivery, Nanomaterials 10(9) (2020) 1655.

[64] F.A. Sheikh, M.A. Hussain, M.U. Ashraf, M.T. Haseeb, M. Farid-ul-Haq, Linseed hydrogel based floating drug delivery system for fluoroquinolone antibiotics: Design, in vitro drug release and in vivo real-time floating detection, Saudi Pharmaceutical Journal 28(5) (2020) 538-549.

[65] X. Ding, Q. Tang, Z. Xu, Y. Xu, H. Zhang, D. Zheng, S. Wang, Q. Tan, J. Maitz, P.K. Maitz, S. Yin, Y. Wang, J. Chen, Challenges and innovations in treating chronic and acute wound infections: from basic science to clinical practice, Burns & Trauma 10 (2022).

[66] A.S. Lee, H. De Lencastre, J. Garau, J. Kluytmans, S. Malhotra-Kumar, A. Peschel, S. Harbarth, Methicillin-resistant Staphylococcus aureus, Nature reviews Disease primers 4(1) (2018) 1-23.

[67] J.S. Novais, C.S. Moreira, A.C.J. Silva, R.S. Loureiro, A.M.S. Figueiredo, V.F. Ferreira, H.C. Castro, D.R. da Rocha, Antibacterial naphthoquinone derivatives targeting resistant strain Gram-negative bacteria in biofilms, Microbial pathogenesis 118 (2018) 105-114.

[68] J. Kurczewska, M. Cegłowski, P. Pecyna, M. Ratajczak, M. Gajęcka, G. Schroeder, Molecularly imprinted polymer as drug delivery carrier in alginate dressing, Materials Letters 201 (2017) 46-49.

[69] C.S. Freitas, P.R. Pereira, R.V. Cardoso, F.P. Pauli, R.C.B. Ribeiro, F.D.C. Da Silva, V.F. Ferreira, V.M.F. Paschoalin, Antimicrobial and wound healing potential of naphthoquinones encapsulated in nanochitosan, Frontiers in Bioengineering and Biotechnology 11 (2024).

[70] L.N. Barde, M.M. Ghule, A.A. Roy, V.B. Mathur, U.D. Shivhare, Development of molecularly imprinted polymer as sustain release drug carrier for propranolol HCL, Drug Development and Industrial Pharmacy 39(8) (2013) 1247-1253.

[71] H. Chen, W. Zhang, N. Yang, C. Chen, M. Zhang, Chitosan-Based Surface Molecularly Imprinted Polymer Microspheres for Sustained Release of Sinomenine Hydrochloride in Aqueous Media, Applied Biochemistry and Biotechnology 185(2) (2018) 370-384

Conclusiones

En este trabajo se demostró la viabilidad de emplear polímeros de impresión molecular como plataformas para la incorporación, retención y liberación controlada y localizada de compuestos con actividad antimicrobiana. Mediante un método de síntesis no covalente se obtuvieron diferentes materiales utilizando ácido láctico y ácido metacrílico como monómeros funcionales, destinados a la liberación de ciprofloxacino, derivados de naftoquinona y antibióticos β-lactámicos, incluidos amoxicilina, piperacilina y tazobactam, de manera individual y combinada para los últimos tres.

Los materiales sintetizados mostraron una elevada capacidad de retención, particularmente los polímeros impresos, con porcentajes superiores al 90 %, lo que confirmó la formación de cavidades de reconocimiento específicas y su mayor afinidad por las moléculas plantilla respecto de los polímeros no impresos. Asimismo, se observó que el método de síntesis, la naturaleza del monómero funcional, la carga superficial del material y el pH del medio influyeron directamente en la capacidad de adsorción y en el comportamiento de liberación.

Los estudios *in vitro* evidenciaron una liberación controlada, sostenida y dependiente del pH, con perfiles condicionados por fenómenos de difusión, relajación de las cadenas poliméricas, hinchamiento y formación de poros. Esta respuesta a valores de pH de 5.4 y 7.4 resulta relevante para aplicaciones cutáneas, ya que reproduce parcialmente las condiciones de la superficie de la piel y de los microambientes asociados con heridas e infecciones. Los modelos cinéticos empleados, particularmente Korsmeyer-Peppas, permitieron describir la complejidad de los mecanismos involucrados en la liberación de los compuestos incorporados.

Los principios activos liberados conservaron su efectividad demostrando su actividad antimicrobiana y produjeron respuestas inhibitorias y bactericidas frente a cepas de referencia y aislamientos clínicos de bacterias de importancia médica, entre ellas *Staphylococcus aureus*, *Escherichia coli* y *Pseudomonas aeruginosa*. De

manera complementaria, los ensayos realizados en fibroblastos dérmicos humanos mostraron que los materiales no presentaron efectos citotóxicos de acuerdo con los criterios de la norma ISO 10993-5, lo que respalda su citocompatibilidad y su potencial uso como matrices para administración local de antimicrobianos.

En conjunto, los resultados muestran que los polímeros de impresión molecular pueden integrar en una misma plataforma el reconocimiento molecular, la alta capacidad de carga, la liberación controlada, la actividad antimicrobiana y la citocompatibilidad. Por lo tanto, estos materiales constituyen una alternativa prometedora para el desarrollo de sistemas farmacéuticos destinados al tratamiento localizado de heridas infectadas. Sin embargo, será necesario realizar estudios posteriores en modelos modelos *in vivo* de heridas infectadas para confirmar su seguridad a largo plazo, comportamiento farmacológico local, eficacia terapéutica y potencial de aplicación clínica.

Perspectivas del proyecto

Como perspectiva del proyecto, la siguiente etapa consistirá en evaluar los materiales diseñados en modelos animales con diabetes mellitus, con el objetivo de determinar su desempeño en condiciones fisiopatológicas más complejas y cercanas al escenario clínico. Estos estudios permitirán analizar la liberación localizada de los antimicrobianos, la eficacia frente a infecciones en heridas diabéticas, la respuesta inflamatoria, la regeneración tisular y el proceso de cicatrización. Asimismo, esta fase permitirá obtener evidencia sobre la seguridad, el comportamiento farmacológico local y la eficacia terapéutica de los MIPs sintetizados, como paso previo a su posible aplicación clínica.

Bibliografía

Adepu, S., & Ramakrishna, S. (2021). Controlled Drug Delivery Systems: Current Status and Future Directions. *Molecules 2021, Vol. 26, Page 5905*, *26*(19), 5905. https://doi.org/10.3390/MOLECULES26195905

Alvarez-Lorenzo, C., & Concheiro, A. (2004). Molecularly imprinted polymers for drug delivery. *Journal of Chromatography B*, *804*(1), 231–245. https://doi.org/10.1016/J.JCHROMB.2003.12.032

Andersson, H. S., & Nicholls, I. A. (1997). Spectroscopic evaluation of molecular imprinting polymerization systems. *Bioorganic Chemistry*, *25*(3), 203–211. https://doi.org/10.1006/BIOO.1997.1067

Aparicio-Blanco, J., Vishwakarma, N., Lehr, C. M., Prestidge, C. A., Thomas, N., Roberts, R. J., Thorn, C. R., & Melero, A. (2024). Antibiotic resistance and tolerance: What can drug delivery do against this global threat? *Drug Delivery and Translational Research 2024 14:6*, *14*(6), 1725–1734. https://doi.org/10.1007/S13346-023-01513-6

Bărăian, A. I., Iacob, B. C., Bodoki, A. E., & Bodoki, E. (2022). In Vivo Applications of Molecularly Imprinted Polymers for Drug Delivery: A Pharmaceutical Perspective. *International Journal of Molecular Sciences 2022, Vol. 23, Page 14071*, *23*(22), 14071. https://doi.org/10.3390/IJMS232214071

Belbruno, J. J. (2018). Molecularly Imprinted Polymers. *Chemical Reviews*, *119*(1), 94–119. https://doi.org/10.1021/ACS.CHEMREV.8B00171

Blair, J. M. A., Webber, M. A., Baylay, A. J., Ogbolu, D. O., & Piddock, L. J. V. (2014). Molecular mechanisms of antibiotic resistance. *Nature Reviews Microbiology 2014 13:1*, *13*(1), 42–51. https://doi.org/10.1038/nrmicro3380

Boulton, A. J. M., Rayman, G., & Wukich, D. K. (Eds.). (2020). *The foot in diabetes* (5th ed.). Wiley. https://doi.org/10.1002/9781119445821

Chen, H., Zhang, W., Yang, N., Chen, C., & Zhang, M. (2018). Chitosan-Based Surface Molecularly Imprinted Polymer Microspheres for Sustained Release of Sinomenine Hydrochloride in Aqueous Media. *Applied Biochemistry & Biotechnology*, *185*(2), 370–384. https://doi.org/10.1007/S12010-017-2658-2

Chen, L., Wang, X., Lu, W., Wu, X., & Li, J. (2016). *Molecular imprinting: perspectives and applications*. https://doi.org/10.1039/c6cs00061d

Choi, V., Rohn, J. L., Stoodley, P., Carugo, D., & Stride, E. (2023). Drug delivery strategies for antibiofilm therapy. *Nature Reviews Microbiology*, *21*(9), 555-572. http://dx.doi.org/10.1038/s41579-023-00905-2

Ciofu, O., Moser, C., Jensen, P. Ø., & Høiby, N. (2022). Tolerance and resistance of microbial biofilms. *Nature Reviews Microbiology 2022 20:10*, *20*(10), 621–635. https://doi.org/10.1038/s41579-022-00682-4

Cirillo, G., Parisi, O. I., Curcio, M., Puoci, F., Iemma, F., Spizzirri, U. G., & Picci, N. (2010). Molecularly imprinted polymers as drug delivery systems for the sustained release of glycyrrhizic acid. *Journal of Pharmacy and Pharmacology*, *62*(5), 577–582. https://doi.org/10.1211/JPP.62.05.0003

Cormack, P. A. G., & Elorza, A. Z. (2004). Molecularly imprinted polymers: synthesis and characterisation. *Journal of Chromatography B*, *804*(1), 173–182. https://doi.org/10.1016/J.JCHROMB.2004.02.013

Davies, J., & Davies, D. (2010). Origins and evolution of antibiotic resistance. *Microbiology and Molecular Biology Reviews, 74*(3), 417–433. https://doi.org/10.1128/MMBR.00016-10

Gao, W., Chen, Y., Zhang, Y., Zhang, Q., & Zhang, L. (2018). Nanoparticle-based local antimicrobial drug delivery. *Advanced Drug Delivery Reviews*, *127*, 46–57. https://doi.org/10.1016/J.ADDR.2017.09.015

Goswami, A. G., Basu, S., Banerjee, T., & Shukla, V. K. (2023). Biofilm and wound healing: from bench to bedside. *European Journal of Medical Research 2023 28:1*, *28*(1), 157-. https://doi.org/10.1186/S40001-023-01121-7

Gullberg, E., Cao, S., Berg, O. G., Ilbäck, C., Sandegren, L., Hughes, D., & Andersson, D. I. (2011). Selection of Resistant Bacteria at Very Low Antibiotic Concentrations. *PLOS Pathogens*, *7*(7), e1002158. https://doi.org/10.1371/JOURNAL.PPAT.1002158

Hasanah, A. N., Safitri, N., Zulfa, A., Neli, N., & Rahayu, D. (2021). Factors Affecting Preparation of Molecularly Imprinted Polymer and Methods on Finding Template-Monomer Interaction as the Key of Selective Properties of the Materials. *Molecules 2021, Vol. 26, Page 5612*, *26*(18), 5612. https://doi.org/10.3390/MOLECULES26185612

Haupt, K., & Mosbach, K. (2000). Molecularly Imprinted Polymers and Their Use in Biomimetic Sensors. *Chemical Reviews*, *100*(7), 2495–2504. https://doi.org/10.1021/CR990099W

Kamaly, N., Yameen, B., Wu, J., & Farokhzad, O. C. (2016). Degradable Controlled-Release Polymers and Polymeric Nanoparticles: Mechanisms of Controlling Drug Release. *Chemical Reviews*, *116*(4), 2602–2663. https://doi.org/10.1021/ACS.CHEMREV.5B00346

Karim, K., Breton, F., Rouillon, R., Piletska, E. V., Guerreiro, A., Chianella, I., & Piletsky, S. A. (2005). How to find effective functional monomers for effective molecularly imprinted polymers? *Advanced Drug Delivery Reviews*, *57*(12), 1795–1808. https://doi.org/10.1016/J.ADDR.2005.07.013

Kempe, H., Pujolràs, A. P., & Kempe, M. (2015). Molecularly Imprinted Polymer Nanocarriers for Sustained Release of Erythromycin. *Pharmaceutical Research*, *32*(2), 375–388. https://doi.org/10.1007/S11095-014-1468-2

Langer, R., & Peppas, N. A. (2003). Advances in biomaterials, drug delivery, and bionanotechnology. *AIChE Journal, 49*(12), 2990–3006. https://doi.org/10.1002/aic.690491202

Lawai, V., Ngaini, Z., Farooq, S., Wahi, R., & Bhawani, S. A. (2024). Current advances in molecularly imprinted polymers and their release mechanisms in drug delivery systems. *Polymers for Advanced Technologies, 35*(2), e6317. https://doi.org/10.1002/pat.6317

Li, J., & Mooney, D. J. (2016). Designing hydrogels for controlled drug delivery. *Nature Reviews Materials, 1*(12), Article 16071. https://doi.org/10.1038/natrevmats.2016.71

Liechty, W. B., Kryscio, D. R., Slaughter, B. V., & Peppas, N. A. (2010). Polymers for Drug Delivery Systems. *Annual Review of Chemical and Biomolecular Engineering*, *1*, 149. https://doi.org/10.1146/ANNUREV-CHEMBIOENG-073009-100847

Liu, R., & Poma, A. (2021). Advances in Molecularly Imprinted Polymers as Drug Delivery Systems. *Molecules 2021, Vol. 26, Page 3589*, *26*(12), 3589. https://doi.org/10.3390/MOLECULES26123589

Lusina, A., & Cegłowski, M. (2022). Molecularly Imprinted Polymers as State-of-the-Art Drug Carriers in Hydrogel Transdermal Drug Delivery Applications. *Polymers 2022, Vol. 14, Page 640*, *14*(3), 640. https://doi.org/10.3390/POLYM14030640

Márquez-Godínez, S. A., Zonana-Nacach, A., Anzaldo-Campos, M. C., & Muñoz-Martínez, J. A. (2014). Riesgo de pie diabético en pacientes con diabetes mellitus tipo 2 en una unidad de

medicina de familia. *Semergen*, *40*(4), 183–188. https://doi.org/10.1016/j.semerg.2013.10.004

Mathieu, T., Favetta, P., & Agrofoglio, L. A. (2024). Molecularly Imprinted Polymeric Nanoparticles as Drug Delivery System for Tenofovir, an Acyclic Nucleoside Phosphonate Antiviral. *Pharmaceutics*, *16*(7), 965. https://doi.org/10.3390/PHARMACEUTICS16070965/S1

Moghadam Omranipour, H., Sajadi Tabassi, S. A., Kowsari, R., Shayani Rad, M., & Mohajeri, S. A. (2015). Brimonidine imprinted hydrogels and evaluation of their binding and releasing properties as new ocular drug delivery systems. *Current Drug Delivery, 12*(6), 717–725. https://doi.org/10.2174/1567201812666150316110838

Murray, C. J., Ikuta, K. S., Sharara, F., Swetschinski, L., Robles Aguilar, G., Gray, A., Han, C., Bisignano, C., Rao, P., Wool, E., Johnson, S. C., Browne, A. J., Chipeta, M. G., Fell, F., Hackett, S., Haines-Woodhouse, G., Kashef Hamadani, B. H., Kumaran, E. A. P., McManigal, B., … Naghavi, M. (2022). Global burden of bacterial antimicrobial resistance in 2019: a systematic analysis. *The Lancet*, *399*(10325), 629–655. https://doi.org/10.1016/S0140-6736(21)02724-0

Naghavi, M., Vollset, S. E., Ikuta, K. S., Swetschinski, L. R., Gray, A. P., Wool, E. E., Robles Aguilar, G., Mestrovic, T., Smith, G., Han, C., Hsu, R. L., Chalek, J., Araki, D. T., Chung, E., Raggi, C., Gershberg Hayoon, A., Davis Weaver, N., Lindstedt, P. A., Smith, A. E., … Murray, C. J. L. (2024). Global burden of bacterial antimicrobial resistance 1990–2021: a systematic analysis with forecasts to 2050. *The Lancet*, *404*(10459), 1199–1226. https://doi.org/10.1016/S0140-6736(24)01867-1

Ndunda, E. N. (2020). Molecularly imprinted polymers—A closer look at the control polymer used in determining the imprinting effect: A mini review. *Journal of Molecular Recognition, 33*(11), e2855. https://doi.org/10.1002/jmr.2855

Norell, M. C., Andersson, H. S., & Nicholls, I. A. (1998). Theophylline molecularly imprinted polymer dissociation kinetics: a novel sustained release drug dosage mechanism. *Journal of Molecular Recognition: An Interdisciplinary Journal*, *11*(1-6), 98-102. https://doi.org/10.1002/(SICI)1099-1352(199812)11:1/6%3C98::AID-JMR399%3E3.0.CO;2-Y

Parisi, I., Fathy Elhabal, S., Abdelmonem, R., Mohamed, R., Nashar, E., Fathi, M., Elrefai, M., Mohsen, A., Hamdan, E., Safwat, N. A., Shoela, M. S., Hassan, F. E., Rizk, A., Kabil, S. L., Ahmed El-Nabarawy, N., Taha, A. A., & El-Nabarawi, M. (2024). Enhanced Antibacterial Activity of Clindamycin Using Molecularly Imprinted Polymer Nanoparticles Loaded with Polyurethane Nanofibrous Scaffolds for the Treatment of Acne Vulgaris. *Pharmaceutics 2024, Vol. 16, Page 947*, *16*(7), 947. https://doi.org/10.3390/PHARMACEUTICS16070947

Pavón-Núñez, D., Cárcamo-Mejía, S., Flores-Moreno, R., Nuñez-Palma, J., Chacón, J. J., Mendoza-Talavera, A., Erazo-Coello, A., Ortiz-Avilés, G., Mejía-Rodríguez, C., Álvarez-Oviedo, G., & Bermúdez-Lacayo, J. (2016). Caracterización de los pacientes con pie diabético atendidos en el Instituto Nacional del Diabético: Tegucigalpa, Honduras, 2013–2015. *Revista Hispanoamericana de Ciencias de la Salud, 2*(3), 215–222. https://dialnet.unirioja.es/servlet/articulo?codigo=5742052

Ruela, A. L. M., de Figueiredo, E. C., de Araújo, M. B., Carvalho, F. C., & Pereira, G. R. (2016). Molecularly imprinted microparticles in lipid-based formulations for sustained release of donepezil. *European Journal of Pharmaceutical Sciences : Official Journal of the European Federation for Pharmaceutical Sciences*, *93*, 114–122. https://doi.org/10.1016/J.EJPS.2016.08.019

Shadabfar, M., Abdouss, M., & Khonakdar, H. A. (2020). Synthesis, characterization, and evaluation of a magnetic molecular imprinted polymer for 5-fluorouracil as an intelligent

drug delivery system for breast cancer treatment. *Journal of Materials Science, 55*(26), 12287–12304. https://doi.org/10.1007/s10853-020-04887-x

Sullivan, C., Fisher, C. R., & Taenzer, J. (2024). Novel Antimicrobial Drug Development and Access: U.S. Government Support and Opportunities. *Novel Antimicrobial Drug Development and Access: U.S. Government Support and Opportunities: Issue Brief*, (November), 1–15. https://www.ncbi.nlm.nih.gov/books/NBK611093/

Tamma, P. D., Avdic, E., Li, D. X., Dzintars, K., & Cosgrove, S. E. (2017). Association of Adverse Events With Antibiotic Use in Hospitalized Patients. *JAMA Internal Medicine*, *177*(9), 1308–1315. https://doi.org/10.1001/JAMAINTERNMED.2017.1938

Tesfaye, S., Boulton, A. J. M., Dyck, P. J., Freeman, R., Horowitz, M., Kempler, P., Lauria, G., Malik, R. A., Spallone, V., Vinik, A., Bernardi, L., Valensi, P., Albers, J. W., Amarenco, G., Anderson, H., Arezzo, J., Backonja, M. M., Biessels, G. J., Bril, V., … Jones, T. (2010). Diabetic neuropathies: Update on definitions, diagnostic criteria, estimation of severity, and treatments. *Diabetes Care*, *33*(10), 2285–2293. https://doi.org/10.2337/dc10-1303

Triadenda, A. ; L. ;, Rahayu, D. ;, Hasanah, A. N. A., Zhang, Z., Pan, J., Niu, X., Murdaya, N., Leatemia Triadenda, A., Rahayu, D., & Hasanah, A. N. (2022). A Review: Using Multiple Templates for Molecular Imprinted Polymer: Is It Good? *Polymers 2022, Vol. 14, Page 4441*, *14*(20), 4441. https://doi.org/10.3390/POLYM14204441

Uhrich, K. E., Cannizzaro, S. M., Langer, R. S., & Shakesheff, K. M. (1999). *Polymeric Systems for Controlled Drug Release*. https://doi.org/10.1021/cr940351u

UNEP. (2022). *Environmental Dimensions of Antimicrobial Resistance: Summary for Policymakers*. https://wedocs.unep.org/handle/20.500.11822/38373

Versey, Z., da Cruz Nizer, W. S., Russell, E., Zigic, S., DeZeeuw, K. G., Marek, J. E., Overhage, J., & Cassol, E. (2021). Biofilm-Innate Immune Interface: Contribution to Chronic Wound Formation. *Frontiers in Immunology*, *12*, 648554. https://doi.org/10.3389/FIMMU.2021.648554/FULL

Wassif, R. K., Elkayal, M., Shamma, R. N., & Elkheshen, S. A. (2021). Recent advances in the local antibiotics delivery systems for management of osteomyelitis. *Drug Delivery*, *28*(1), 2392–2414. https://doi.org/10.1080/10717544.2021.1998246

World Health Organization. (2024). *WHO bacterial priority pathogens list, 2024: Bacterial pathogens of public health importance to guide research, development and strategies to prevent and control antimicrobial resistance*. https://iris.who.int/handle/10665/376776

World Health Organization. (2023, November 21). *Antimicrobial resistance*. https://www.who.int/news-room/fact-sheets/detail/antimicrobial-resistance

Wu, Z., Hou, J., Wang, Y., Chai, M., Xiong, Y., Lu, W., & Pan, J. (2015). Preparation and evaluation of amoxicillin loaded dual molecularly imprinted nanoparticles for anti-Helicobacter pylori therapy. *International Journal of Pharmaceutics*, *496*(2), 1006–1014. https://doi.org/10.1016/J.IJPHARM.2015.10.065

Yang, Y., & Shen, X. (2022). Preparation and Application of Molecularly Imprinted Polymers for Flavonoids: Review and Perspective. *Molecules 2022, Vol. 27, Page 7355*, *27*(21), 7355. https://doi.org/10.3390/MOLECULES27217355

Zhao, G., Zhang, Y., Sun, D., Yan, S., Wen, Y., Wang, Y., Li, G., Liu, H., Li, J., & Song, Z. (2023). Recent Advances in Molecularly Imprinted Polymers for Antibiotic Analysis. *Molecules 2023, Vol. 28, Page 335*, *28*(1), 335. https://doi.org/10.3390/MOLECULES28010335

Carátulas de artículos

ScienceDirect

Journals & Books Help Search My account Sign in

Research article Get rights and content ↗

Research paper

Development and evaluation of ciprofloxacin local controlled release materials based on molecularly imprinted polymers

Vanessa Galván-Romero [a], Fernando Gonzalez-Salazar [a], Karla Vargas-Berrones [b], Luz Eugenia Alcantara-Quintana [c], Fidel Martinez-Gutierrez [d e], Sergio Zarazua-Guzman [d], Rogelio Flores-Ramírez [f] Show more

European Journal of Pharmaceutics and Biopharmaceutics

Date: February 2024
Article: 114178
Volume: Volume 195

Cite Add to Mendeley Share | 10.1016/j.ejpb.2024.114178 ↗

Access through **Universidad Complutense d...** Purchase PDF Other access options

Article preview Cited by (16) Metrics

ScienceDirect

Journals & Books Help Search My account Sign in

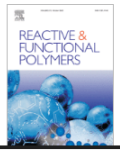

Research article Get rights and content ↗

Molecularly imprinted polymer systems for the controlled release of naphthoquinone derivatives with antimicrobial activity

Vanessa Galván-Romero [a], Fernando Gonzalez-Salazar [a], Karla Vargas-Berrones [b], Francisco Castro Flores [a], Blanca Nohemí Zamora Mendoza [a], Denisse Atenea de Loera Carrera [c], Fidel Martínez Gutiérrez [d], Luz Eugenia Alcántara-Quintana [e], Rogelio Flores-Ramírez [f] Show more

Reactive and Functional Polymers

Date: October 2025
Article: 106388
Volume: Volume 215

Cite Add to Mendeley Share | 10.1016/j.reactfunctpolym.2025.106388 ↗

Access through **Universidad Complutense d...** Purchase PDF Access through another organization

Article preview Recommended articles Cited by (3) Metrics